ASSESSMENT OF DAMAGE IN CORRODED AND FRP REPAIRED CORRODED BEAMS USING ADVANCED NDT TECHNIQUES

A Thesis

Submitted in fulfilment of the requirement for the award of degree

of

DOCTOR OF PHILOSOPHY

in

CIVIL ENGINEERING

Submitted by

Sunil Garhwal

Reg. No.: 951602008

Supervisor(s)

Dr. Shruti Sharma
Professor
Civil Engineering Department

Dr. Sandeep Kumar Sharma
Associate Professor
Mechanical Engineering Department

THAPAR INSTITUTE
OF ENGINEERING & TECHNOLOGY
(Deemed to be University)

DEPARTMENT OF CIVIL ENGINEERING

PATIALA – 147 004

August 2021

"Dedicated to my Beloved parents"

Mr. Tarachand Garhwal

Mrs. Bhirma

I learned from my mother

"where there's a will, there's a way"

I learned from my father

Always do the best job, your reputation is worth more than a quick profit"

CERTIFICATE

I, **Sunil Garhwal,** hereby declare that the thesis entitled, **"Assessment of damage in corroded and FRP repaired corroded beams using Advanced NDT Techniques,"** submitted to Thapar Institute of Engineering & Technology, Patiala, in partial fulfilment of the requirement for the award of Degree of **Doctor of Philosophy** in **Civil Engineering** is a record of original and independent research work done by me during 2016-2021. This thesis has been conducted under the supervision and guidance of **Dr. Shruti Sharma,** Professor, Civil Engineering Department, and **Dr. Sandeep Kumar Sharma**, Associate Professor, Mechanical Engineering Department, Thapar Institute of Engineering & Technology, Patiala. It has not formed the basis for the award of any Degree to any candidate of any university.

Sunil Garhwal

Date: 14/10/2022

This is to certify that above statement made by the candidate is correct to the best of my knowledge.

Shruti Sharma 14/10/2022

Dr. Shruti Sharma
Supervisor
Professor
Civil Engineering Department

14/10/22

Dr. Sandeep Kumar Sharma
Supervisor
Associate Professor
Mechanical Engineering Department

ABSTRACT

Corrosion of steel in concrete is inevitable and is a worldwide problem which causes heavy losses to the economy and industry. Concrete due to its alkaline nature (pH > 13.5) provides a passive protective layer of oxides around the reinforcing steel initially but when exposed to severe environmental conditions (like marine exposure) corrosion in steel bar is initiated due to depassivation of this layer. Corrosion product formed has a tendency to exert tensile pressure on surrounding concrete as rust product has volume about 6-10 times that of parent steel leading to cracking and spalling of surrounding concrete. Bond deterioration at steel concrete interface and reduction in steel area due to corrosion which ultimately reduces the load carrying capacity of Reinforced Concrete (RC) structure and can be catastrophic. In countries like India with diverse environmental condition, losses due to corrosion has been estimated USD 40 billion per year for industrial and infrastructural segments. Due to this, most of the structures need repair with 10-15 years of their construction. Therefore, it becomes very important to monitor corrosion in RC structures alongwith sustained loading so that proper timely remedial measures can be adopted before degradation leads to catastrophic failures. Numerous studies have been reported by researchers in last few decades for monitoring corrosion in RC structures like visual inspection, electrochemical, optical methods, measurement of linear polarization resistance and concrete resistivity, X-ray, gamma rays, etc. But these techniques only provide qualitative information on the presence of corrosion but do not indicate the rate or extent of corrosion.

In this study, an effort has been made to monitor various stages and aspects of real time corrosion in RC structures using a judicious combination of various non-destructive monitoring tools of active Ultrasonic Guided Wave (UGW), passive Acoustic Emission (AE) technique and optical Infra-Red Thermographic (IRT) technique. Bars with simulated corrosion damage representing pitting and delamination in the bars prepared and were tested in air and concrete using UGW and IRT. Further RC beams (80 x 80 x 400 mm) were subjected to real time actual accelerated impressed current corrosion and were simultaneously monitored using advanced NDT techniques of UGW, IRT and AE. As the corrosion progresses in RC beams a significant drop in transmitted signal strength of a specific core seeking guided wave mode is observed

representing efficiency of UGW in picking progression of corrosion but UGW is not very effective in picking up the initiation of corrosion. It was well corroborated by AE testing which successfully picks up the initiation of corrosion along with its progression in the surrounding concrete. It is well depicted by various micro-cracking and macro-cracking phases at different stages of corrosion in the corroding beam as picked up by increase in number of cumulative AE hits and their amplitudes with progressive corrosion. AE X-Y event plots clearly demonstrate the initiation and progression of cracks in pictorial representation. But localisation of corrosion damage still remains a challenge and is explored in this study. IRT effectively picks up corrosion in rebars in concrete as the rust products produced get heated at a fast rate than the parent steel and the same is represented as differential temperature profiles in the IRT. Hence, it can be concluded from the detailed qualitative as well as quantitative NDT monitoring of corrosion that initiation is effectively picked up by AE, well supported by UGW for picking up progression and localisation by thermographic images in IRT. It is important to mention that UGW picks up deterioration only in embedded rebars while AE picks up the effect of corrosion on the surrounding concrete.

Further in this study, effect of varying levels of corrosion alongwith sustained loading on the overall performance of real size RC beams (127 x 227 x 4100 mm) was investigated using a combination of global vibration diagnostics and local Acoustic Emission technique. With the increase in corrosion level in RC beams, a shift and drop in fundamental frequency and drop in Frequency Response Function (FRF) amplitudes is observed as vibration signal attenuates due to increasing corrosion cracks. An attempt has been made to establish a correlation between damage index (based on FRF amplitude) and ultimate load of corroded as well as Glass Fibre Reinforced Polymer (GFRP) repaired corroded beams. During flexural testing of corroded beams there is a drop in the ultimate load carrying capacity and mid span deflection. For severely corroded samples, ultimate failure behavior changed from ductile to brittle which is alarming. AE monitoring during flexural testing of corroding beams indicate variation in a number of AE hits and their corresponding amplitudes with an increase in corrosion level. In healthy beams, specific micro-cracking (Phase I) and macro-cracking (Phase III) phases of damage progression are depicted by AE monitoring but with the increase in corrosion levels, a significant drop in cumulative AE hits along with depletion of different AE cracking phases is observed due to the attenuation of the captured AE

signals caused by pre-existing cracks as compared to healthy beam. Hence, AE monitoring can serve as a non-destructive tool to monitor initiation and progression of damage and cracks much before they are observed on the surface and also pick up effect of increasing corrosion and sustained loading marked by depletion of AE phases.

Further the beams corroded to different levels were repaired using GFRP wraps to investigate the efficacy of FRP wrapping for strengthening corroded structures. The performance of GFRP repair was assessed using global vibration and local AE monitoring during flexural loading. Micro-concrete and GFRP repair of corroded RC beams leads to a significant improvement in dynamic characteristics of beams both in terms of frequency as well as FRF amplitudes. Also as a result of repair, AE phases reappeared with an increase in the number of AE hits pointing towards improved integrity of beams after GFRP repair. AE X-Y event plots give a pictorial representation of actual cracking inside the concrete much before it is observed on the surface. All the cracking events right from initiation to the progression of micro-cracks into macro-cracks is well presented by AE X-Y event plots. AE also aids in the visualization of the repaired concrete beneath the FRP wrap as the surface of structure is not exposed for visual observation. Also a correlation is established between non-destructive parameters of cumulative AE hits and ultimate loads in both corroded and GFRP repaired corroded beams to facilitate non-destructive evaluation of RC structures.

Hence it can be concluded that global vibration monitoring and local AE monitoring of RC structures can serve as a potential tool for non-destructive evaluation of effect of corrosion with loading and its efficacy post repair of corroded RC structures which would help in deriving a post-corrosion maintenance strategy for RC structures.

ACKNOWLEDGEMENT

First and foremost, I am beholden to the Almighty and I bow before Him for his umpteen blessings and bestowing in me the grit and confidence to carry out the research work.

I extend my thanks to **Dr. Prakash Gopalan**, Hon'ble Director, Thapar Institute of Engineering and Technology, for giving me the opportunity to undertake Ph.D.

I convey heartfelt and sincere gratitude to my research supervisor **Dr. Shruti Sharma**, Professor, Civil Engineering Department and **Dr. Sandeep Kumar Sharma**, Associate Professor, Mechanical Engineering Department. Their valuable support, advice, and encouragement inspired me to complete the research work on time.

I am honour bound and profoundly thankful to the doctoral committee members-, **Dr. Prem Pal Bansal**, Head & Professor, Civil Engineering Department, **Dr. Shweta Goyal**, Professor, Civil Engineering Department, **Dr. A.B. Danie Roy,** Assistant Professor, Civil Engineering Department, and **Dr. Raj Kumar Gupta,** Professor, Department of Chemical Engineering Thapar Institute of Engineering and Technology, for their support and invaluable comments.

Further, I wish to thank those persons who helped me in structural lab and concrete lab: Ram Sumiran, Virendran Sharma, Hitesh sharma, Manreet singh, Amarjeet Singh, Roop Kumar and many others.

I would also like to acknowledge the most important person of my family: my father, Sh. Tarachand Garhwal, my mother, Smt. Bhirma, Sh. Jagdish Garhwal (Baba ji), Smt. Kalavati (Maa ji), Dr. Sunita Garhwal (sister), Ms. Rekha Gharwal (sister), Dr. Ajay Laura (brother-in-law), Mr. Yogesh Siwach (brother-in law), Anil Garhwal (brother cum friend), Priyanka Garhwal (sister-in-law) for their endless support. Their love, patience, persistent encouragement, and good virtuous understanding enabled me to complete the research work successfully.

I would also take this opportunity to thank my beloved wife, Anjali Chauhan for always supporting and believing in me. She has been the constant source of positivity and motivation for me.

Sincere, thanks to all my friends especially Dr. Manpreet singh, Ashish Tiwari, Savy dagar, Akshay Sharma and Nirmal for their support and cooperation throughout the entire process. Thanks for the friendship and memories.

I would like to thank all my little siblings Anaya, Dishita, Aashna and Vivan. They have given me so much love and happiness. Finally, my thanks go to all the people who have supported me to complete the research work directly or indirectly.

Sunil Garhwal

TABLE OF CONTENTS

LIST OF FIGURES

LIST OF TABLES

ACRONYMS AND ABBREVIATIONS

AE	Acoustic Emission
CC	Chloride Corrosion
CFRP	Carbon Fiber Reinforced Polymer
GFRP	Glass Fiber Reinforced Polymer
CSS	Cumulative Signal Strength
DT	Destructive Testing
FRP	Fiber Reinforced Polymer
UGW	Ultrasonic Guided Wave
HCP	Half-Cell Potential
MS	Mild Steel
DT	Destructive testing
NDT	Non-destructive testing
RC	Reinforced Concrete
WT	Wavelet Transform
IC	Impressed current
IRT	Infra-Red Thermography
VMT	Vibration Monitoring Technique
PE	Pulse Echo
DI	Damage Index

CHAPTER 1

INTRODUCTION

1.1 BACKGROUND AND MOTIVATION

Reinforced Concrete (RC) is the most commonly used construction material throughout the world as it can be moulded into any shape and provides high compressive strength along with promising durability. Due to its high alkaline pore solution (pH > 13.5), concrete provides a protective covering to the reinforcement against corrosion by forming dense impermeable film on the steel surface. Aggressive environments like chloride or carbonation leads to depassivation and breakdown of this protective layer thus leading to corrosion [1]–[3]. Rust produced as a result of corrosion is estimated to have 4-6 times the volume as that of parent steel and thus tend to exert tensile stresses on the surrounding concrete leading to its cracking and spalling [4]. It can be very catastrophic for RC structures as it results in pitting and de-bonding of bars from surrounding concrete thus affecting its overall strength and integrity [4]–[10]. According to Melchers the process and mechanism of corrosion in severe marine conditions is typically divided into four different phases [11]. Initiation of corrosion is due to breakdown of passive layer and is referred to as '***Phase I***' of corrosion. The corrosion product formed in this phase acts as a protective layer for reinforcing steel and reduces the corrosion activity for a small duration in '***Phase II***'. Further protective layer of rust dissolves due to accelerated corrosion in '***Phase III***' and results in sudden increase in corrosion. This is the most damaging phase of corrosion. Finally, a small corrosion rate is recorded in the later stages of corrosion is termed as '**Phase IV**'.

Corrosion along with physical damage results in massive economic losses in the form of maintenance and repair of structures [12]. Structures near coastal regions and the structures exposed to severe tides or storms are more prone to corrosion. In Middle East countries and in countries with a long coast line (like India) problem of corrosion is predominant and most of the structures deteriorate within 15-20 years of their construction. It has been estimated that in India, annual losses due to corrosion are about around 100 billion USD where as it is about 2.5 trillion USD worldwide [13]. Hence, it becomes very important to monitor corrosion and pick its initiation at early stage so that proper and timely remedial measures and repair can be adopted before degradation leads to catastrophic stages.

In the last few decades lot of research have focused on monitoring corrosion in RC structures. Visual inspection (VI) is the most commonly used technique and is characterized by simplicity and virtually no cost but it gives indication at very late stages when damage is beyond repair [14]–[16]. Numerous other techniques have been suggested by researchers worldwide to pick up corrosion in RC structures [6], [17]–[19]. These techniques fall broadly in two categories Destructive techniques (DT) and Non-Destructive techniques (NDT). DT involve the inspection of reinforcing steel bars by removing the concrete cover so as to estimate the extent of corrosion damage. Most commonly adopted destructive testing techniques are pull out test and mass loss estimator [20]–[22]. But, these DT are rarely adopted as it can damage the structure fully or partially thus increasing the cost of repair exponentially. NDT on the other hand, helps in detecting corrosion without affecting the integrity of the structure and its use. Some commonly suggested NDT techniques used for picking corrosion in RC structure include electrochemical based techniques like Half-Cell Potential (HCP)[25], [9], [16, 17], linear polarization resistance [26], [27], galvanostatic pulse transient method [28], concrete resistivity [29] and electrochemical noise [30], [31]. But these electrochemical techniques only provide information on the presence of corrosion but fails to quantify its extent or rate. Alternately specific methods like fiber optic technology which is a strain sensing method and monitors strains in a localized region due to corrosion is also proposed by some researches [32], [33]. Other specialized NDT methods include impact-echo method, use of X-ray, gamma rays, etc.[34]–[36]. But these techniques require skilled labor and suffer from the drawback of their application in monitoring large sized RC structures. When applied to RC structures for corrosion evaluation, the above-mentioned famous NDT techniques suffer from several constraints as discrete access, and limited qualitative or quantitative monitoring data.

Recently wave propagations tool have been suggested by researchers for damage detection in RC structures. They typically fall in two regimes: Active and Passive techniques. Active monitoring techniques involve external excitation of wave into the structure and monitoring the variation in its propagation characteristics with damage. The change in wave propagation characteristics as compared to the healthy specimen represents the severity of damage like impact echo method or Ultrasonic Guided Wave approach. Ultrasonic Guided Wave (UGW) approach involves the injection of a high-frequency wavelet pulse into a structure and the subsequent

observation of transmitted or reflected waves after interaction with damage. Recently UGW have been used for damage detection in RC structures typically for corrosion monitoring. Drop in transmitted waves amplitude of specific guided wave modes have been used to identify pitting and delamination effects of corrosion [37]–[42]. Specific core seeking and surface seeking modes were identified which were sensitive to different stages of corrosion in RC structures along with identifying different types of corrosion (chloride or oxide) in RC structures. Similarly, passive monitoring techniques of Acoustic Emission (AE) has been established as one of the most promising methods for effectively monitoring corrosion damage in RC structures. It has been sucessfully used to pick up initiation of corrosion as increased volume of rust exerts pressure on surrounding concrete which results in minor cracking at the interface of concrete and steel. It leads to formation of elastic waves which are recorded by the AE sensors mounted on the surface of specimen and processed using AE win software. Hence, AE can be used as a non-destructive testing and assessment tool for RC structures which are at risk of corrosion, providing an early warning before the damage becomes severe. The approach has also shown promising in predicting damage during load testing of various structures and materials, such as Fibre Reinforced Polymer (FRP), steel, Reinforced Concrete (RC) and Prestressed Concrete (PC) structures [25], [38], [43]–[53]. Similarly, another monitoring technique of Infrared Thermography Technique (IRT) also has been used as an advanced tool for monitoring damage in structures. IRT has been used to identify the damage beneath the surface. IRT works on the principle that every material has different thermal conductivity. This change in thermal conductivity is used to detect damage underneath the surface. Rust formed due to corrosion tends to transmit heat at a different rate as compared to healthy steel and hence change in surface temperature profile called thermogram is recorded to identify the damage due to corrosion [37], [54]–[62].

While considerable research has been independently done concentrating solely on either detecting corrosion, localizing it or limiting its progress, a combination of a thorough qualitative and quantitative methodology which can pick up the initiation, progression and advancement at all stages of corrosion still needs to be developed. In this research work, an effort has been made to monitor real time initiation and progression of corrosion in concrete beams utilizing a combination of active wave propagation tools of UGW (Ultrasonic Guided Wave) along with passive AE (Acoustic

Emission) monitoring tool assisted by advanced thermal imaging technique of IRT (Infra-Red Thermography). The research work tries to utilize the advantages of each NDT tool to pick up whole process of corrosion at different stages in RC beams.

Another aspect of corrosion monitoring is application of the developed NDT technique to real sized structures. In this work, it is attempted to extend the developed NDT of local AE and global vibration monitoring to assess the performance of differently corroded RC beams under flexural loading. It closely relates to real life RC structures undergoing corrosion along with sustained loads (applied flexural loading). Vibration monitoring technique is a universally adopted global NDT technique which is sensitive to damage even when cracks are located well within a structure. The underlying concept behind this technique is that modal parameters are functions of the structure's physical properties, such as mass, damping, and stiffness. Hence it is expected that as a result of corrosion the development of cracks would lead to change in modal parameters damage or cracks would lead to attenuation of the vibration response leading to quantification of damage [63]–[70]. A change in vibration parameters of a damaged structure marked by shift in frequency and amplitude of the vibration signals is compared with the baseline signature of same undamaged structure would help to quantify damage clubbed with local AE monitoring tool, localization of corrosion damage is expected. Another aspect of the research work undertaken in this thesis is the monitoring of beams corroded to different levels when repaired with Glass Fibre Reinforced Polymer (GFRP) wraps. Differently corroded and corrosion repaired RC beams were then monitored using global vibration monitoring technique. The GFRP repaired beams were subjected to flexural testing and were simultaneously monitored using local Acoustic Emission technique. Due to repair of corroded specimen surface of specimen is not exposed for inspection thus it becomes essential to monitor repaired specimens using NDT tools so as to monitor their condition.

Hence, it is proposed in this study to monitor RC structures using a combination of global and local NDT techniques so that corrosion can be first detected in its early stages and timely remedial measures can be adopted. Further monitoring the beams subjected to corrosion and sustained loading simulating real like structures is attempted using well established local global vibration monitoring and AE technique tools. The corroded structures repaired with GFRP wrapping are also monitored after repair to

investigate the efficacy of repair using NDT. The aim of the work is to develop a novel methodology for assessing damage progression in large sized RC structures undergoing simultaneous corrosion and subjected to sustained loading and further their assessment where corroded beams are GFRP wrapped and subjected to flexural loading. This approach facilitates non-destructive evaluation of GFRP repaired RC structures with a prior indication of their damage post repair.

1.2 CORROSION IN RC STRUCTURES AND REPAIR METHODS

In RC structures the corrosion of steel is one of the major problem faced by concrete industry as it directly influences the durability of structures. In RC structures surrounding concrete layer around steel reinforcement act as a barrier to corrosion and prevent penetration of corrosive agents. Further a passive layer of oxides exists around steel bar which delay corrosion but fails to prevent it completely. It does not sustain long due to penetration of aggressive agents like carbon dioxide and chloride ions leading to initiation of corrosion due to depassivation of reinforcement (**Figure 1.1 b**). Further, corrosion progresses resulting delamination of steel from surrounding concrete. It is due to the formation of voluminous rust product which is about 4-6 times the volume of original steel [53] (**Figure 1.1 c**). The expanded steel exerts tensile pressure on concrete leading to the cracking and spalling of concrete (**Figure 1.1 d**). Eventually these cracks accumulate and travels to the concrete surface [71] and result in cracking and spalling of concrete cover and further exposes the steel rebar to corrosion. Progression of corrosion finally leads to pits in the steel bar ultimately causing huge loss in load carrying capacity of structure and can lead to its catastrophic failure. To mitigate effects of corrosion and enhancing the service life of structure various methods have been suggested by researchers. Use of FRP bars, stainless steel or epoxy coated bars, galvanized steel bars etc. in place of tradition bars have been proposed. [72]–[79]. But these special type of bars are uneconomical and their long term effectiveness is questionable. Their application is still in nascent stages of research. Various conventional methods have also been suggested like removing spalled concrete and addition of extra concrete layer or steel rebars etc [80]–[83]. But these methods suffer from practical limitations like compromising the overall appearance of structure, adding extra weight to the structure etc.

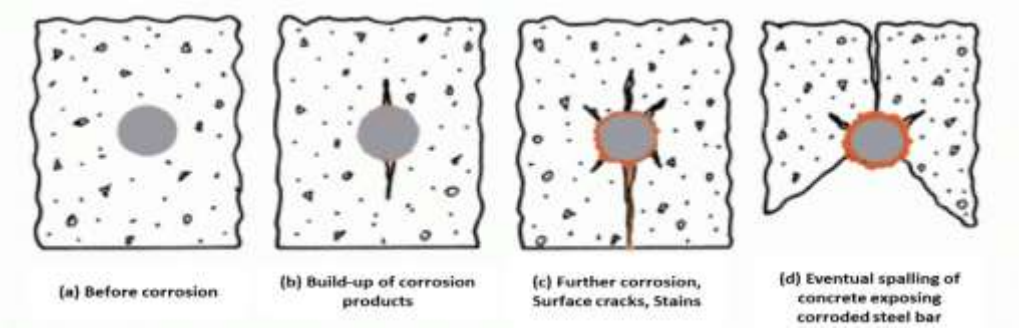

Figure 1.1: Cracking and spalling of concrete cover due to corrosion of reinforcement [71]

During last few decades, an effective measure of FRP wrapping around concrete has been suggested for repair and rehabilitation of damaged corroded structures. To attain high strength and longer life of structures FRP materials are being used on large scale in countries like North America, Western Europe, and Japan. Glass Fiber Reinforced Polymer (GFRP) offers very high strength-to-weight ratio, stiffness-to-weight ratio and increased corrosion resistance [84]–[87]. Thus, GFRP sheets not only provide high flexural and shear strength to the RC structures but also provides resistance to acids, alkalis and similar corrosive agents [84], [85], [88]–[91][20], [91]–[98]. Additionally, FRP sheets are easy to handle and perform wonderfully in adverse environments. Two major advantages of FRP for repair against corrosion has been reported by various researchers [86], [97], [99], [100] which are summarized as below:

- Acts as a barrier to the infusion of corrosive agents on the reinforcement.
- Provides a confinement pressure on the damaged concrete hence preventing the displacement of concrete cover.

Both Glass Fibre Reinforced Polymer (GFRP) and Carbon Fibre Reinforced Polymer (CFRP) both most commonly used as repair or strengthening techniques, CFRP provides better strength, stiffness and are durable. On the other hand, GFRP sheets offers much superior electrical resistance making them comparatively better for passive protection from corrosion.

A brief review of use of FRP wrapping for corrosion protection is presented below:

Masoud et al. (2001) examined the feasibility of using externally bonded FRP laminates to rehabilitate corrosion damaged reinforced concrete beams with varying chloride level (i.e. 0 to 3%) and subjected to four-point bending. The results indicate

successful confinement to the corrosion cracking and spalling by FRP wrapping. Test results also revealed that FRP strengthened beams exhibited higher stiffness in comparison to un-strengthened beams, and increase in the ultimate and yield strength was also recorded.

Maaddway and Soudki (2005) studied the viability of using externally bonded carbon-fibre-reinforced polymer (CFRP) laminates to increase the serviceability or service life of reinforced concrete beams. The RC beams were subjected to different levels of corrosion damage upto 15% mass loss in bars. The corroded samples were repaired using CFRP laminates. It was concluding that corrosion of reinforced steel reduces the load carrying capacity of RC beams but their repair with GFRP wrapping resulted in increase in ultimate strength of the corroded beams in comparison to non-corroded or virgin beams but the deflection capacity was significantly reduced.

Kenneth et al., (2005) investigated the effects of FRP wrapping on restoring strength losses due to steel corrosion as well as inhibiting further corrosion damage. Two sets of experimental studies were performed to ensure the protection and rehabilitation of corrosion damaged reinforced concrete columns. The first investigation involved the use of three different types of FRP (glass/epoxy, carbon/epoxy and aramid/epoxy), as well as two additional conventional waterproofing systems (a siloxane sealer and polymer concrete overlay) to compare different techniques for protecting steel rebars from corrosion. The results indicated that the FRP materials provided superior protection against corrosion, even for specimens already damaged by corrosion. However, the extent of protection was independent of the type of FRP. Protection provided by the siloxane sealant and polymer concrete overlay was found to be limited in time. In the second study, an accelerated corrosion process is initiated on concrete columns with both axial and spiral reinforcement. The main goals of the FRP rehabilitation of corrosion damaged column were to restore the initial strength as well as restricting the further damage. The corroded and then repaired specimens exhibited 40 % more strength when compared with the un-corroded unstrengthened ones. Furthermore, the ductility was improved without increasing the stiffness.

Masoud and Soudki (2006) presented an experimental study on RC beam specimens subjected to corrosion and further repaired with GFRP and CFRP. Corrosion

activity of rebar was evaluated using half-cell potential measurements and mass loss method. The average mass loss of FRP repaired specimen was 16% lower than unrepaired specimen. The decrease in corrosion rate and average mass loss was attributed to the reduction in diffusion rate of moisture and oxygen into concrete due to FRP wrapping. It was concluded that GFRP wrapping reduces the corrosion activity but CFRP provides only flexural strengthening and provides no considerable effect on decreasing the corrosion activity.

Gadve et al. (2009) investigated the efficiency of using surface bonded FRP composites for rehabilitation of corrosion damaged concrete. Electrochemical tests of half-cell potential and cell voltage, mass loss and pull out strength test were used to evaluate the performance of corroded as well as repaired corroded cylinders. The test results demonstrate that surface wrapping of FRP decreases the corrosion rate, increases the pull out strength, and decreases the mass loss.

Gadve at al. (2010, 2011) investigated passive and active corrosion protection of the reinforcing steel with surface bonded FRP's. For passive protection investigation, sheets of GFRP and CFRP wraps were adhesively bonded to the beam specimen, while for active protection electrically conducted carbon fibre wrap was made an anode and reinforcing bar was used as cathode. Various tests were also performed like flexural strength, mass loss and half-cell potential to report the performance of the samples. The application of FRP increases the flexural capacity and decreased the mass loss due to corrosion activity. It was also reported that the loss in bond between steel and concrete was also eliminated by the confinement pressure exerted by the FRP sheets.

Sharma et al. (2015) investigated the efficacy of using CFRP and GFRP wrapping against accelerated chloride induced corrosion. Specimens subjected to different levels of corrosion were repaired by wrapping with CFRP and GFRP and further subjected to corrosive exposure to study post-repair behaviour. To study the pre- and post-repair behaviour of RC cylinders pull out strength and mass loss tests were performed alon with ultrasonic monitoring. The results obtained shows that FRP bonding increases the cell voltage by 300% indicating increase in corrosion resistance. The comparative performance of GFRP and CFRP was also tested and it was concluded that GFRP samples exhibited higher electrical resistance than CFRP. Fall in surface seeking mode and core seeking mode indicates the initiation aand progression of corrosion.

Sharma et al. (2021) investigated the efficacy of dual protection offered by CFRP sheets against active and passive protection for corrosion inhibition. The performance was evaluated by Ultrasonic Guided Wave (UGW). Results concluded that CFRP wrapping reduces the corrosion rate by preventing the diffusion of oxygen and moisture. Destructive tests also confirmed the beneficial effect by a decrease in mass loss and increase in pull out strength of CFRP wrapped samples.

Hence, in this research effort, in addition to developing a comprehensive corrosion monitoring strategy for picking up initiation and progression of corrosion, the effect of GFRP wrapping on differently corroded RC beams when subjected to flexural loading would also be investigated to assess the performance by use of NDT tools of local AE technique clubbed with global vibration monitoring tool. Repairing and re-strengthening of structures with FRP wrapping prohibits the inspection of surface as it is not exposed. Hence, to evaluate the performance of FRP repaired structures, NDT tools needs to be developed so as to estimate the actual condition of structures when they are further subjected to adverse environmental conditions combined with sustained loads.

1.3 GAPS IN RESEARCH AREA

From the literature, major gaps identified can be summarized as:

1. Real time corrosion monitoring in concrete using Infra-Red Thermography (IRT) has not been investigated till date.
2. Combination of advanced NDT local techniques of AE, UGW and IRT for actual corrosion monitoring in RC structures has not been reported.
3. Effect of simultaneous corrosion in real sized RC beams with loading has not been investigated using non-destructive tools.
4. Effect of FRP repair against corrosion in beams under flexural loading has not been investigated using Non-Destructive Testing tools.

From these identified gaps in the literature, the objectives of the proposed research work are out lined.

1.4 OBJECTIVES OF RESEARCH

From the identified gaps in the research area, the objectives of the research are outlined as follows:

- Assessment of damage due to real time corrosion in concrete using Infra-Red Thermography, Acoustic Emission and Ultrasonic Guided Waves.
- Fracture monitoring of beams subjected to different corrosion levels under flexure using Acoustic Emission and Vibration Monitoring Technique.
- Analysis of fracture in corrosion repaired beams with FRP using Acoustic Emission and Vibration Monitoring Technique.

1.5 OUTLINE OF THESIS

CHAPTER 1: Introduces the problem of corrosion and its effect on RC structures and the review of corrosion monitoring techniques. Further control strategies and repair for corrosion protection and inhibitor are discussed. The gaps in the research area are identified and objectives and scope of the research work is outlined.

CHAPTER 2: Carries out a review of damage monitoring techniques used for corrosion assessment in this work. The first segment throws light on the studies carried using ultrasonic guided waves for damage monitoring in RC structures. Further, review of work done using advanced NDT tools of Acoustic Emission Technique and Infrared Thermography along with global vibration monitoring for damage monitoring in RC structures has been presented.

CHAPTER 3: This chapter focusses on the experimental details and methodology adopted for the research work.

CHAPTER 4: This chapter focusses on real time monitoring of accelerated corrosion damage in RC beams using Advanced Non-destructive Techniques of Ultrasonic Guided waves, Infra-Red Thermography and Acoustic Emission Technique.

CHAPTER 5: This chapter focusses on the monitoring of corroding and corrosion repaired RC beams when subjected to flexural loading using AE and Vibration Monitoring Technique.

CHAPTER 6: This chapter focusses on monitoring of corroded beams and GFRP repaired corroded beams under flexural loading using a combination of local Acoustic Emission Technique and global vibration monitoring tool.

CHAPTER 7: Presents the conclusions derived from the entire research work and provides a few recommendations for further study.

1.6 CLOSING REMARKS

This chapter outlines the basic background and motivation for this research work. The basic aim is to develop a comprehensive corrosion monitoring methodology for RC structures using a combination of various advanced (wave) NDT tools of AE, UGW and Vibration diagnostics (wave based tools) along with IRT- a thermographic technique. These NDT tools would be further used for monitoring corroded and GFRP repaired corroded RC beams when subjected to simultaneous loading. The gaps in this research area and the objectives of the present work have also been outlined. Further, the outline of the thesis is presented.

CHAPTER 2

DAMAGE MONITORING TECHNIQUES – A REVIEW

2.1 GENERAL

Quality monitoring of infrastructure systems is critical for extending service life, ensuring protection by identifying damage and deformations early, and taking timely corrective action. Non-Destructive Testing (NDT) is commonly used to track materials such as steel in the aerospace industry and other industries without causing any damage to the structure. The principle of NDT technique is to find out the integrity and quality of materials, components or assemblies without disturbing the ability to perform their anticipated functions. As briefed in chapter 1, this research work is focussed on developing a comprehensive real time corrosion monitoring technique in RC structures utilizing combination of various NDT techniques of ultrasonic guided waves, acoustic emission technique, infrared thermography and global vibration monitoring technique. Further the beams corroded to different loads would be repaired with GFRP wrapping and simultaneously were subjected to flexural loading and their behaviours and performance would be assessed using these NDT tools.

This chapter throws light on the basic principles of these NDT tools of Ultrasonic Guided Wave (UGW), Acoustic Emission (AE), Infra-Red Thermography (IRT) and global Vibration Monitoring technique and the review of latest works done specifically with reference to assessment of corrosion damage.

2.2 ULTRASONICS FOR DAMAGE MONITORING

Ultrasonic bulk waves propagation has been used since centuries for damage monitoring in various infrastructures and a brief discussion of the same is presented below:

2.2.1 Basic Principle

The basic principle of ultrasonic non-destructive testing technique is based on the propagation of sound waves in any medium. A typical ultrasonic testing system consists of various functional units such as ultrasonic pulser/receiver which excites piezoelectric transducers for excitation of waves in media, and display devices to display the reflected or transmitted waves after their interaction with damage / defect. The sound

waves with certain velocity propagates large distances through the structure under examination and is received by a sensor located at different positions. The signal received by the sensor are further analysed further for locating as well as determining the degree of damage in the structure. The applied voltage produces mechanical disturbance that travel through the structure as wave. These waves are vibration frequencies having range above 20 kHz, with the upper range varying between 15-30 kHz. It is to be taken into consideration that there are no structural and dimensional changes when the test is being performed. This could only be possible when the applied stress is lower than the elastic limit and to achieve the same low energy and high frequency wave packet is introduced into the structure to be inspected and further observing the subsequent propagation and reflection of this energy. It is possible to identify fundamental properties of materials such as elastic constants, damping characteristics and use them for damage diagnosis by investigating the propagation, reflection, and attenuation of ultrasonic pulses. Most commonly used methods for ultrasonic testing are: -

(a) Pulse Echo Method (b) Pulse Transmission Method

(a) *Pulse Echo Technique*

In pulse echo method, a piezoelectric transducer is mounted over the surface of the test specimen where it transmits and receive ultrasonic waves. The waves transmitted in the specimen gets reflected back by the opposite face of specimen or due to any lack of continuity, cracks, voids, or any other damage in the material. This reflected wave is received by the same transducer and converted into electrical signal which is further displaced on monitor as two echo peaks, one referencing to Back Wall Echo (BWE) and appearance of a Crack Echo (CE) (Figure. 2.1). This method offers the advantage of damage localization in addition to quantification of damage measured by magnitude of crack echo. The display is used to calculate the travel time between the excited and reflected pulses. The position of defect can be identified by using the following formula:

$$D = Vt \qquad (2.1)$$

where,

D is the defect distance from transducer end,

V is the wave velocity, and

t is the flight time

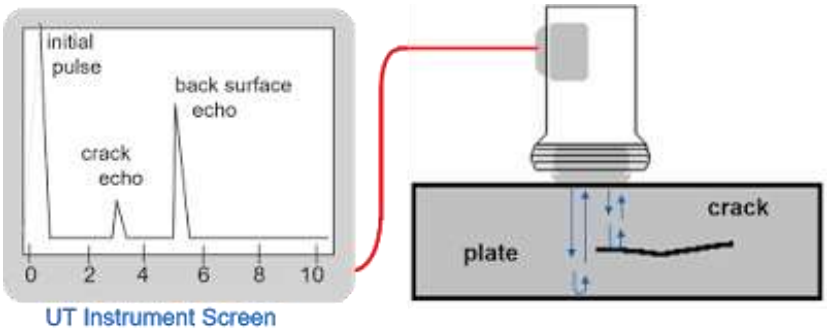

Figure. 2.1: Test set-up for pulse echo technique [40]

(b) Pulse Transmission Method

In pulse transmission method two transducers are used where one acts as a transmitter (T) which transmits the wave into the system and other act as a receiver (R) which records the wave transmitted on the other end. Testing of specimen with this method helps to locate damage (defect, holes and gaps) in the X-Y plane **(Figure. 2.3)**. The relative change in amplitude of the transmitted signal is used to estimate the degree of a damage in the specimen undertesting shows cracks/ gap. Ultrasonic pulse transmission technique helps to quantify damage accurately but does not localize it.

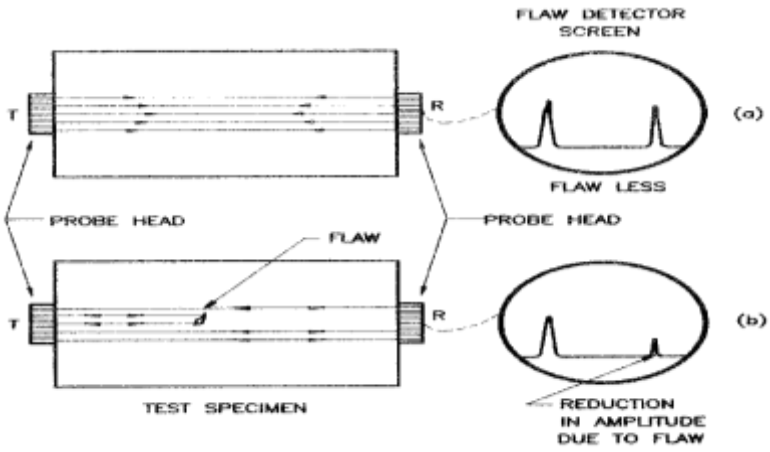

Figure. 2.2: Schematic representation of Pulse Transmission method [104]

Both these methods can be used together with advantage to exactly localize or quantify damage. This type of ultrasonic testing for damage detection fall in ultrasonic bulk wave propagation. But the ultrasonic bulk wave propagation is not suited for damage monitoring in large structures like civil engineering applications due to high attenuation of signal and limitation in scanning the large RC structures. Hence, guided wave propagating through specific geometries are preferred for structural health monitoring due to their enhanced and long range inspection capabilities.

2.2.2 Ultrasonic Guided Waves (UGW)

The types of elastic wave that exist in all frequency range (i.e. ultrasonic, sonic, and subsonic) are typically classified as ***body waves (also called bulk waves) and surface waves (also known as guided waves).*** As discussed body waves offer limited scanning capabilities whereas guided waves guided by geometry of the structure are capable of travelling long distance with minimal energy loss. The expression "waveguide" refers to the mechanism that directs the wave. The thickness of the waveguide must be equal to the operating wavelength for an ultrasonic wave to be considered guided. For the occurrence of bulk wave and surface wave, the thickness of material should be much greater than the working wavelength. Guided waves for damage diagnosis and detection offer a large number of benefits as follows:

- Access to a small area of the specimen is required using guided wave, such as small area of the structure or a rebar end.
- Guided wave has the capacity to examine the entire structure from a single point as they can spread throughout the structure.
- Guided waves are highly sensitive and allows to identify minor defects.
- Detection of flaws deep within the structure is also possible due to its high penetrating power.
- Mode tuning and frequency may be used to assess various forms of damage in systems using guided waves.

Depending upon the geometry through which the guided waves propagate, they can be further classified as Plate waves or Lamb waves, rod waves or bar waves, cylindrical guided waves as in rebar in concrete and pipes, Rayleigh waves and Generalized Rayleigh-Lamb waves. The directed wave propagating along the half space's surface is

known as a **Rayleigh wave,** if the wave guide's configuration is a homogeneous half space, while **Lamb waves** are waves that propagate across a plate-like system with two adjacent stress-free boundaries. The elastic waves that propagate through a hollow / solid cylindrical or pipe structure are called **as cylindrical guided waves**. The waves travelling through the reinforcing bars in concrete fall in this category.

2.2.3 Cylindrical Guided Wave

- ***Guided Waves in Bar in Air***

The sound waves when transmitted through a perfectly elastic bulk material gets dispersed through the material as bulk wave which results in drop in amplitude. Whereas in case of a perfectly elastic material like steel bar, the sound wave is constrained and reflected back by the boundaries of the material and is termed as guided wave. Wave propagation is influenced by the dispersion effects of boundaries in cylindrical system resulting in three modes of propagation namely longitudinal (L), flexural (F) and torsional (T) modes. All three modes are represented by the first letter and two reference numbers i.e L (m, n), T (m, n) and F (m, n) for longitudinal, torsional and flexural modes respectively. Two reference number 'm' and 'n' represent variation in displacement around the circumference of the bar and counter variable. By selecting a frequency band, specific modes can be excited and the relationship representing the velocity-frequency relationships of guided waves is known as **dispersion curves.**

Various guided waves modes based on solution of wave propagation equation are obtained using dispersion curves. Dispersion curves are used to analyse the properties of the phase velocity, wave number, and group velocity for a free, perfectly elastic bar to explain the guided wave behaviour. For this purpose, DISPERSE software has been developed and used [105]. Dispersion curves can also be used to find the relationship between the velocity of guided waves and their frequency for a free elastic structure. Phase velocity and group velocity are two widely used parameters for free elastic structures. Phase velocity (V_{ph}) is the velocity of a wave at a certain frequency.

$$V_{ph} = \frac{\omega}{\xi} \tag{2.2}$$

where,

ω is the angular frequency of wave which is related to frequency as $\omega = 2\pi f$;

ξ is the real wavenumber which is related to wavelength as $\xi = 2\pi/\lambda$.

On the other hand, group velocity is the velocity of entire group of waves traversing through the structure. Group velocity (V_{gr}) is associated with the angular frequency (ω) and real wave-number (ξ) as,

$$V_{gr} = \frac{\partial \omega}{\partial \xi} \tag{2.3}$$

- ***Guided Waves in Rebars in Concrete***

The monitoring of material become more complex when additional layers are added around them such as in the case of embedded steel bar in concrete. In this case, the elstic and damping properties of the different layers determine how the ultrasonic wave propagates through the system. Further, the energy that leaks into the surrounding layers like concrete leads to the attenuation of waves it becomes a leaky wave. To analyse and monitor leaky wave energy velocity and attenuation characteristics are used. Energy velocity is defined as the rate at which a wave packet propagates along a structure, and it can be measured using data recorded from mode shapes (stress and displacement fields). In a situation like the perfectly elastic steel bar in a vacuum it is equal to the group velocity. However, there are variations in group and energy velocities in leaky or attentive systems. Further, attenuation is caused by two factors: energy absorption into the surrounding media like concrete around rebars and damping in the waveguide material (steel rebars). Damping occurs as all the materials are not perfectly elastic and some loss occurs due to visco-elastic losses. Disperse's typical damping model assumes a constant attenuation per wavelength, which means that attenuation increases with frequency in a bulk wave. In case of guided waves, the frequency-attenuation relationships are much more complicated and are influenced by a variety of other considerations, including leakage into the surrounding concrete media.

For rebar in concrete, input properties (**Table 2.1**) for steel and concrete properties were used in modelling in DISPERSE software. To select a guided wave mode in an embedded system, dispersion curves are plotted. Phase velocity, energy velocity and attenuation curves are used to arrive at a particular mode and frequency of excitation. The guided wave tends towards highest energy velocity (**Figure 2.4 a**) and minimum attenuation (**Figure 2.4b**) is selected further for testing. **Figure 2.4 (b)** shows energy velocity curve for 12 mm diameter steel bar embedded in concrete where L (0,7) tends

towards maximum energy velocity and hence was chosen as the excitation longitudinal guided wave mode at an excitation frequency of 1 MHz. Here, excitation frequencies can be varied to excite the various longitudinal modes in the bars in concrete. The selection of frequency is also dependent on signal accuracy. It is also important to mention that this L (0,7) mode at 1 MHz proceeds towards decreasing or minimum attenuation values (**Figure 2.4 c).** Hence, this L (0,7) mode at 1 MHz was selected for 12 mm bars in concrete for further ultrasonic investigations.

Table 2.1. Material properties of steel and concrete [105]

S.No.	Material Property	Steel	Concrete
1	Modulus, E (GPa)	210	29.6
2	Density (ρ), (kg/m^3)	7932	2200
3	Longitudinal Attenuation (dB/m)	0.003	0.2
4	Shear Attenuation (dB/m)	0.008	0.5
5	Longitudinal Velocity (m/s)	5960	4100
6	Shear Velocity (m/s)	3260	2300
7	Poisson's Ratio	0.2865	0.27

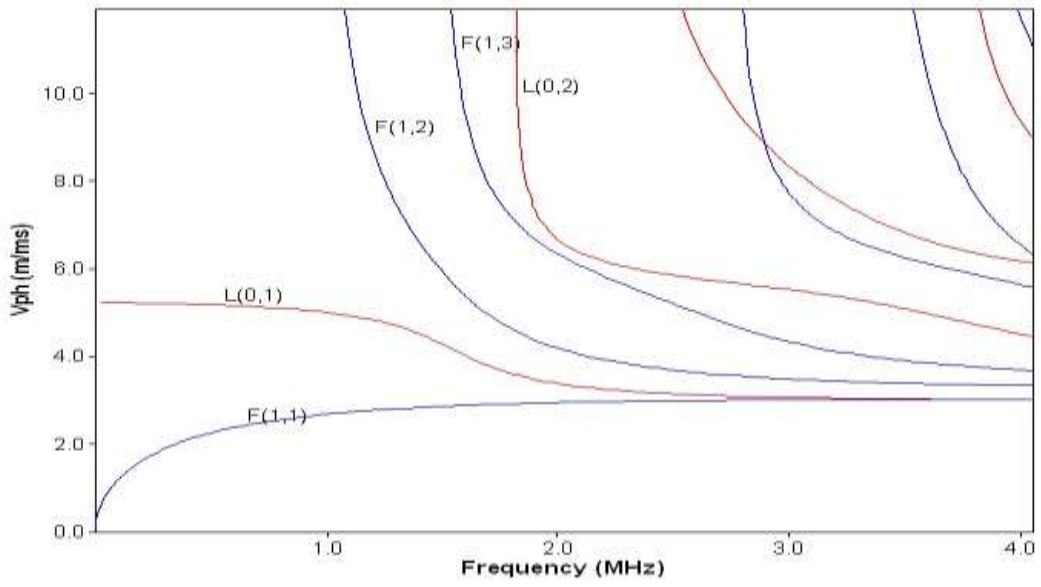

(a) Phase Velocity Vs Frequency

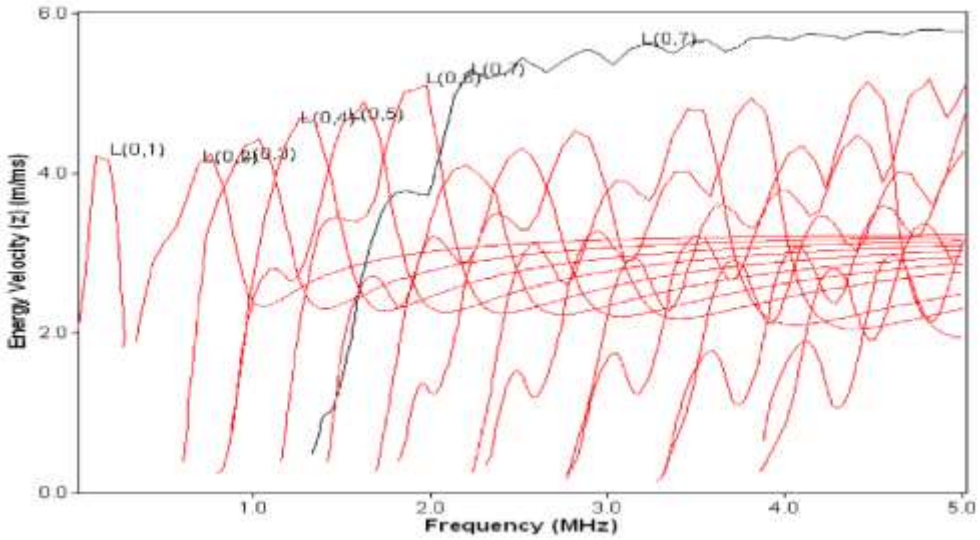

(b) Energy Velocity Vs Frequency

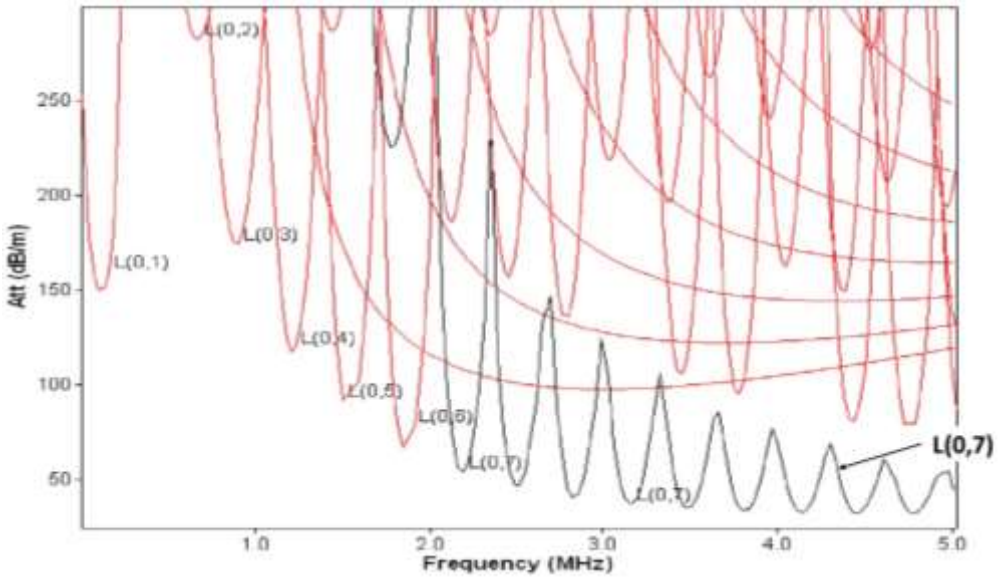

(c) Attenuation Vs Frequency

Figure. 2.3: Illustration of dispersion Curves for 12 mm bar in concrete [105]

2.2.4 Limitations for Use in RC structures

Ultrasonic guided wave faces some major problem in field application which are discussed below:

- The modes and frequencies used for inspection of corrosion in reinforced concrete structures have a restricted inspection spectrum.
- Due to absorption into the surrounding concrete, wave energy transmitted in embedded steel bar is attenuated at higher rates.

- The reflection coefficient of defects in addition to leakage of ultrasonic guided waves is a concern. Although the reflection coefficients from defects cannot be calculated, the recent finding of high frequency, low-leakage driven modes [105] have the ability to minimize reduction due to leakage.
- Other disadvantages of the ultrasonic guided wave technique include the requirement for technical expertise for accurate monitoring.

Despite these challenges, ultrasonic guided waves have been effectively researched in last two decades for monitoring various kinds of defects and damages especially corrosion related damages in RC structures. **Section 2.2.5** outlines the major works done in the application of Ultrasonic guided wave for corrosion monitoring in RC structures.

In this work it is proposed to use ultrasonic guided wave (UGW) for corrosion monitoring in RC bars along with other advanced local NDT tools of Acoustic Emission (AE) and Infrared Thermography (IRT) while the corroded beams are subjected to sustained flexural loading.

2.2.5 Review of Ultrasonic Guided Waves for Corrosion Monitoring

Pavlakovic et al. (2001) investigated the behaviour of ultrasonic guided wave modes with minimum attenuation for a steel bar embedded in low impedance grout. Both pulse-through and pulse-echo were employed in the studies. The dispersion curves for circular bar with low impedance grout were calculated to establish attenuation minima at higher frequencies. The findings are beneficial for inspecting tendons in post-tensioned bridges.

Maia et al., (2003) studied the delamination as well as corrosion at the interface between steel bar and concrete using guided ultrasonic waves. Plain and Rebar steel bars with corrosion and physical separation were used as specimen for the study. Ultrasonic cylindrical guided waves propagating along the reinforced steel bar were found to be sensitive to the interface conditions between concrete and steel bar. The transducers employed during the course of experiment were Electromagnetic Acoustic Transducer (EMAT) and the Piezoelectric Transducer (PZT). The ultrasonic guided waves were also found to be sensitive to the type of steel used and the rib patterns on the deformed steel bars. The studies indicated that the guided ultrasonic waves are a bit

uncertain in quantifying the amount of corrosion or delamination at the steel-concrete interface.

Na et al., (2003) assessed the feasibility of employing generalized Rayleigh-Lamb waves and cylindrical guided Lamb waves for inspection of concrete–steel interface. Generally, the conventional ultrasonic methods use reflection, transmission, and scattering of longitudinal waves by internal defect for inspecting defects in concrete. However, the same was not found to be very efficient in detecting delamination at the interface between concrete and steel bars. Therefore, Lamb waves which can propagate a long distance along the reinforcing steel bars embedded in concrete and is sensitive to the interface bonding condition between the steel bar and the concrete were taken into account. The proposed transducer–receiver arrangements in the study has successfully inspected reinforced concrete beams for delamination at the steel concrete interface when the bars were accessible or not.

Sharma and Mukherjee (2010) investigated the use of longitudinal guided ultrasonic waves to monitor notch and debond defects in steel bars in concrete simulating pitting and delamination phenomena caused by corrosion. The two ultrasonic techniques of pulse transmission and pulse echo were applied for in situ corrosion monitoring of embedded reinforcements in RC beams. The combination of both techniques not only indicated the presence of damage but also gave the exact location and magnitude of damage. The specific core and surface seeking modes of ultrasonic guided wave successfully identified the corrosion mechanism in a bar embedded in concrete.

Sharma and Mukherjee (2011, 2013) investigated chloride and oxide induced corrosion in RC beams using specific core and surface seeking mode. In case of chloride corrosion, high freequency core-seeking mode were effective for picking up signal showing pitting and non-uniform area loss at later stages of corrosion. In the initial stages, surface seeking mode of low frequency picked up delamination and debonding marked by increase in signal intensity. In case of oxide induced corrosion surface-seeking mode indicated gradual decrease in signal intensity pointing towards only delamination and not pitting.

Sharma S.K. and Mukherjee (2015) reported on the development of a non-contact, in-situ, and non-destructive approach for monitoring corrosion in submerged

plates using ultrasonic guided waves. Two modes operating at different frequencies, 0.1 MHz and 1 MHz, were used to track corrosion-induced damage in plates. In addition to the ultrasonic signals, certain metrics such as plate mass loss, stress-strain behaviour, and tensile strength were also measured. The research was found to be extremely useful in the development of a non-destructive technique for measuring progressive degradation in plates and evaluating their degradation in strength due to corrosion, as measured by stiffness and mass loss, which would eventually aid in the assessment of residual life of various kind of plate infrastructure assembles.

Sharma et al. (2015) monitored corrosion progression in FRP wrapped RC cylinders using ultrasonic guided waves. The cylinders were repaired after exposing them to corrosive environments at different rates using glass and carbon fibre reinforced polymer wraps. An increase of 300% in the cell voltage was recorded for FRP wrapped samples representing increase in corrosion resistance. By carefully monitoring the performance of surface and core seeking modes of signal it was concluded that the FRP reinforced bars were less prone to corrosion than the unwrapped samples. The ultrasonic results were well supported by reduced mass loss and higher pull out strength in wrapped samples.

Farhidzadeh et al. (2015) investigated use of ultrasonic guided waves to repair corrosion damage in steel strands. A reference-free technique, continuous wavelet transformations, and wave velocity measurements were developed on the basis of the dispersion curves in order to achieve estimated loss in cross-section of the strand.

Beena et al. (2017) developed a non-contact damage monitoring technique for detecting corrosion damage in Concrete Filled Steel Tubes (CFST) using guided waves. UGW were used to identify corrosion-induced notch and debond flaws in CFST components. The loss in cross-sectional area and pitting caused by accelerated corrosion was picked successfully by guided waves.

Kairu et al. (2019) observed that, application of thin layer of epoxy on the reinforcement bars will allow smooth propagation of the ultrasonic guided waves in rebar. Rebar embedded in the concrete could only transmit 3% of the energy. After the application of 0.3mm layer of epoxy, energy detected at 3.5 meters from the excitation point was 27%. It was observed that these relative amplitudes are taken with respect to signal amplitudes for reinforcement bars in air.

Sriramadasu et al. (2019) investigated UGW for detection of early cracks in the rebars. It was aimed to develop robust and non-destructive assessment technique by scattering the guided waves for estimation of local damages and early cracks in rebars referred to as corrosion pits. Observing the energy and timing of arrival of the guided wave modes back and front margins of damages could be picked up. The scatter coefficient is defined by the factors affecting the scatter energy. It was observed from the UGW studies that estimated size of the damage increases with the increase in corrosion length of the rebar i.e. with 50% and 100% increase in corrosion length there was increment of 29.5% and 78% in estimated size of damage respectively.

Hence, it can be seen that ultrasonic guided waves of specific nature can not only pick up debonding and pitting effects of corrosion but also successfully differentiate between corrosion in different environments. It can also be observed from literature review that UGW can pick up corrosion in various steel geometries like plates, ribbed bars, CFST sections, tendons in pre-stressed concrete structures etc. Hence, they can be used with advantage for monitoring damages in various forms and conditions in RC structures as explored in this work under combined effects of corrosion and sustained flexural loads.

2.3 ACOUSTIC EMISSION TECHNIQUE

2.3.1 Principle and Advantages of AE

Acoustic emission with its ability to detect dynamic process of deformation has outlined the existing NDT techniques. The deformation in material / structure can be due to the initiation of minor or major cracks, bond failure, yielding, etc. This deformation generates energy which transmit to the surface of structure in the form of elastic waves which are termed as ‘acoustic emission’. These elastic waves are recorded by the AE sensors which are mounted on the surface of the specimen being investigated (**Figure 2.4**). These piezoelectric transducers convert the sound waves generated as a result of deformation into electric signal and transmit it to the AE data acquisition system for further analysis (**Figure 2.4**). This method is very sensitive and enables to detect flaws much before they are visible to the naked eyes. Various factors such as distance and direction of the source with respect to the sensor as well as nature of transferring material affects the AE signal strength. After processing the recorded data depending upon the wavelength signature and time of arrival, type of damage, damage

intensity and its location can be classified using AE win software. The detected AE signals are usually referred to as ***AE hits***. AE technique has been effectively used for monitoring structures subjected to loading and re-strengthen structures with materials like FRP, steel, RC and Pre-Stressed Concrete (PC) structures. In case of repair with engineered material it becomes difficult to monitor the surface of structure as it is not exposed thus in such case AE plays a key role in determining the level of damage and condition of structure underneath.

There are number of benefits of using the Acoustic Emission Technique (AE) over other usual Non Destructive Testing Techniques (NDT) methods. Some of these advantages are:

- Real time monitoring
- Detection of defects, flaws, cracks etc rapidly.
- High sensitivity
- Cost reduction especially maintenance cost

For these reasons, AE method is an influential aid for real time monitoring for detection of deformation, fracture and cracks inside structures. It indicates about the behaviour of materials which directly influence their strength, damage and failure at a very early stage. Thus it is proposed in this study to use passive AET along with UGW and IRT to monitor damages in RC structures subjected to combined corrosion and sustained flexural loading. **Section 2.3.5** throws light on the recent works done for damage monitoring in concrete structures using Acoustic Emission Technique.

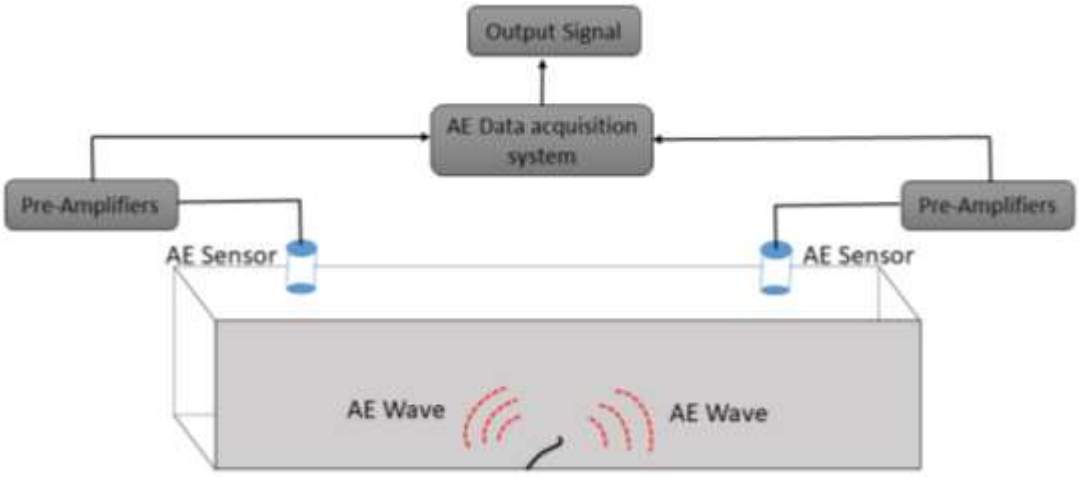

Figure 2.4: Schematic illustration of AE Monitoring Process [114]

2.3.2 AE Test setup

AE test setup comprises of various devices which serve a specific role in monitoring and recording of AE signals through any structure. The various components involved are:

- **AE Sensors: -** These are piezoelectric transducers which are mounted on the surface of test specimen and coverts sound waves into electric signals. In order to monitor the specimen accurately and to locate the damage location the sensors must be placed at the appropriate location. In order to avoid any discontinuity in the signal received at the surface of specimen, proper contact should be maintained between the specimen and sensor surface. To achieve this usually a coupling gel is used.
- **Pre-Amplifiers**: The signal received by the AE sensors is very weak and contains other disturbances. Thus to eliminate all noises and to amplify the received signal to a better level pre-Amplifiers are used.
- **Data acquisition system:** The signal received at the sensor end is transferred to modern AE systems which comprises of computers and associated software. All the signal received are stored by the acquisition system for further analysis. AE system offers a wide range of post-processing options for the recorded data for further analysis.

2.3.3 AE signal parameters

The recorded AE signal waveforms are analysed to determine the properties of wave source originating from the damage/crack/fracture To understand the AE signal, it is necessary to understand certain fundamental terms which are required to analyse a structure (**Figure 2.5**).

- **Threshold**: To eliminate sound waves from the surroundings a predetermined voltage level is set for acoustic signal to surpass before it can be recognized and processed.
- **Hit:** It is a AE waveform which surpasses the threshold limit and is recorded and processed by Acoustic Emission channel. The AE hits also points towards the deformation experienced by the structure under observation.

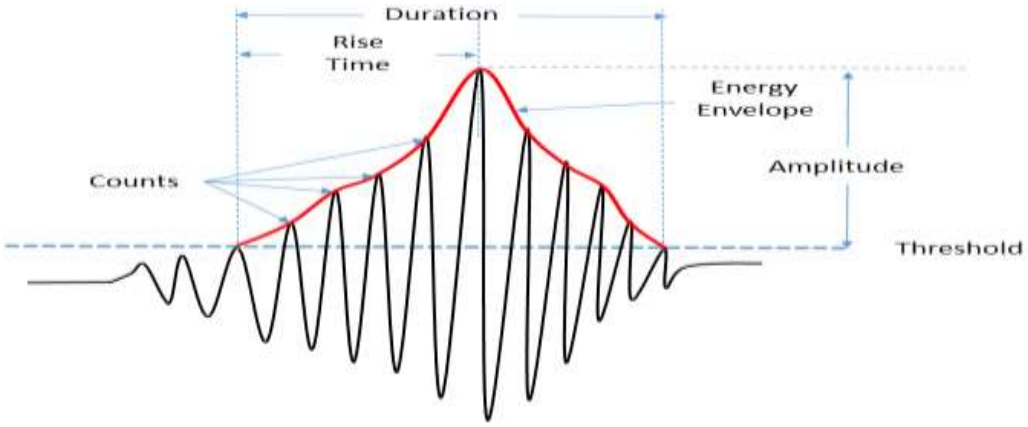

Figure 2.5: Typical Waveform of Acoustic Emission signal [114]

- **Peak Amplitude:** It is the maximum amplitude attained by an acoustic signal burst. The size of source event is related to the corresponding amplitude.
- **Rise Time**: The time between the first signal crossing threshold and the peak amplitude is known as the rise time**.**
- **Signal Duration:** It is the duration of time between the first and final time signal burst which has surpassed the threshold limit.
- **Counts:** The number of times the amplitude of the signal surpasses the threshold limit.
- **Event**: The AE sound wave generated gets transmitted into all the direction which when recorded by one or more AE sensors are struck. As a result, an event is defined as a collection of AE hits from a single source. Events are generally used for the location of AE source.
- **Signal-Strength:** The "signal-strength" represents the amount of energy emitted by a source or material or structure. It is a direct function of the recorded Acoustic Emission signal's amplitude (dB) and duration.

These characteristics of AE waveform signals received are analysed vis-à-vis damage to characterize damage to localize and quantify the same

2.3.4 AE Signal Analysis

The analysis of detected AE signals is normally done in two ways:

- Waveform Analysis
- Parametric Analysis

Waveform analysis

Waveform analysis is the process of capturing and analysing AE signals in order to identify and localize damage. It records the acoustic signal and calculates the damage depending on the signal's behaviour. This kind of analysis can distinguish between the waveform of an acoustic signal and noise. The disadvantage of using this method is that it necessitates a large amount of data storage, as well as a wait/pause after each waveform to save it, which creates a delay and loss of intermediate data.

Parametric Analysis

The study entails capturing the AE signal in order to generate quantitative and qualitative damage estimates in structures. The rapid recording and data storage speed of this technology makes it superior to waveform analysis. The most commonly used parameters for qualitative damage estimation are AE hits, AE amplitudes and Cumulative Signal Strength.

- C**umulative AE hits** can be used to identify the regions of micro- and macro-cracking. Increase in AE activity corresponds to higher number of AE strikes which are directly associated with a higher crack evolution rate.
- **Cumulative Signal Strength:** It is accumulation of each AE hit's signal strength over time. This curve can be used to identify sudden or unexpected damage in a reinforced concrete structure. The sharp rise in CSS value refers to as ‘Knee’, shows the existence of micro- and major macro cracks in RC structures.
- Acoustic signals of smaller **amplitude values** are indicative of micro-cracks that are usually produced in larger numbers and higher amplitude hits indicate macro-cracks that are produced in small numbers.

In this work, the various AE parameters used for damage estimation and evaluation are AE hits, Amplitude of AE hits, AE X-Y plots etc. for monitoring corrosion in RC beams and further when differently corroded beams are subjected to sustained loading.

A brief review of recent works utilizing AE technique for corrosion monitoring is presented below:

2.3.5 AE for corrosion monitoring – A review

Yoon et al., (2000) explored methods for assessing the damage mechanisms in reinforced concrete using both conventional Acoustic Emission parameter analysis and the wavelet transform method. It was found that AE responses exhibit different characteristics such as amplitude, duration etc. for different failure mechanisms like localized cracking, micro-cracking, flexural cracking, and shear/bond cracking. Both AE event rate and AE generation behaviour signified much different characteristics depending upon the degree of corrosion of reinforcing steel. Also, with an increase in the degree of corrosion there was a reduction in the total cumulative AE events. The results of wavelet transform and frequency spectrum for signals provided useful insight about the relationship between AE generation mechanisms and damage mechanisms of concrete. Conclusively, both AE parameter analysis and AE signal analysis unveiled a positive correlation with the damage mechanisms in reinforced concrete beams

Kawasaki et al., (2010) study the corrosion process in cyclic wet and dry environment. Stage 1 represented initiation of corrosion in which passive layer on the rebar surface was damaged. Very small number of AE events were recorded this stage 1 representing minor damage. Tensile cracks were generated with increase in accelerated corrosion around rebar which later changed to shear cracks. This change was identified as Stage 2 and was detected by sigma analysis in AE monitoring. AE sources were clearly observed as nucleation sites as the cracks developed around the rebar. SiGMA analysis during the corrosion process was in remarkable agreement with location of the cracks on the surface.

Kawasaki et al., (2013) used AE to study corrosion mechanisms in reinforced concrete. Beginning of reinforcement corrosion could be identified by AE parameter of decrease RA value and increase in Average Frequency (AF) with increase in corrosion level. At later stages corrosion induced cracks increases and there was an increase in RA value and decrease in AF values. Fluctuation in ib-value could identify both onset of corrosion and progression of corrosion induced cracking due to corrosion.

Zaki et al. (2015) studied the influence of corrosion on the performance of RC beam during a three-point flexure testing and monitored using AE testing. According to the mass loss of reinforcement, the estimated steel corrosion induced in beam specimen were at 0%, 4.55% and 32.37% respectively. AE data analysis shows distinguishable

trend for RA value and AF values for dissimilar corrosion levels respectively. A Weibull damage function was introduced for the estimation of residual flexural capacity in differently corroded beams. It was observed that with increase in the corrosion levels tensile failure becomes more dominant.

Sharma et al. (2018) investigated the combination of Acoustic Emission (AE) and Ultrasonic Guided Waves (UGW) technique for monitoring propagation of the corrosion in RC structures. RC beams were subjected to anodic corrosion. UGW technique could differentiate pitting and surface corrosion using specific surface and core sensitive modes at later stages of corrosion. During the early stages of corrosion, AE technique is very effective in tracking of initiation and progression of corrosion.

Abouhussien and Hassan (2018) presented an extensive study on the application of acoustic emission monitoring for the estimation of the bond strength of corroded RC beam specimen, which is exposed to the accelerated corrosion. RC beams are corroded to level such that mass loss of steel reached to 5, 10, 20, and 30 %. Beams were constantly monitored via three attached AE sensors at varied distances from the source of damage. This study indicates the effectiveness of AE analysis for the assessment of propagation of corrosion in large scale RC beams at different severity levels of corrosion. The increase in the corrosion induced cracks and the steel mass loss were associated with the AE parameter. At all corrosion levels, increase in the distance of sensor from the source of corrosion results in the decline of cumulative number of hits, signal amplitude values also.

Nair et al. (2019) studied the application of Acoustic Emission (AE) technique for identifying the failure mechanism of a damaged specimen repaired using CFRP was studied. Pattern recognition methods were developed with the use of the AE approach. It was seen that (a) In some specimens, micro-cracks aggregated into a flexure crack. Early on, matrix fractures were seen, which eventually lead to debonding failure. (b) In shear-failure specimens, micro-cracks build into debonding and flexure cracks, eventually leading to shear failure. (c) The specimen collapsed due to mix failure, microcrack accumulation in localised flexure, shear failure, and eventually debonding failure.

Yu et al. (2020) used AE technique to correlate AE characteristics with level of corrosion damage in bar. With the help of Gaussian distribution function a model for

damage distribution in form corrosion was established. This model was based on the normalization of local energy with respect to total energy over the corroded steel bar. The observation from this model were seen to provide more possibilities for the improvement in the health monitoring as well as better structural performance.

Prem et al. (2021) investigated the AE monitoring with combination of mechanical testing for identification of different failure mechanisms (such as flexure, shear-flexure and shear) in RC structures. The major failures (like major cracks & steel yielding etc.) could be observed through transitions in the AE energy Vs deflection curve. The differentiation of the AE energy was done in four stages where yielding of specimens shows maximum activity. Afterwards, maximum AE energy was showed by specimen failed in shear followed by mixed and flexure failed specimens. It was observed that there was an inverse relation in RA and AF values. The study of AE chart shows quantitative and qualitative information about the failure mode identification and damage evolution.

The review of recent works done in the area of AE for corrosion monitoring indicates that it is successful for picking up initiation and progression of corrosion in bars in concrete, various damage levels in concrete by using various AE parameters of AE hits, AE event, ib-value, AE energy etc. The effect of corrosion on bond characteristics of rebars in concrete is also picked up by AE.

In this research effort, it is proposed to use AE technique for monitoring real time corrosion in RC beams along with monitoring when beams corroded to different levels would be subjected to sustained loading.

2.4 INFRARED THERMOGRAPHY (IRT)

2.4.1 General

Thermography can be defined as the science of acquirement and investigation of data from non-contact thermal imaging device. The images taken with an infrared camera determine the distribution of temperature at the surface of the object. If the temperature changes on the surface, it represents defect below the surface such as void, crack etc. Thus infrared technology is the basis of thermography method and can give the data about subsurface structure of a material by observing differences in thermal emission from the surface.

Depending upon the heat transfer thermography methods are divided into **Active** and **Passive thermography**.

- An **active thermography** approach entails the use of an external energy source to increase the temperature of an object which results in transfer of heat in it. Thermal conductivity and diffusivity, density, moisture content, and other physical factors influence the transfer of heat inside the material. As depicted in **Figure 2.6**, If a flaw under the surface has better insulating characteristics than the remainder of the material, it will tend to operate as a heat transmission barrier. As a result, the emissivity of the surface over the greater defect is higher. [120].

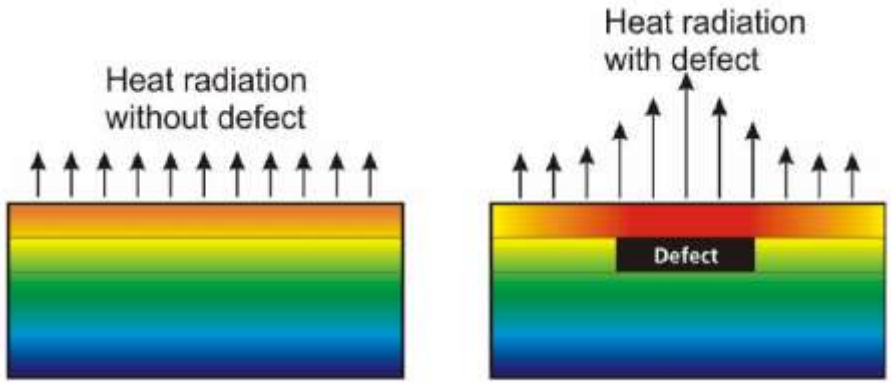

Figure 2.6: Principle of subsurface detection using thermography [121]

- The **passive thermography methods** have no external energy excitation unlike in the case of active thermography. The change in thermal emission of the objects is observed when it placed in colder surroundings with a certain temperature. The example of passive thermography in industrial application is when the material is transferred from high temperature in one process to another where it cools down and this rate of heat transferred is being observed. Difference in surface temperature gives information about the possibility of defects underneath the surface. The area above the defect appears as a cold spot as it act as a barrier to the heat transfer of the core material as compared to undisturbed material [121], [122].

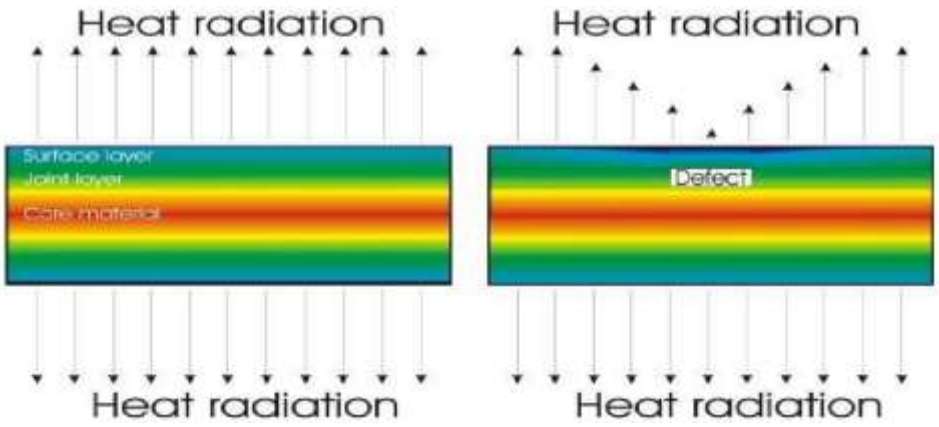

Figure 2.7: Principle of the passive thermography [121]

Active thermography methods are further classified as reflection mode and transmission mode. These classifications are dependent upon the placement of an IR camera and energy source. If both are placed on same side of the test specimen it is classified as reflection mode and if both are placed on opposite sides it is termed as transmission mode. Variants of the active thermography methods are: pulse, step heating, lock-in and vibrio thermography[123].

External energy stimulation, such as electromagnetic radiation or ultrasound, is commonly used to start a heat transfer. Infrared cameras are thermal imaging devices that are sensitive to the infrared component of the thermal radiation, which is a region between visible and microwave radiation in the electromagnetic spectrum, similar to ordinary cameras that produce images using visible light (wavelengths 760 nm - 1 mm). Infrared testing results are generally obtained by picture processing and analysis. A brief of the IRT tools to detect damage in concrete / steel structures is presented below:

2.4.2 IRT setup & Methodology

IRT technique comprises of a heating device and Infrared camera. The concrete sample under observation is subjected to heat by an external source. The rise and fall in surface temperature of the specimen is continuously monitored using IRT camera (**Figure 2.8**). The difference in heat transfer as a result of any defect, discontinuity, damage etc. is recorded and is represented by variation in colors in thermograms. The same data recorded is transferred and processed in computer for further classification. This variation in surface temperature helps in identifying the damage area in a clear

pictorial view. Section 2.4.3 presents a brief review of some latest works done in concrete structures.

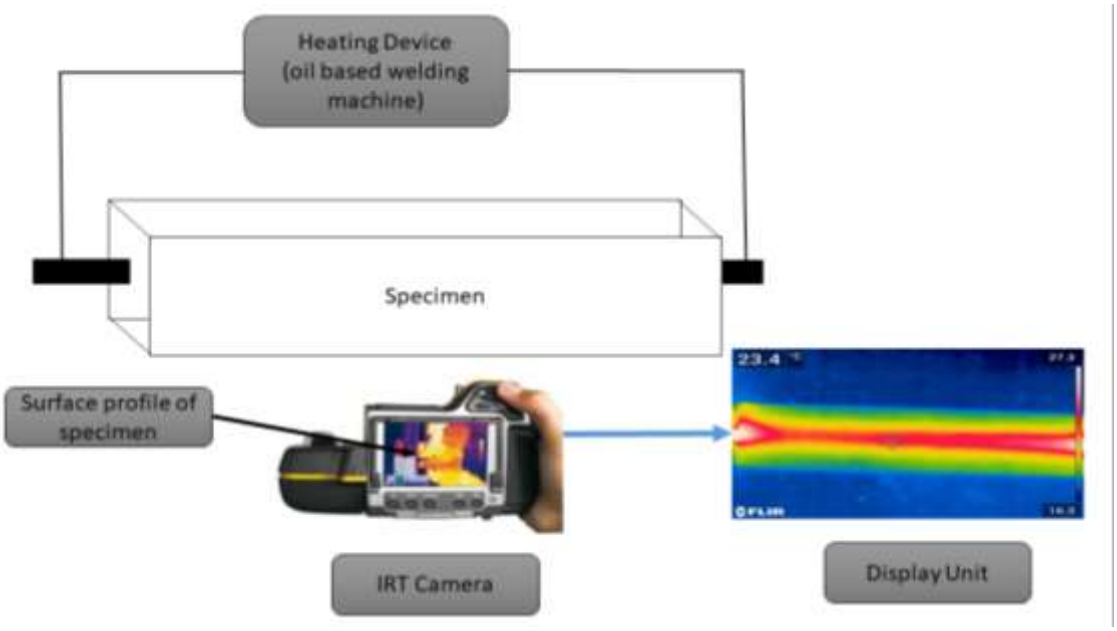

Figure 2.8 Schematic illustration of IRT Process

2.4.3 IRT for monitoring RC structure- A Review

Chung et al. (2006) used Infrared Thermographic technique to measure corrosion in reinforcing bar. The intention of this study was to develop a new technique to determine the level of rebar corrosion using accumulated thermal data. Heating rate of rebar rose with anticipated higher level of corrosion which shows corrosion of steel has negative impact on infrared emission. Thermal data was collected using an infrared camera and processed to discern between different levels of rebar corrosion. The results of the tests revealed that the higher the amount of corrosion, greater is the temperature.

Lai et al. (2010) used quantitative infrared thermography for identification of the deterioration of externally bonded CFRP-concrete composites. Flaws and delamination are two different forms of defects in FRP wrapped structures. Flaws emerge during the first application of the CFRP strips onto the concrete surface as a result of poor craftsmanship, and delamination occur as a result of stress concentrations caused by chemical/physical deterioration of the binding layer.

Aggelis et al. (2010) studied subsurface cracks in concrete using a combination of infrared thermography and ultrasonic Rayleigh waves techniques. In this study, the

concrete specimens were scanned using an infrared camera to point out position of the crack. Simultaneously, ultrasonic sensors were placed on the specified part of the surface in order to make a more comprehensive estimation of the depth of the crack. The combination of these two NDT techniques seemed to be promising for real life structures assessment.

Baek et al. (2012) proposed an integrated system of infrared thermography and heat induction for observation of corrosion in rebars in RC structures. The heating rate as well as cooling rate and the peak IR intensity rose with rise in extent of corrosion due to change in electrical resistivity on the steel surface with increase in corrosion. The author reported that the efficiency of induction heating decreased with increase in cover depth as it took more time for heat to reach the concrete surface from rebar. The relationship between heating or cooling rate and the amount of corrosion was difficult to find out.

Milovanović and Banjad Pečur (2016) used infrared thermographic technique to illustrate and identify faults in reinforced concrete. The author concluded that infrared thermography has a number of advantages, including the ability to reduce the time required to inspect a concrete structure because the defected area can be identified immediately as compared to the sound test which requires the structure to be inspected at multiple locations. Post-processing approaches improve flaw identification and reduce susceptibility to non-uniform heating, imperfections, and colour differences on the surface. For increased precision and dependability, it has been proposed that infrared thermography can be used in conjunction with other non-destructive methods.

Janku et al. (2019) assessed corrosion in rebar using combination of infrared thermography (IRT) and non-destructive ground penetrating radar (GPR) methodology. GPR identified corroded bars, detachment and voids beneath separate concrete, as well as areas having higher moisture and mineral salts content. The joint analysis of both GPR and IRT data established the independent interpretation provided, which allowed for a better understanding of the behaviour of the GPR signals.

The review of recent works done in the area of IRT for corrosion monitoring indicates that it is successful for picking up damage, corrosion and delamination in RC concrete. The variation in surface temperature immediately identify the damage beneath the surface and it was also concluded that efficiency of induced heating

decreases with increase in cover depth. The intensity of corrosion of rebars in concrete is also picked up by IRT as higher rate of corrosion anticipates higher surface temperature. In this research, it is proposed to use IRT technique for monitoring simulated damages in concrete beams as well as for real time corrosion monitoring in RC beams.

2.5 VIBRATION MONITORING TECHNIQUE

2.5.1 General

Crack initiation and propagation can occur at loads much lower than those required for actual structural failure; early stages can be detected by means of visual inspection and other traditional methods. Vibration measurements, on the other hand, are thought to be sensitive enough to detect and track damage even when cracks are deep inside a structure. For structural health monitoring, a variety of vibration-based parameters have been used. The fundamental principle behind this technology is that modal parameters, such as frequencies, mode shapes, and modal damping, are a function of the structure's physical properties, such as mass, damping, and stiffness of the structure. As a result, changes in the physical properties can result in measurable changes in modal parameters. Previous researches have shown that damage can be detected in structures using modal analysis and characterisation of damage can be done by investigating changes in various modal parameters like:

(1) Modal Frequencies

(2) Mode Shapes

(3) Amplitude of Signals like FRF amplitudes

(4) Curvature

(5) Modal Damping Characteristics

2.5.2 Test Setup and Methodology

Vibration monitoring setup includes instrumented force hammer that is connected to the force input channel, accelerometers and data analysers like FFT analyzer. Generally, the hammer is connected to the force channel of FFT analyzer gives power to an integrated circuit piezoelectric (ICP). The frequency excited into the system by

the impact hammer is recorded by the accelerometer. Each accelerometer is connected to the input channel of the FFT analyzer. The response data received by the FFT analyzer is recorded on a computer as Frequency Response Function (FRF) (**Figure 2.9**). The various components of a typical vibration test set up consists of following:

- **Impact hammer**

The vibration response is measured by performing impact testing on the structure. The impact excitation is applied by an impact hammer having a hard rubber impact tip which is swung from a horizontal distance of approximately 50 mm from the specimen. The amplitude and frequency of forced impulse is directly associated with the material of hard rubber tip, size and length of hammer. The impact consisted of a nearly constant force over a broad frequency range and was capable of exciting all resonances in that range by changing the impact tip of different mass.

- **Accelerometer**

Accelerometers are made of piezoelectric material which produces an electric charge when exposed to forced vibration. These forced vibrations are recorded and transmitted to FFT analyzer for further monitoring. In order to allow reasonable resolution at all times, data signal for each accelerometer is recorded at several sensitivity levels over the exponentially decaying vibration signal. To mount the accelerometer to the surface of the test specimen, high strength cement plaster is used specifically for monitoring concrete structures.

- **FFT Analyzer**

Spectrum analysis is defined as the transformation of a signal from a time-domain representation into a frequency-domain representation. There are four forms of the Fourier Transforms which are generally used.

a) Fourier Series
b) Fourier Integral Transform
c) Discrete Fourier Transform (DFT)
d) Fast Fourier Transform (FFT)

The time domain signal obtained from vibration monitoring was subjected to FFT to get FRF (frequency response function). Normally a software performs this and it is displayed as FRF. Comparison of FRF plot at different stages of damage indicates

the level of damage. A brief review of recent works done in the area of global vibration monitoring technique is presented below.

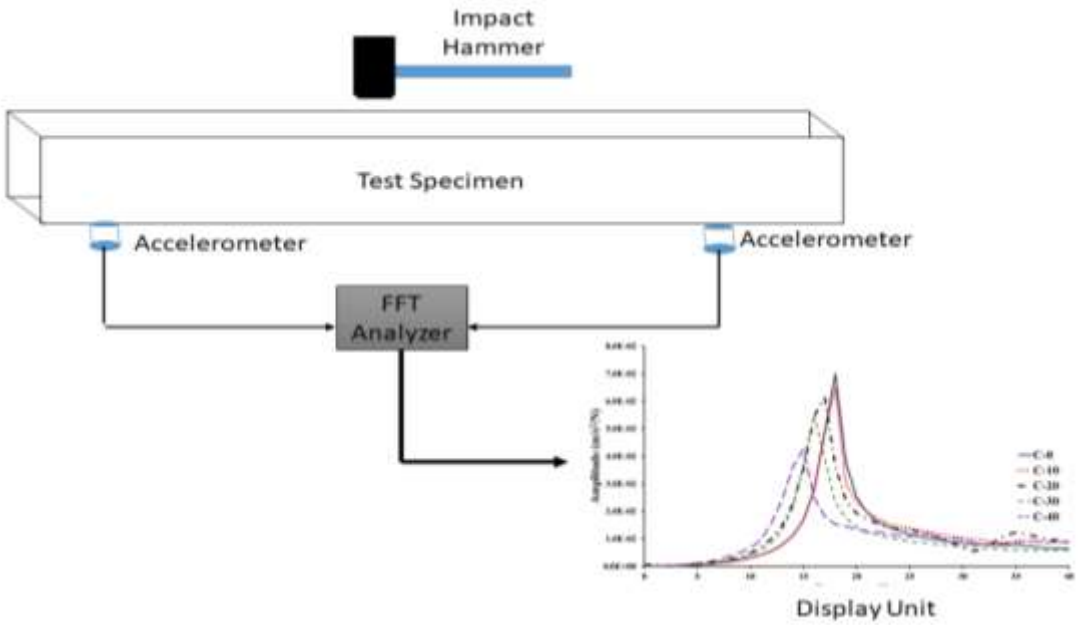

Figure 2.9 Schematic illustration of Vibration monitoring

2.5.3 Vibration Monitoring in RC structures- A Review

Razak and Choi (2001) studied the effect of general corrosion on the modal parameters of reinforced concrete beams. The full scale beams were corroded until a substantial amount of reinforcement corrosion damage was introduced. The measurement of crack width and spalling was performed to assess the states of damages in the test beams. As per the results obtained, the modal parameters especially natural frequencies and damping ratio showed significant change. Also, the changes in modal damping ratio for the transfer function method and the normal mode method were observed. Additionally, the static load test was used to determine the load carrying capacity and the results were correlated with the changes in the modal parameters. The study offers further understandings on the application of modal parameters for damage detection in structural concrete elements which can be helpful for the structural appraisal and assessment purposes when applied to full scale structures.

Burgueno et al. (2001) dynamic characteristics of a full-scale FRP composite bridge prototype investigated the Kings Storm Water Channel Bridge. They discovered that modal vibration studies were an efficient, cost-effective, and fast method of determining dynamic structural properties. Change in structural behaviour due to

changes in boundary conditions, as well as structural damage caused by loading, were successfully determined using the modal vibration test results when compared with healthy non-destructive health monitoring system.

Maia et al., (2003) analysed the possibility of using various damage detection methods without the requirement for modal identification. It was found that the damaged locations were identified where the change in mode shape was greatest. Also, the use of direct measurement in the form of frequency response function found to be considerably beneficial. The false damage location is although an issue in the methods and needs close attention. The author suggested that some improvements could be made in the interpolation process, in defining a noise level under which the results are not considered, in the method to calculate the maximum occurrences, in applying statistics to the results and, finally, in the set-up and skill of the experimentalist.

Kao and Hung (2003) proposed a method, consisting of two stages. The first stage, System Identification, involves identifying the damaged and undamaged states of a structure using neural networks. The damage detection phase employing neural networks to produce free vibration responses with the same initial state constitutes the second stage. The inputs in neural networks are typically structural responses in the time or frequency domain, or structural modal parameters (frequency, damping ratio, and mode shape), and the outputs are usually damage levels in the structures. The author demonstrated that changes in structural properties of stiffness and damping results in changes in the free vibration amplitudes. As a result, the intervals and amplitudes of free vibration are helpful indices for detecting structural changes.

Baghiee et al. (2009) studied the changes in the dynamic parameters in specimens undergoing gradual damage and further when they are CFRP repaired from initial to failure state. The efficiency of the methods like frequency changes, modal assurance criterion (MAC), Coordinate Modal Assurance Criterion (COMAC) and modal curvatures was also investigated. Author concluded that frequency change method was not effective for damage detection and prediction of strength. The MAC values could predict the overall change in the stiffness of the beam due to damage. Whereas COMAC evaluates the change of stiffness at each degree of freedom of beams. It was concluded that the damage classification of the specimens was best described by modal curvature method.

Prasad et al., (2010) examined the changes occurred in the modal parameters in response to the damage induced to the beams by cyclic loading. The dynamic characteristics were related to the damage pattern of the structures for the purpose of damage assessment. With the increase in the damage level on the beams, Natural Frequency decreased and damping values increased. Furthermore, the Natural frequency displayed more percentage drop in the over-reinforced beam than under-reinforced beam.

Ede et al. (2015) used modal based parameter to assess damage in reinforced concrete beam under four-point static loading. Dynamic test was done to identify the degree of stiffness degradation after each static loading. The result obtained during the investigation showed that dynamic based assessment method was good in monitoring damage evaluation and stiffness degradation of structural element in RC beams under static loading.

R. Capozucca (2018) investigated the behaviour of undamaged and damaged reinforced concrete beams with dissimilar end conditions. The beams were strengthened using near surface mounted glass fibre reinforced polymers. Damage was achieved by developing cracks under bending in one beam and by artificial notches in remaining beams. Dynamic experimental tests were performed for development of Frequency Response Functions (FRFs) and the variations in natural frequencies were correlated to the degree of damage. Finally, modelling of undamaged and damaged with notches beams was done using finite element method. Only 10% maximum difference was observed between theoretical frequencies and experimental frequencies in both the cases. In strengthened beams; the damage was limited with small variation in frequencies even for greater values of bending moments.

Kırlangıç (2020) investigated a nonlinear vibration based diagnostic technique to measure the magnitudes of the corrosion-induced damage in the reinforced concrete. The developed method utilizes an adaptive higher order spectral analysis, which included wavelet transform in place of the Fourier transform, with the aim to suit the transit vibration signals produced under an impact hammer. It was found that the wavelet transform-based bicoherence (WTB) generated from the damaged and undamaged cases are well separated from each other compared to the Fourier transform-based bicoherence (FTB). The WTB features showed less variation than the

FTBs. The implementation of the wavelet transforms in the bispectral analysis improved the bicoherence sensitivity to damage by decreasing the variation in the extracted features.

Pourrastegar et al. (2021) investigated damage in RC slabs using vibration testing using random decrement signal processing techniques and fibre-optics. The test was conducted in two stages: first stage focussed on the identification of damage and second stage focussed on identifying damage intensity through change in frequency and damping dynamic parameters. Accurate evaluation of damage location through change in the first mode shape could be done by a damage recognition multi-channel random decrement (MCRD) technique, and using an embedded smart network of fibre optic sensors.

From the literature review, it can be summarized that damage initiation and progression in RC structures leads to modification in modal characteristics of RC structures in the form of shift in frequency and change in amplitude of signal. Hence, this technique can be successfully used to relate to corrosion damage with simultaneous loading in RC structures.

2.6 CLOSING REMARKS

The chapter focusses on the basics of various damage monitoring methodologies adopted for RC structures which are utilized further to assess corrosion induced damage in concrete structures in this thesis and also for monitoring GFRP repaired corroded beams subjected to sustained loading. Various NDT tools described along with their state of art (review) are local Acoustic Emission (AE), Ultrasonic Guided Wave (UGW), Infrared Thermography (IRT) and global Vibration Monitoring Technique.

CHAPTER 3

EXPEIMENTAL DETAILS AND METHODOLOGY

3.1 GENERAL

In this research effort, the work is subdivided according to the three outlined objectives. First study deals with the monitoring of bars in air and concrete involving simulated corrosion damages using advanced NDT techniques of UGW and IRT. Further, continuous monitoring of RC beams subjected to accelerated corrosion was done using local techniques AE, UGW and IRT. Second study deals with the monitoring of real sized RC beams subjected to varying level of corrosion damage using global vibration monitoring technique. Further the corroded and GFRP repaired corroded were subjected to flexural loading to assess their mechanical behaviour and performance using various load–deflection characteristics such as change in ultimate deflection, load, energy etc. These RC beams were also monitored simultaneously using AE during flexural testing by surface mounted AE sensors and their damage and fracture was assessed using various AE parameters like AE hits, amplitude of AE hits and damage localization using AE X-Y event plots.

3.2 MONITORING REAL TIME ACELERATED CORROSION

In this study bars with simulated corrosion damage representing pitting and delamination were prepared and then cast in concrete and were monitored using advanced NDT tools of UGW, IRT and AE. Further, continuous monitoring of RC beams subjected to varying level of corrosion damage was done using these NDT tools and the results were compared with simulated damaged beams.

3.2.1 Specimen Details

For developing real time corrosion monitoring methodology for RC structures, corrosion was first simulated as pitting / area reduction damage and debond and monitored using UGW and IRT. Further concrete beams with embedded rebars was subjected to actual corrosion and corrosion initiation and progression was monitored using UGW, AE and IRT technique. It is important to note that AE monitoring was not done for simulated corrosion damage samples since it is an active technique which only monitors damage while the dislocation, cracking or damage is taking place.

For this purpose, two type of samples were prepared for simulating corrosion damage in the form of area reduction / pitting (Simulated Damage 1, **Table 3.1**) and increasing debonding simulating delamination of bars from surrounding concrete were prepared (Simulated Damage 2, **Table 3.2**). Plain Mild Steel (MS) bars of 12 mm diameter and 500 mm length were used in the study. Bars with Simulated Damage 1 (pitting) as in **Table 3.1** had reducing diameter of 10 mm, 8 mm, 6 mm and 4 mm in a constant length of 50 mm in the middle of each rebars (**Figure 3.1 b**). Bas with Simulated Damage 2 (representing de-bonding) had increasing debond length of 50 mm, 75 mm, 100 mm and 125 mm in the middle of bars with a constant diameter of 10 mm (**Table 3.2 and Figure 3.1 a**). Three samples of each type of bars with simulated damages were prepared. A total of 24 concrete beams were prepared for the study (**Table 3.1 and 3.2**).

First the Mild Steel (MS) samples with simulated damages were tested without concrete in air using Ultrasonic Guided Wave (UGW) and Infra-Red Thermography (IRT). Then they were embedded in concrete and subjected to UGW and IRT monitoring. Further, 4 rebar samples of plain MS of 12 mm diameter were cast in concrete and subjected to accelerated impressed current corrosion to varying degrees of corrosion (Section 3.2.2). For this purpose, beams of size 80×80×400mm with the MS bar of length 500 mm were placed in the center of the cross section of beam were cast (**Figure 3.1 c**). Ordinary Portland Cement (53 grade), aggregates of size not more than 20mm, river sand, portable tap water with mix proportions of 1:1.4:2.7 (cement/sand/aggregates) and water cement ratio of 0.45 was used for casting of beam [136]. The average characteristic compressive strength of the concrete mix prepared was obtained as 28.5N/mm^2.

Table 3.1: Nomenclature of rebar's having Simulated (Pitting) Damage

Nomenclature of specimens	Sample details	Number of samples
D10	Bars with reduced diameter of 10 mm tested in air	3
D8	Bars with reduced diameter of 8 mm tested in air	3
D6	Bars with reduced diameter of 6 mm tested in air	3
D4	Bars with reduced diameter of 4 mm tested in air	3
CD-10	Bars with reduced diameter of 10 mm cast in concrete	3

CD-8	Bars with reduced diameter of 8 mm cast in concrete	3
CD-6	Bars with reduced diameter of 6 mm cast in concrete	3
CD-4	Bars with reduced diameter of 4 mm cast in concrete	3

Table 3.2: Nomenclature of the rebar's having Simulated (De-bond) Damage

Nomenclature of specimens	Sample details	Number of samples
L-50	Bars with increasing debond length of 50 mm tested in air	3
L-75	Bars with increasing debond length of 75 mm tested in air	3
L-100	Bars with increasing debond length of 100 mm tested in air	3
L-125	Bars with increasing debond length of 125 mm tested in air	3
CL-50	Bars with increasing debond length of 50 mm cast in concrete	3
CL-75	Bars with increasing debond length of 75 mm cast in concrete	3
CL-100	Bars with increasing debond length of 100 mm cast in concrete	3
CL-125	Bars with increasing debond length of 125 mm cast in concrete	3

(a) Simulated Damage 1 (Change in Diameter)

(b) Simulated Damage 2 (Change in Length)

(c) Concrete Beam

Figure 3.1: Rebars with simulated damages

3.2.2 Inducing Accelerated Corrosion and Methodology

Concrete beams with embedded rebars were subjected to accelerated impressed current corrosion using a constant voltage power supply (Aplab Dual DC Power Supply 64V,05A). For accelerating corrosion beam samples (80x80x400 mm) were wrapped with cotton gauge all around in the middle 100 mm length and stainless steel wire mesh was wrapped around it to create cathode and connecting to the negative terminal of the power supply. A constant 20V power was supplied throughout the experiment and to maintain conductivity continuous supply of 3.5% NaCl solution was maintained by drip arrangement in the middle portion of the beam. One end of the rebar was exposed at the end by 50 mm was connected to the positive terminal of the power supply to act as anode (**Figure 3.2**).

During corrosion UGW readings were taken every 24 hours along with continuous AE monitoring. Concrete was subjected to corrosion till UGW signature vanishes in 33 days. Further 3 different stages / levels of corrosion were identified and three more beams were subjected to 8, 19 and 26 days of corrosion. Corrosion current, UGW signal strength and AE signal were continuously monitored for all samples (S-8, S-19, S-26 and S-33) (**Table 3.3**). After corrosion to specified days, the corroded beams were visually inspected and further subjected to IRT monitoring. Lastly the corroded bars were removed from concrete for quantitative analysis of level of corrosion by checking the mass loss and residual tensile strength to relate to the effect of corrosion on non-destructive testing parameters.

Table 3.3: Nomenclature of samples subjected to accelerated corrosion

Corrosion Exposure	Nomenclature	No. of concrete beam samples
8 Days	S8	3
19 Days	S19	3
26 Days	S26	3
33 Days	S33	3

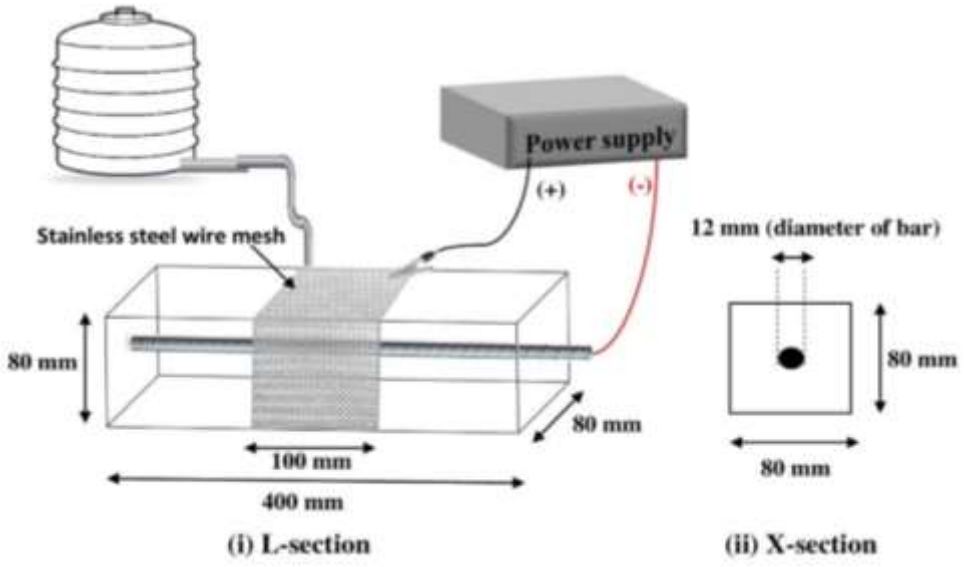

(a) Schematic of corrosion set up

(b) Actual corrosion set up

Figure 3.2. Accelerated impressed current corrosion set up

3.2.3 Ultrasonic Testing Set up Used

In this study, a standard ultrasonic research device is used to excite longitudinal guided waves in bars. A pulser/receiver system (DPR 500, JSR Make) (**Figure 3.3 b**), cylindrical transducers (Karl Deutsch Make) (**Figure 3.3 a**), and display devices were used. The compression transducer, which is operated by the pulser, produces an ultrasonic pulse that passes through the bar in the form of longitudinal waves. There are generally two modes of ultrasonic testing - Pulse Echo and Pulse Transmission. In the Pulse-Echo method, a single touch transducer is used to produce and obtain wave signatures while in the pulse transmission mode, two contact transducers are used – one to transmit the signal called transmitter and the other to receive the waveforms called receiver. In this study, pulse transmission is used for propagating guided waves through bars in air as well in concrete. The transducers with a central frequency of 1 MHz were used to produce longitudinal guided wave modes through bars in air as well as through bars embedded in concrete. L(0,7) mode at 1 MHz which is the least attenuative and easiest to excite, being a longitudinal mode is used for testing. The choice of a particular frequency and mode for UGW monitoring is based on previous studies [22], [39], [42], [108], [109], [137] and further detailed in Section 2.3.4.

Further, as explained 12mm bars embedded in concrete were also subjected to accelerated corrosion for 8, 19, 26 and 33 days. The corrosion monitoring of these bars in concrete was carried out using same L(0,7) mode at a frequency of 1 MHz for ultrasonic testing. L(0,7) mode is a core seeking mode and is sensitive to pitting [108]. A Pulser/Receiver combination with a specific gain (0-66dB) and a maximum input voltage of 475 V drives the transducers. The obtained signal is captured and processed using a computer digitizer card (Acquiris Make- 12 Bit resolution). Also, an industrial coupling gel is used to bind the transducer to the specimens, and is placed in a tray. Afterwards, a compressive spike pulse with a length of 10-70 ns acts as the excitation signal. The obtained signals are further analysed using ORIGIN software and each waveform received is plotted. From the waveforms, the peak amplitude values are normalised with respect to healthy amplitude to plot.

Hence it is important to note that guided waves are propagated and monitored through rebars and not in concrete. The transmitted signal strength through the bars

reduces as the bars undergo deterioration due to corrosion. Fall in signal strength is quantitative indicator of extent of the corrosion.

(a) Transducer (S12 HB 1) (12 mm diameter) of 1 MHz frequency

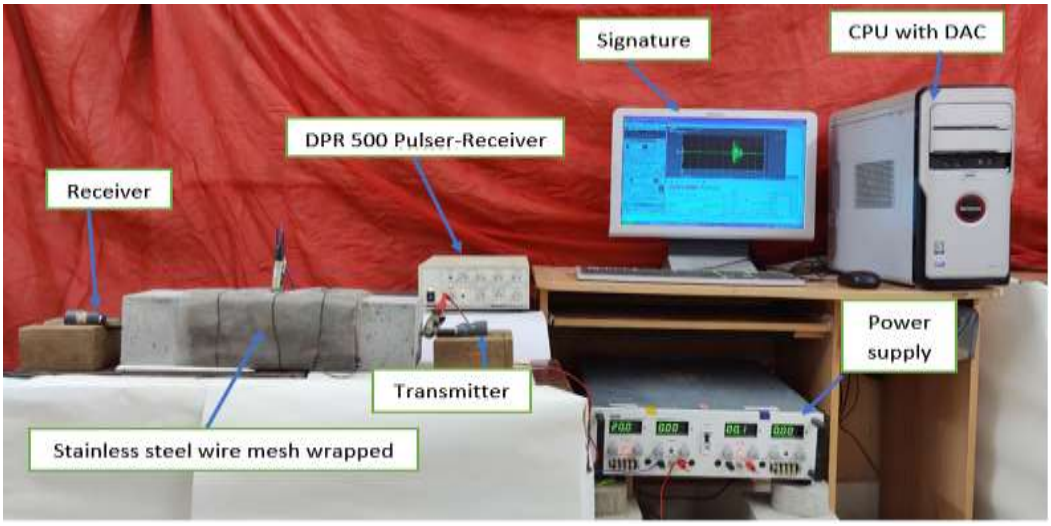

(b) Ultrasonic Guided Wave Set-up

Figure. 3.3 Experimental Set up

3.2.4 Infra-Red Thermography (IRT) Monitoring and Details

IRT is the non-destructive technique which is very useful for the visual analysis of the corroded samples since it requires no physical contact with the structure. All the objects in the proportion to their surface temperature emits infrared radiations which can be read and analysed by IRT.

3.2.4.1 IRT Set-up

Infrared thermo-imager with spectral range of 7.5 to 13 µm (FLIR T360 Prism DS) was used for capturing IRT images. It had an infrared resolution of 464 x 348 pixels

with temperature range of -20°C to +120°C (**Figure 3.4 a**). In this work it IS proposed to use infrared thermography for monitoring real time corrosion as well as simulated corrosion damage in concrete along with combination of AE and UGW. First the samples were heated using a source of heat (Welding machine used) within temperature range of 20-200°C. The IR camera was placed at the constant distance of 1.6m from the samples to take IRT images at regular intervals as the beams were subjected to increasing damage (**Figure 3.4 b**). First the IRT images of bars with simulated damage in air were taken, then they were cast in concrete and IRT images were again taken. For beams subjected to corrosion IRT images were taken for thermal wave inspection and analysed after corrosion for 8, 19, 26 and 33 days (S8, S19, S26 & S33).

(a) FLIR T-540 used in study

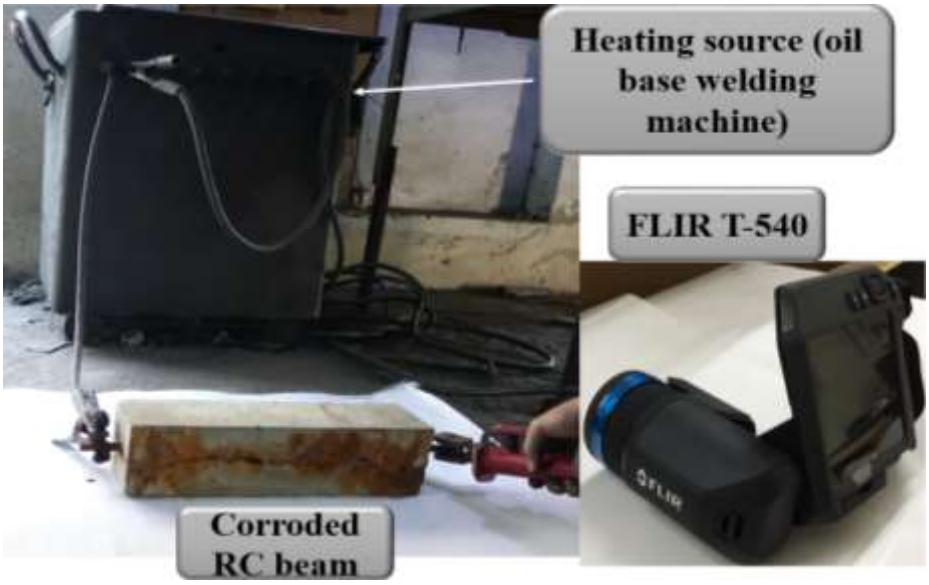

(b) IRT set up

Figure 3.4: IRT setup used

IRT works on the principle that every material has different heat conducting properties and reduced area of steel gets heated at a faster rate as compared to its surrounding. Thus these material properties are used to detect damage beneath the concrete surface. Rebars with simulated damage 1 and 2 were cast in concrete and monitored using IRT showed high intensity color at the middle portion representing the severity of damage. Similarly, for corroded sample, rust induces higher temperature as compared to the parent steel thus high temperature difference and different color patches were observed representing the intensity of corrosion.

3.2.5 Acoustic Emission Monitoring

In this study, AE monitoring was only resorted for beams undergoing actual corrosion for varying days and levels (S8, S19, S26 and S33). For this, 8 channel AE data acquisition system (SAMOS Micro-II digital, Physical Acoustics, USA) along with AE sensors and pre-amplifiers was used. Any deformation or damage in the form of micro or macro cracks produces waveforms which are recorded by surface mounted AE sensors. All the AE sensors are mounted using coupling gel and tape to hold sensors in their passion and to avoid any gap between the AE sensor surface and specimen.

In our study six AE sensors (R3α) (**Figure 3.6 a**) with a resonant frequency of 30 kHz, three on the front face and three on back face forming the triangular pattern were surface mounted on concrete beams (80 x 80 x 400 mm size) (**Figure 3.5**). The signal recorded by the sensors is very weak to study thus it is amplified using pre-amplifier (**Figure 3.6 b**). The amplified signal is then transferred to Micro digital acquisition system (**Figure 3.6 c**) and with the help of AE Win software and AE data is further extracted in the form of amplitude, signal energy, signal strength, duration, count, rise time etc. to relate to the progression of damage. The characteristics of damage source, distance of the source from AE sensor, characteristics of AE sensors etc. are the prime aspects effecting the recording of AE signals.

AE waveform received comprises of various AE parameters such as cumulative AE hits their amplitudes, signal strength and signal energy **(Figure 3.7)**. Initiation and progression of cracks releases energy which are recorded by the surface mounted sensors in the form of signals are known as **AE hits**. The energy released due to cracking is represented by the area under the AE waveform (**signal energy**) and the number of AE signals which crosses the threshold limit is known as **AE counts**. The

crest of the AE waveform which is influenced by the source and type of crack is termed as AE signal amplitude and the duration for which the waveform is above the threshold is known as **duration of AE signal (Figure 3.7)**.

In this study, cumulative AE hits and their amplitude along with pictorial AE X-Y event plots for damage localization have been used to relate the corrosion damage. AE X-Y plots will provide pictorial representation of cracking beneath the concrete surface, which help us to understand the progression of damage inside concrete. Hence, it is expected that change in AE parameters with corrosion damage will lead to quantitative assessment of corrosion. The flow chart for the methodology followed for objective 1 real time corrosion monitoring is detailed in **Figure 3.8.**

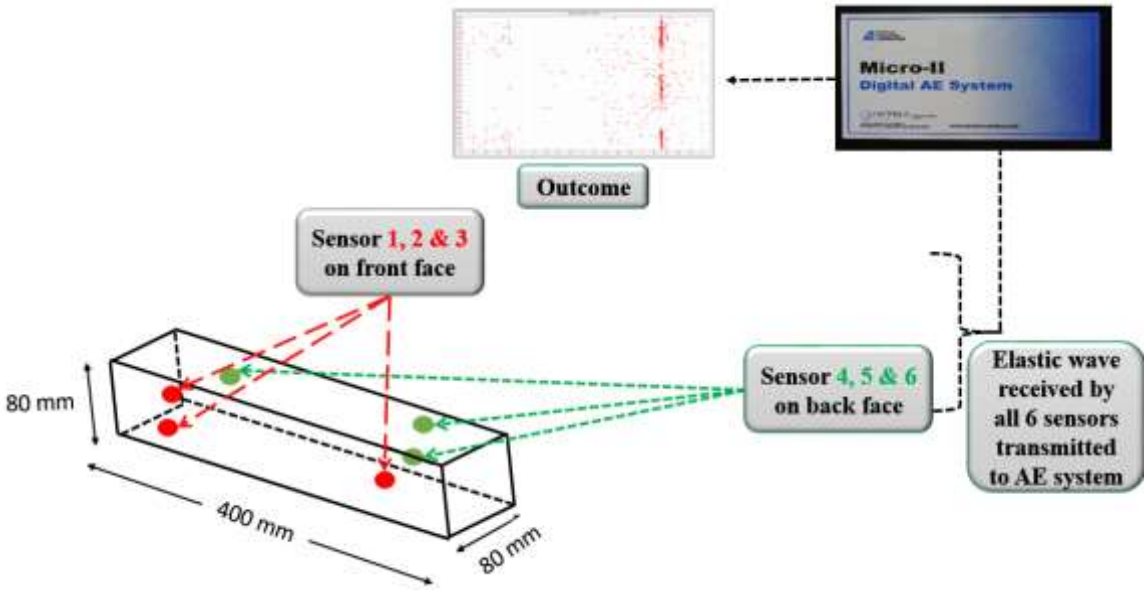

Figure 3.5: Schematic of AE setup

(a) R3α Sensors used

(b) Pre-amplifier

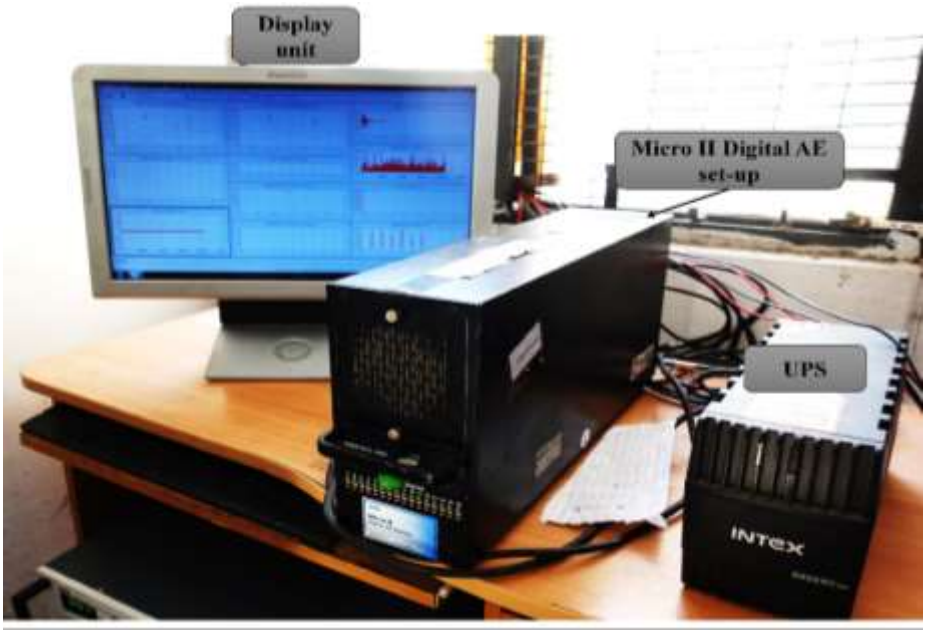

(c) Actual Set-up

Figure 3.6: Actual Acoustic emission monitoring set-up used in the study

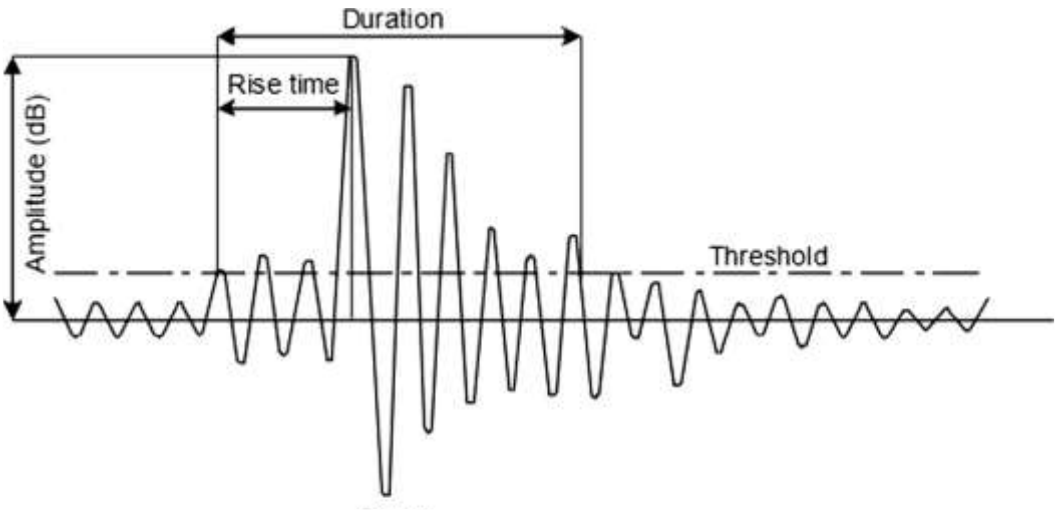

Figure 3.7. Characteristic of a burst type of AE signal [138]

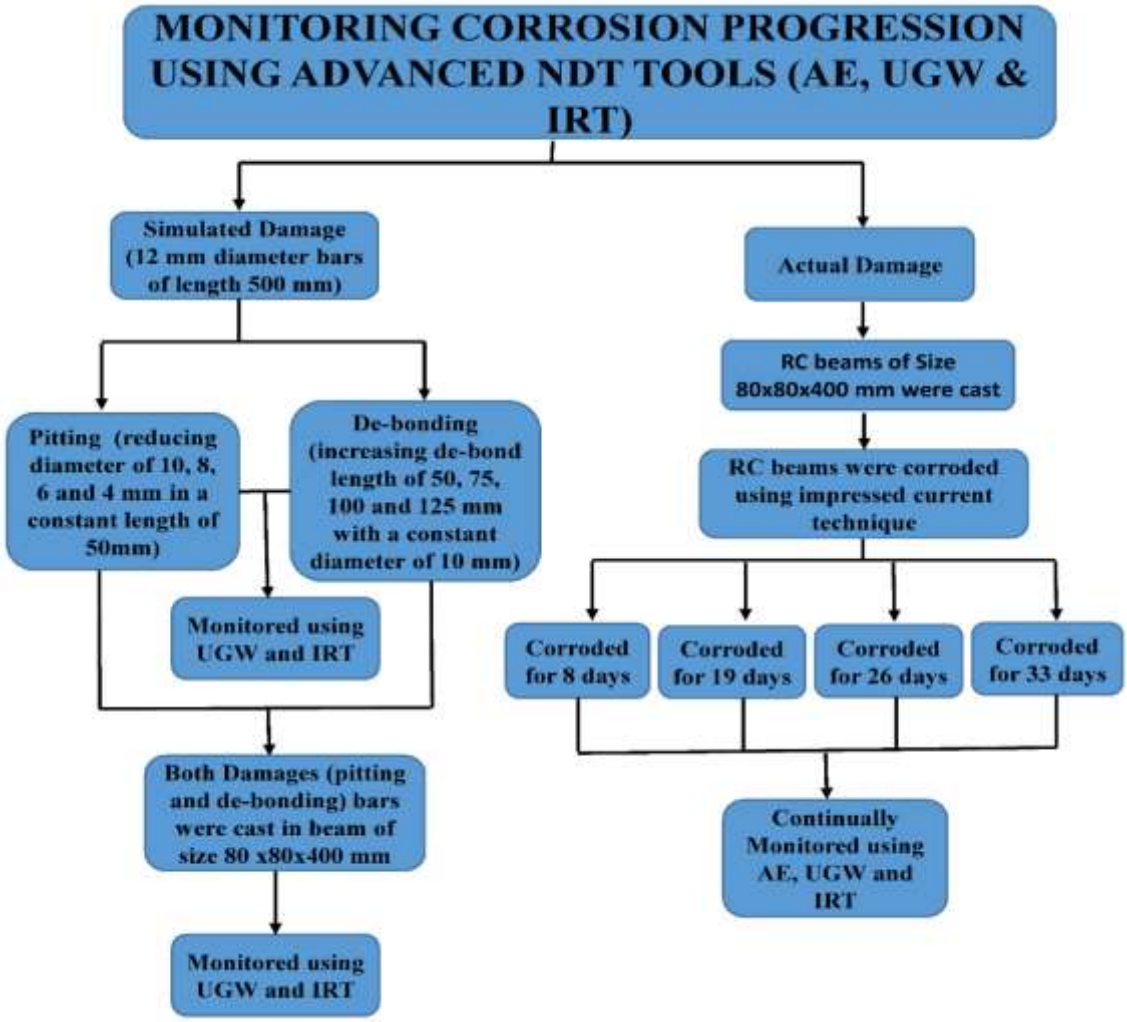

Figure: 3.8 Flow chart for monitoring real time corrosion

3.3 MONITORING CORRODED AND GFRP REPAIRED CORRODED RC BEAMS USING VIBRATION MONITORING

In this study, real sized RC beams were subjected to varying level of corrosion and were repaired using GFRP sheets wraps. The corroded and corrosion repaired RC beams were monitored using vibration monitoring technique and finally tested under flexural loading along with simultaneous AE monitoring.

3.3.1 Specimen Details

Ten identical RC beams measuring127 x 227x 4100 mm were cast for this study. The beams were designed as under reinforced sections using design mix proportions of 1:1.4:2.7 (cement: sand: aggregate proportions by volume) and water: cement ratio (w/c) of 0.46. The average 28 days compressive strength of the concrete used for casting

of RC beams was observed as 28.5 MPa. The reinforcement details of the RC beams cast in the study is shown in Figure 3.9. They comprise of two bars of 10 mm ϕ bars on the tensile face and two bars of 8 mm ϕ at on compression face. 6 mm ϕ diameter bars at a centre to centre spacing of 150 mm was used as shear reinforcement.

Eight out of ten RC beams were corroded to different levels for 10, 20, 30 and 40 days with 2 samples of each using impressed current chloride induced corrosion at a constant voltage of 10 V. two beams are used as control beams (C-0) with no corrosion. The other beams are named as given in Table 3.4 (C-10, C-20, C-30 & C-40). One sample of each C-10, C-20, C-30 and C-40 beams was further repaired against corrosion by micro-concreting and GFRP wrapping as detailed below in Section 3.3.4. The control beam along with corroded and GFRP repaired corroded beams were evaluated using vibration monitoring to observe the variation in dynamic parameters with increasing corrosion damage and their subsequent repair. Further, all the corroded RC beams (Set 1) and corrosion repaired RC beams (Set 2) were further then subjected to flexural testing in four-point bending to record the load deflection characteristics and to relate to the NDT vibration parameters.

Table 3.4. Nomenclature of specimens

Specimen	**Details (corroded at constant voltage)**
C-0	Control
C-10	Corroded for 10 days
C-20	Corroded for 20 days
C-30	Corroded for 30 days
C-40	Corroded for 40 days
R-10	C-10 repaired with GFRP
R-20	C-20 repaired with GFRP
R-30	C-30 repaired with GFRP
R-40	C-40 repaired with GFRP

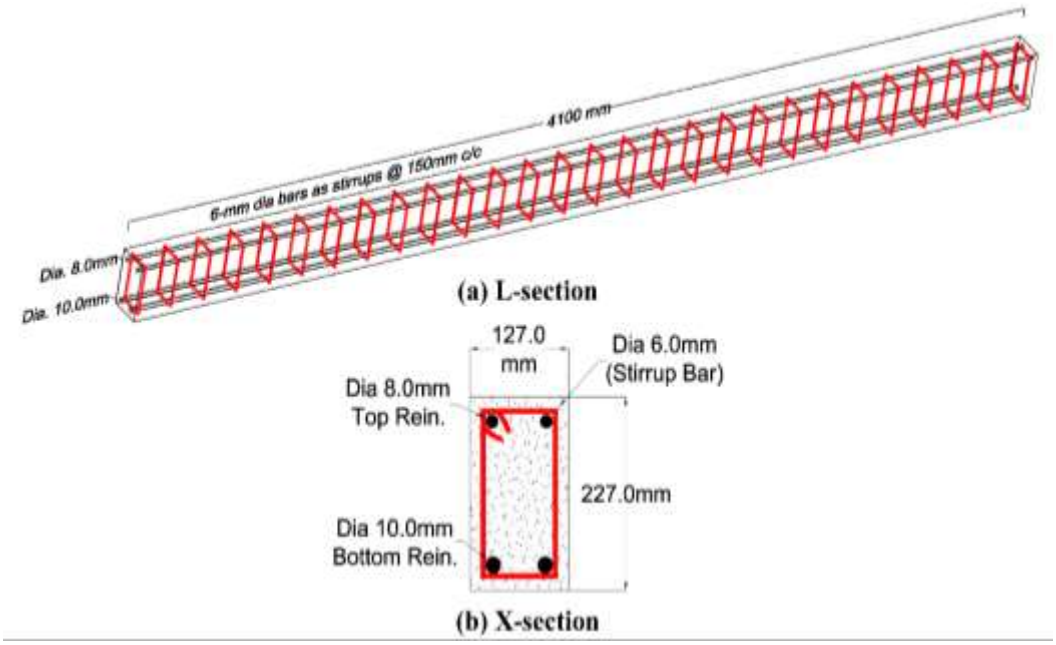

Figure 3.9. Longitudinal and X-section details of RC beams cast

3.3.2 Vibration Measurement Set-Up

Vibration monitoring is executed by exciting the specimen through impact hammer which generates a signal, which is observed by an accelerometer placed at the opposite face of the specimen. This signal is further transferred to dual channel signal Fast Fourier Transform (FFT) Analyzer, where refining and simplification of the signal take places before displaying the Frequency Response Function (FRF) representing the relation between frequency and amplitude. Vibration monitoring technique does not interfere with the service of the structure, thus making it user-friendly [67], [139]–[141]. Fall in the FRF amplitude and shift in the modal frequencies are related to damage level in structures.

As per authors' knowledge, no study has been carried out for assessing the dynamic properties of GFRP repaired corroded RC beams using global vibration monitoring technique. In this study, behaviour and change in dynamic properties of natural frequency and amplitude of the received FRF signals is investigated to relate to corrosion induced damage in RC beams and further when the corroded beams are repaired with GFRP. For this, a hard rubber tip impact hammer (PCB 20135, OROS make) with a sensitivity of 0.00225 V/N (**Figure 3.10 b**) was dropped vertically from a height of 100 mm and two accelerometers (Dytron model 11197, 11305) with a sensitivity of 1.055 V/g (**Figure 3.10 a**) were used to measure the response. The

accelerometers were placed at mid-span and one third points in the RC beams at the soffit with the help of high strength cement paste for recording the signal generated by impact hammer (**Figure 3.11**). The output was observed in the form of Frequency Response Function (FRF) using FFT real time multi-analyzer (Make- OROS, OR-35, 8 ch-102.4 KS/s-24 bits) (**Figure 3.10 c**). The RC beam with the impact hammer and sensors in place is shown in **Figure 3.11** below. It is important to note that for plotting a typical FRF record, average of 8 impact hits was taken. Maximum deviation in vibration signals received was observed at mid-span and thus FRF signatures were plotted and studied at this location. In a typical FRF, the first peak corresponds to 1st fundamental mode and variation in its response is measured in term of frequency shift. Also change in amplitude of received FRF signal with progressively increasing corrosion in RC beams is measured.

(a) Accelerometer

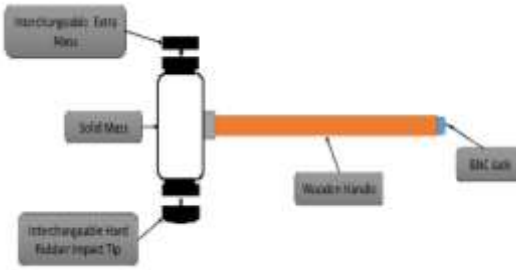

(b) Typical impulse-force hammer.

(c) FFT Analyzer

(d) Impact hammer instrument with impactor tips

Figure. 3.10. Vibration monitoring Set-up

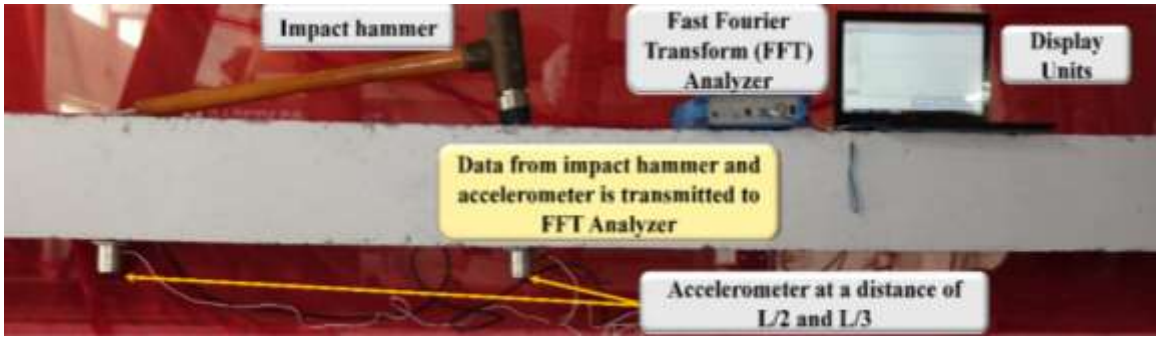

Figure 3.11. Experimental set up for Vibration Monitoring

3.3.3 Accelerated Corrosion

All eight RC beams were subjected to accelerated corrosion using impressed current technique, where a constant electric potential of 10V is supplied using a constant voltage source (APLAB Make, 64V, 5 A). The tensile reinforcement acting as anode is connected to the positive terminal of power source.

Figure 3.12. Accelerated impressed current corrosion set up

Middle 1.5 m portion of the beam was wrapped with cotton gauge to retain the moisture and was kept moist with uninterrupted supply of 3.5 % NaCl solution using a water tank arrangement as shown in **Figure 3.12**. Thereafter, the cotton gauge is covered on the top with stainless steel wire mesh acting as cathode and connected to the negative terminal of power supply. RC beams with four different levels of corrosion were prepared with two samples for each level of deterioration as detailed outlined in **Table 3.4**. To track the level of corrosion in various specimen, the corrosion current was recorded at regular intervals. The increase in the corrosion current at constant voltage is an indication of increasing deterioration due to corrosion in the RC beams.

3.3.4 Repair of corroded beams using GFRP wraps

After RC beams were exposed to different level of corrosion damage, repairing was carried out to attain its lost strength and ductility. Damaged concrete cover was removed by tapping with hammer till sound concrete appears. Micro-concrete consisting of good quality cement, fine grade aggregates and additives (Trade Name- Dr Fixit Repair Pro, Pidilite Construction Chemicals) having average 28 days characteristic compressive strength of 57 MPa was used to replace removed concrete [142]–[144]. After sufficient curing of new concrete for 21 days, bottom and side surfaces of beam were well grounded to make them smooth to avoid any air gap between concrete and the GFRP sheet to be wrapped onto the concrete beams. To strengthen the beam in flexural, two strips of GFRP sheet 127 mm wide and 4100 mm long were applied at the bottom surface (**Figure 3.13**). To prevent spalling of micro-concrete, an additional single layer of U-wrap was provided in the middle 2 m length of beam. The main objective of GFRP repair was to investigate the efficacy of GFRP wrapping on improving the strength and capacity of RC beams when subjected to deterioration due to corrosion at increasing levels. **Figure 3.14** shows the steps involved for repair of corroded RC beams.

RC beams corroded to different levels (C-10, C-20, C-30 and C-40) and subsequent GFRP repaired beams (R-10, R-20, R-30 and R-40) were inspected for assessing the extent of damage due to corrosion by vibration monitoring technique. Further these beams were then subjected to flexural testing until failure for determining their load carrying behaviour after corrosion and further when repaired against corrosion by GFRP wrapping (**Figure 3.15**).

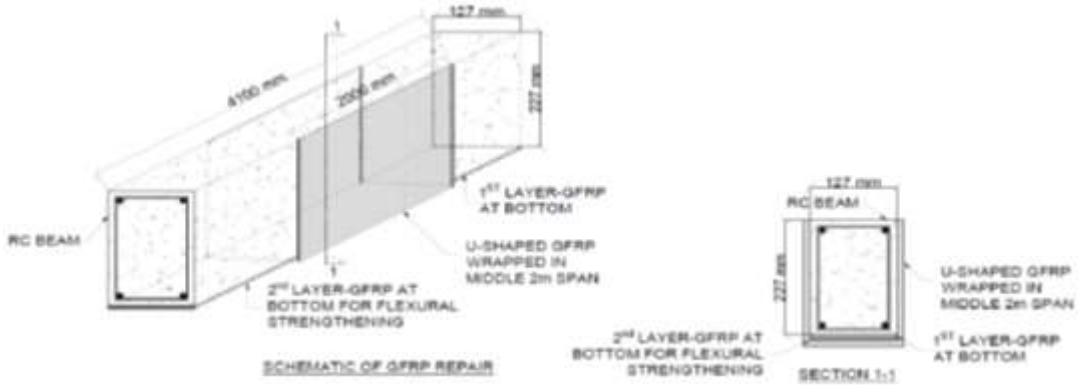

Figure 3.13. Schematic of GFRP repair

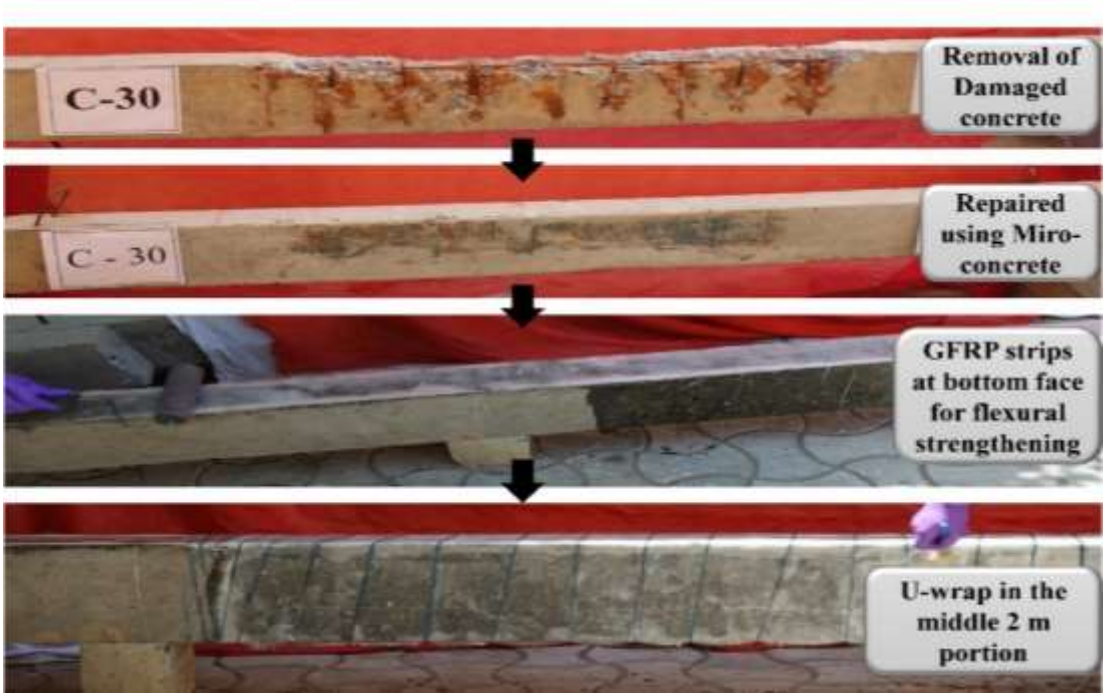

Figure. 3.14. Steps involved in GFRP Repair of Beams

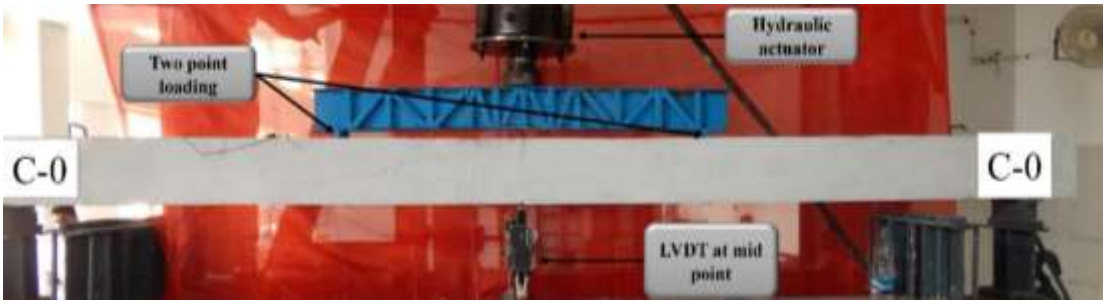

Figure. 3.15. Flexure testing set up

3.4 MONITORING CORRODED AND GFRP REPAIRED CORRODED BEAMS USING AE

RC beams corroded to different levels (C-10, C-20, C-30 and C-40) and GFRP repaired corroded beams (R-10, R-20, R-30 and R-40) were tested under flexural (**Figure 3.16 b**). During flexural testing, simultaneously AE monitoring was also performed using surface mounted AE sensors to investigate the failure and cracking pattern in all corroded as well as repaired RC beams. The AE sensors are placed away from GFRP wraps because practically they cannot be placed on the GFRP wraps (applied 2m in the middle). The AE sensors are mounted over the surface of the beam for detecting the elastic waveforms generated by micro-cracking under static loading with a threshold of 45 dB to eliminate unwanted waveforms. AE-Win software

(SAMOS Make) is used for extracting AE data providing various characteristics of AE signals such their number and amplitude of AE hits, AE signal energy, duration and counts of AE signal and rise time etc. (**Figure 3.16 a**).

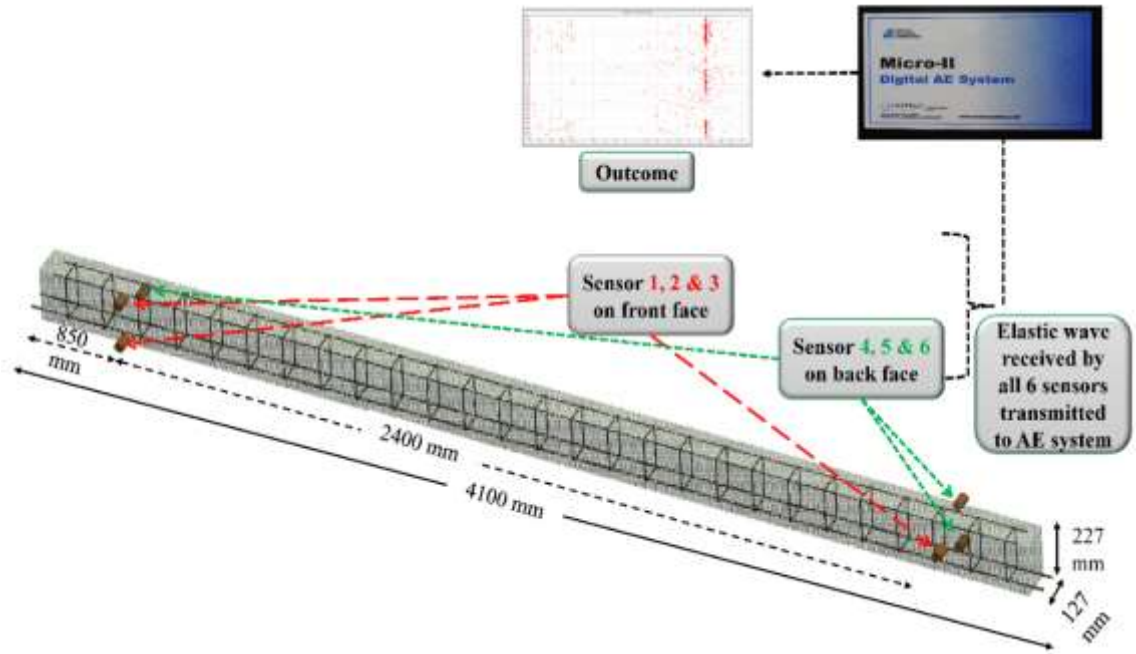

(a) Schematic of AE set-up

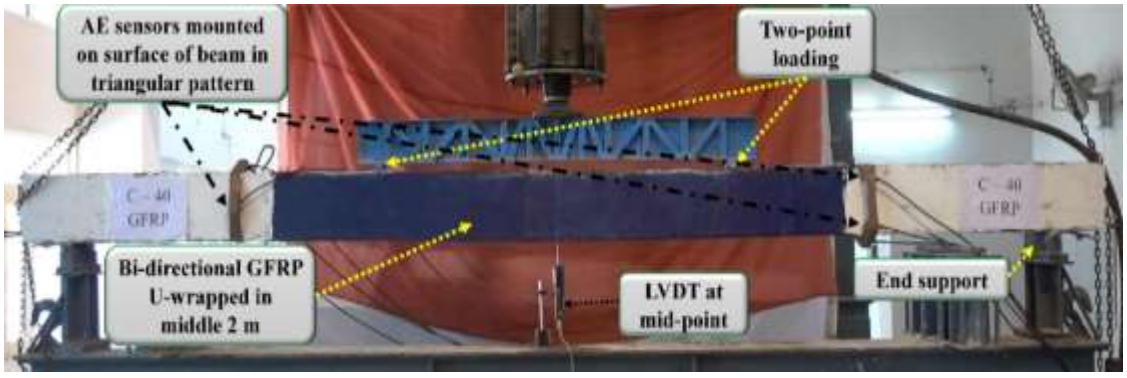

(b) Actual AE set up used

Figure 3.16 Flexural testing set up in combination with AE

Figure 3.17 shows the flow chart for the methodology followed for objective 2 and 3 monitoring corroded and GFRP repaired corroded beams using NDT tools.

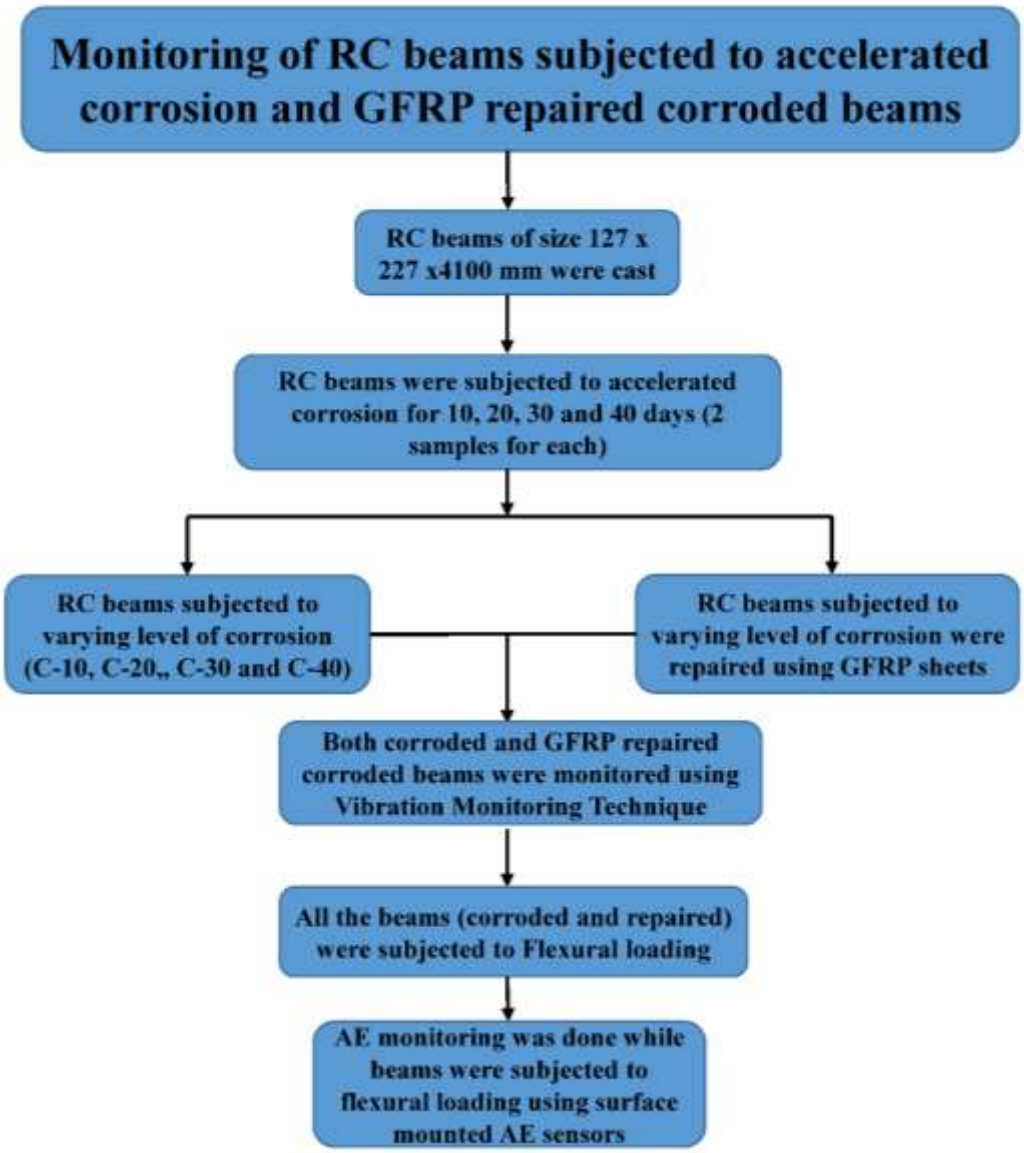

Figure: 3.17 Flow chart for monitoring corroded and GFRP repaired corroded beams using NDT tools

3.5 Closing Remarks

In this chapter, experimental details and methodology used in this study are explained in detail. The specimen cast and NDT techniques used for monitoring real time corrosion are discussed in detail. Further to explore behaviour of real size beams corroded to varying level and repaired using GFRP using global vibration monitoring and local acoustic emission technique has been explained in detail.

CHAPTER 4

MONITORING REAL TIME CORROSION USING NDT TOOLS

4.1 GENERAL

Non-destructive techniques that are able to estimate the residual strength of corroding structures would help a great deal in strategizing post-corrosion maintenance. This chapter reports combination of three non-destructive techniques for monitoring corrosion initiation and progression, based on active wave propagation of ultrasonic guided waves (UGW), passive wave propagation of Acoustic Emission (AE) and Infra-Red Thermography (IRT) based thermographic images.

In this study, two types of damage simulating corrosion in the form of pitting and delamination were introduced to the reinforcing steel bars and were analysed both in air and as well as in concrete using UGW, AE and IRT techniques. Further, reinforced concrete (RC) beam of 80 x 80 x 400 mm size were corroded to varying levels of accelerated corrosion and progression of damage due to corrosion was monitored using the combination of three NDT tools of UGW, AE and IRT. The results of rebars with simulated corrosion damage was compared with actual corroding RC beams using the three NDT techniques of AE, UGW and IRT.

4.2 SIMULATED DAMAGE MONITORING

4.2.1 UGW Monitoring

Bars in Air and Concrete

The bars with simulated corrosion damage representing pitting (Damage 1) and debond damage (Damage 2) were subjected to UGW monitoring as explained in **Section 3.2.3**. The transmitted signals were recorded in healthy and in bars with simulated corrosion damages as shown in **Figure 4.1** and **Figure 4.3** respectively. The relative change in the transmitted pulse with respect to transmitted signal in healthy bar are plotted as pk-pk voltage ratio (transmitted voltage / pulse voltage of healthy bar) for both types of simulated corrosion damage bars.

From **Figure 4.1** it can be observed that ultrasonic transmitted signal strength reduces with reducing diameter of the bar indicating increasing pitting in bar. Since the

guided wave propagating through the bar reduces with reducing diameter it is observed that for D4 (diameter reduced from 12 mm to 4 mm), the ultrasonic signal completely vanishes, indicating that there is no more sufficient material left to transmit the signal. Initially for D10 (reduced diameter to 10 mm), the fall in signal strength is lower but thereafter shows a steep drop for D8 and D6 and ultimately drops to a very low for D4 bar. Similar trends and signatures were obtained as shown in **Figure 4.2** when these bars with simulated damage were cast in concrete. Bars with Simulated Damage 1 (simulating pitting) were cast in the concrete and ultrasonic signals were taken for the same settings to consider the effect of concrete on the signals. UGW signatures and their pk-pk voltage ratio trend with reducing diameter are represented in **Figure 4.2**. From **Figure 4.2 (a-e)** similar trends are observed for bars with simulated damage 1 when embedded in concrete. A drop in signal is observed with reduction in diameter. UGW signature for D6 is very small and it completely disappears in D4. An important observation is the drop in signal strength when the same rebars are embedded in concrete and UG signal are taken at same setting. It is due to attenuation caused by leakage of the ultrasonic signal into surrounding concrete.

Similarly, for bars with increasing debond (simulated damage 2) in rebar in concrete, it is observed that initially with increasing de-bond, signal attenuation is low but at larger lengths of de-bond from 75 mm to 125 mm, a drop in voltage observed is significantly higher. This is because the tapered length of bar from center attenuates the waveguide travelling on the surface or the circumference of the bar. Similar trends were observed as shown in **Figure 4.4** when these bars with simulated damage 2 were cast in concrete. **Figure 4.4** presents UGW signatures and pk-pk voltage ratio trends for increased length of debond in rebars embedded in concrete. Disturbances in the signature can be noticed and similar trend of reduction in the pk-pk voltage is observed as for the rebars in air. When debond length increases from 75mm to 100mm, highest drop in the signals is noted indicating that the steel bar has lost sufficient area caused by increase in tapered length and transmitted signals strength drops drastically.

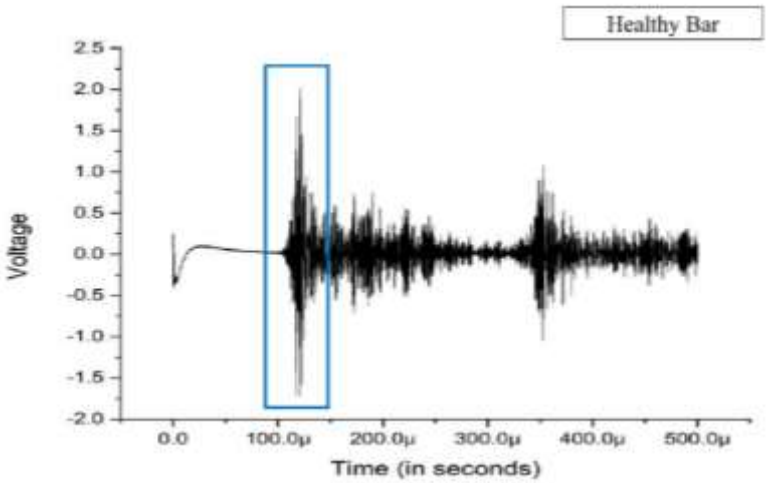

(a) Healthy Bar

Total voltage 3.57V

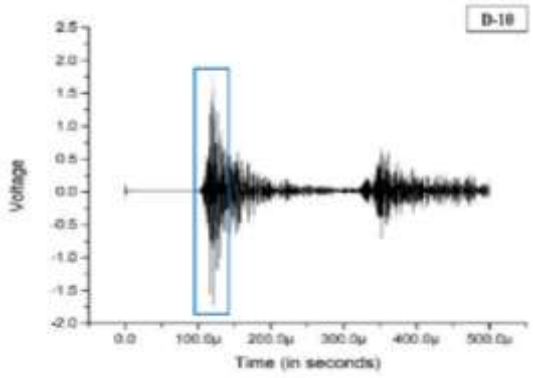

(b) D-10

Total voltage 2.38V

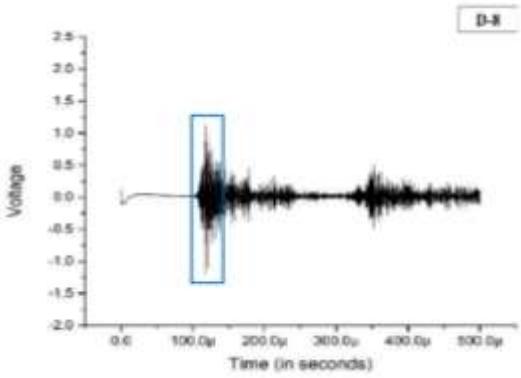

(c) D-8

Total voltage 1.13V

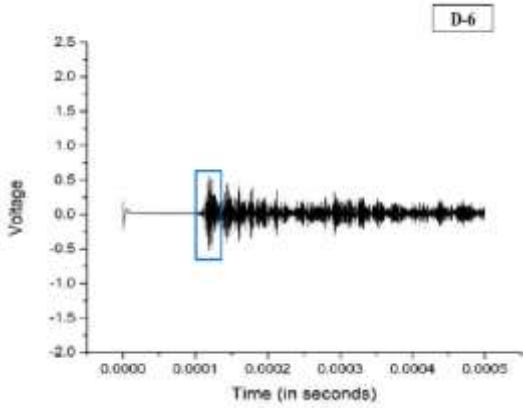

(d) D-6

Total voltage 0.311V

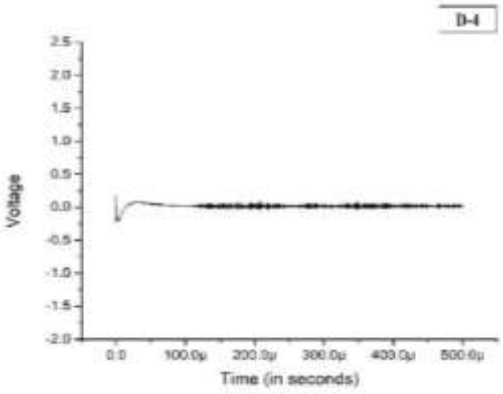

(e) D-4

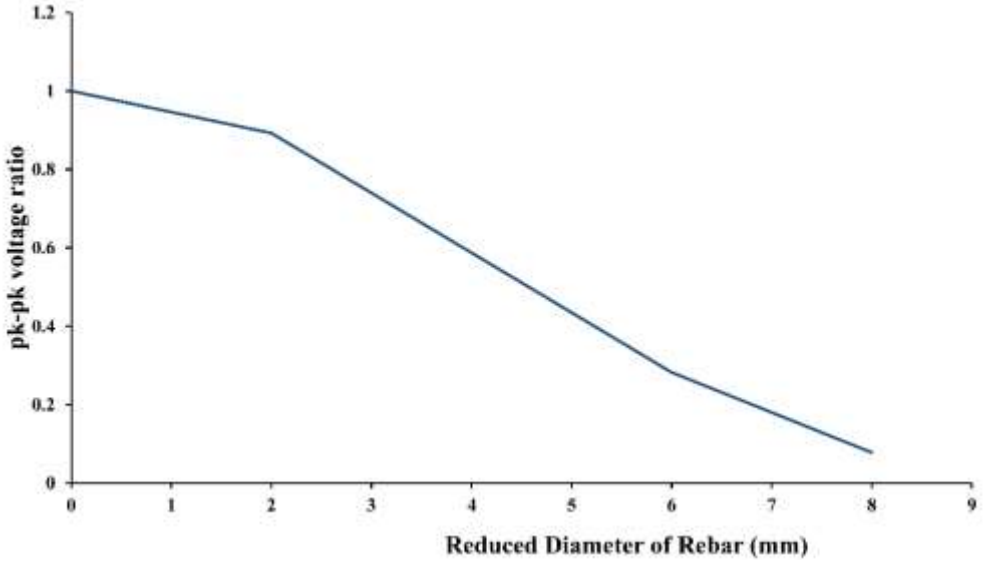

(f)

Figure 4.1: UGW signatures for the Simulated Damage 1 bars in air (Pitting)

Total voltage 3.8V

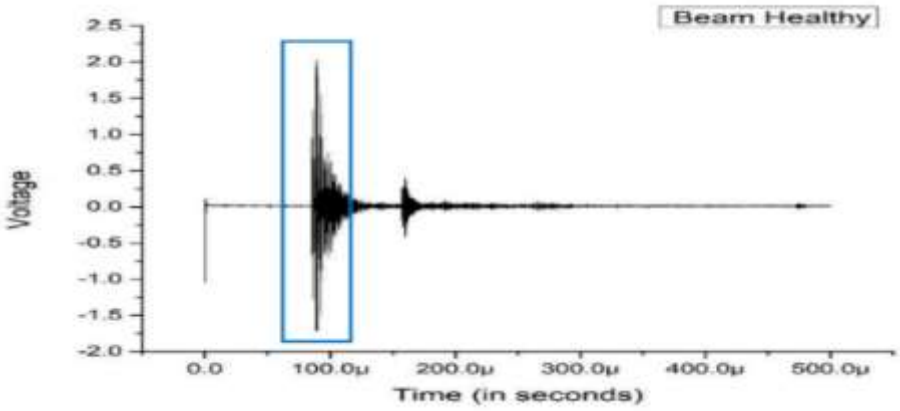

(a) Healthy Beam

Total voltage 3.39V

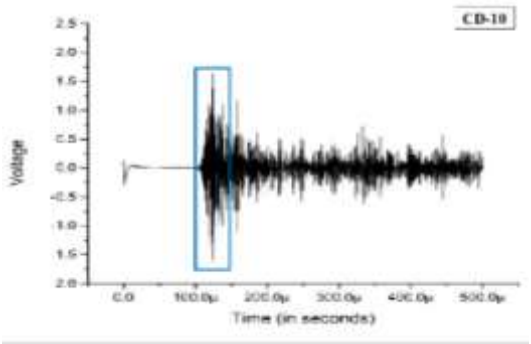

(b) CD-10

Total voltage 2.2V

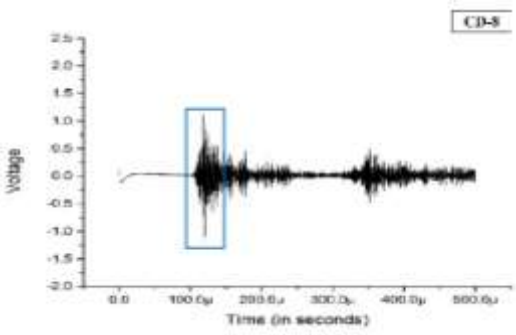

(c) CD-8

Total voltage 0.787V

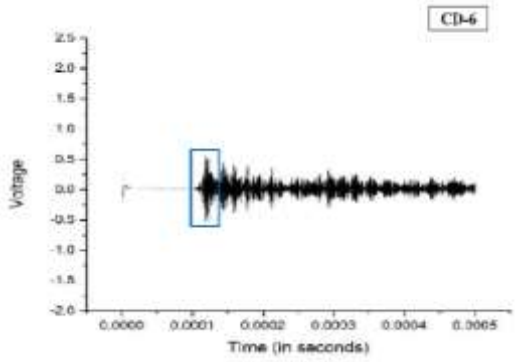

(d) CD-6

Total voltage 0.179V

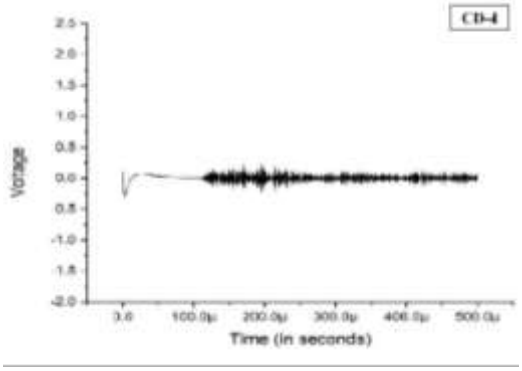

(e) CD-4

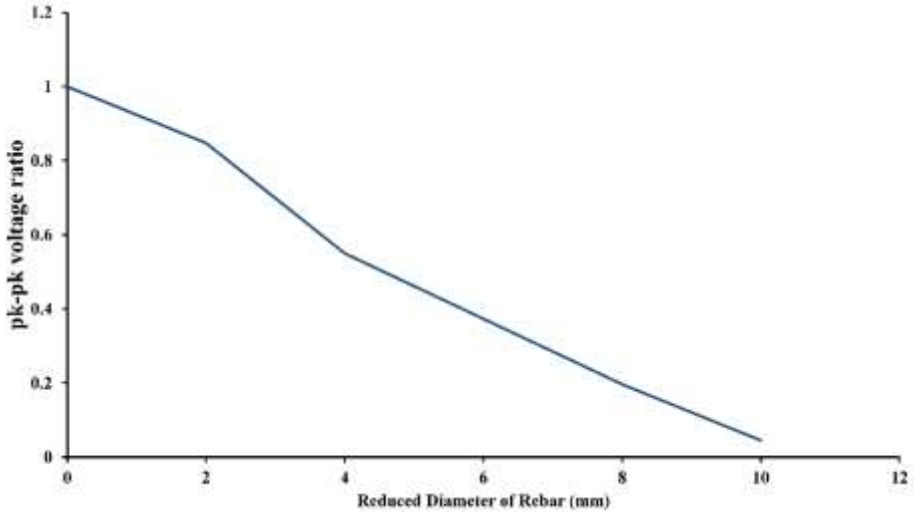

(f)

Figure 4.2. UGW signatures for the Simulated Damage 1 bars in concrete

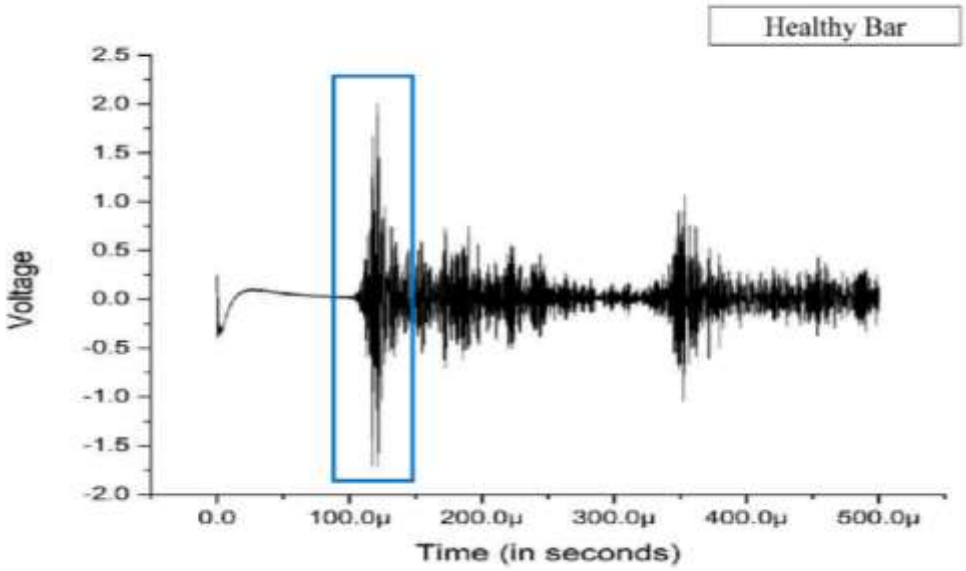

(a) Healthy Bar

Total voltage 3.413V

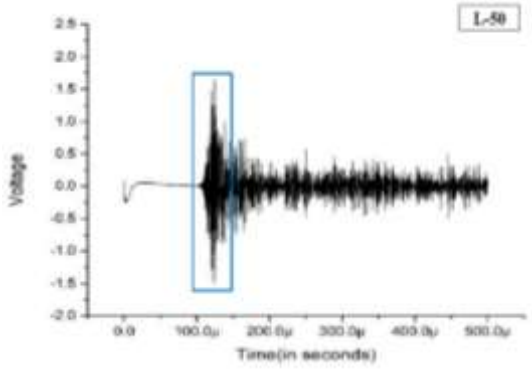

(b) L-50

Total voltage 3.1V

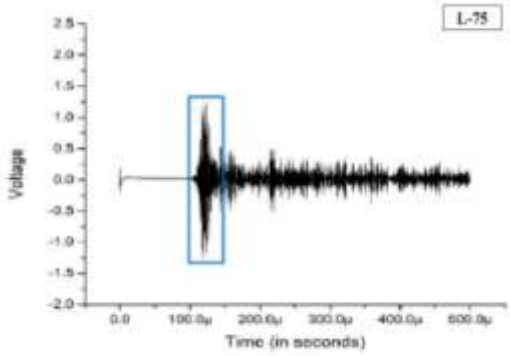

(c) L-75

Total voltage 2.5V

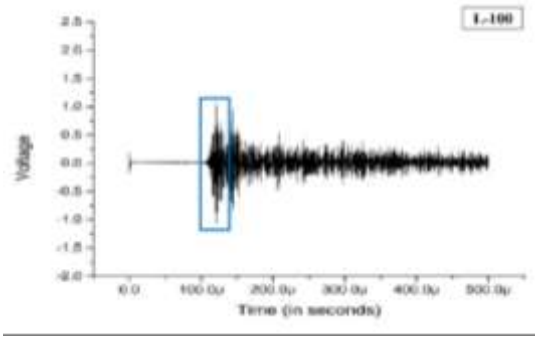

(d) L-100

Total voltage 2.01V

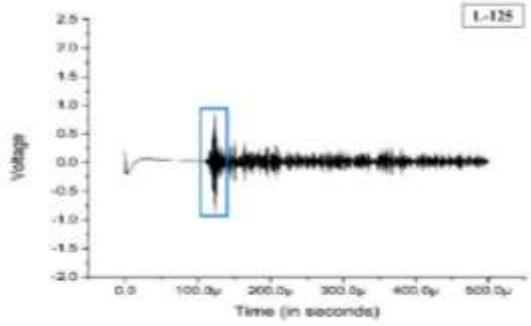

(e) L-125

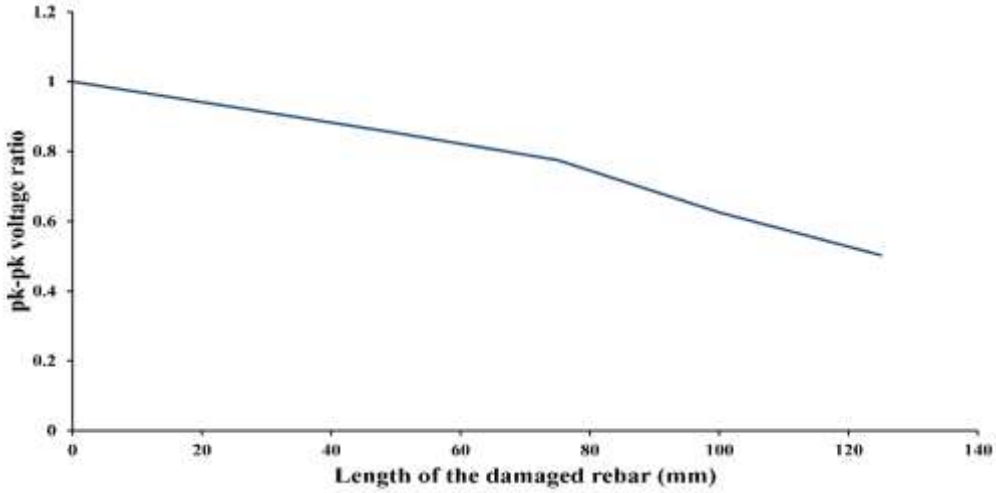

(f)

Figure 4.3. UGW signatures for the simulated damage 2 bars in air (De-bond)

Total voltage 3.8V

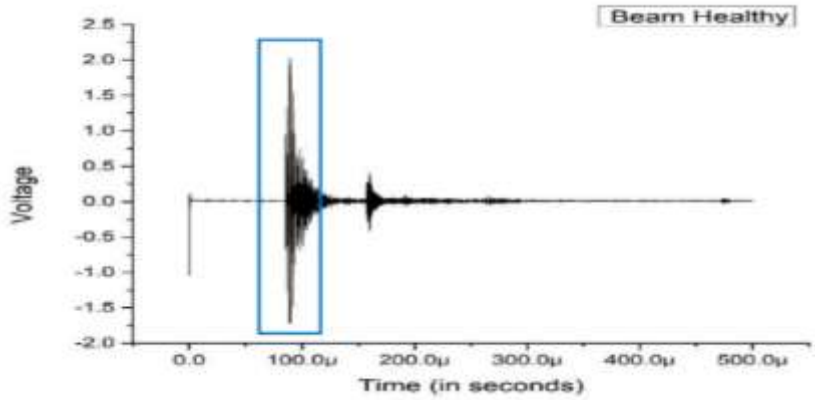

(a) Healthy Beam

Total voltage 3.27V

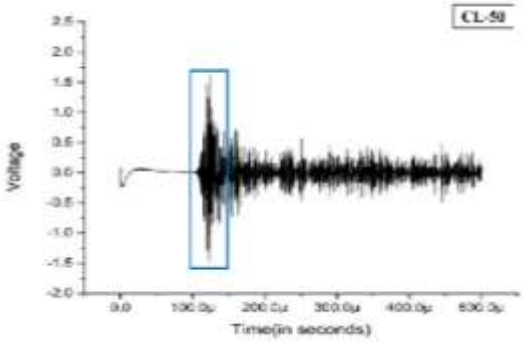

(b) CL-50

Total voltage 3.11V

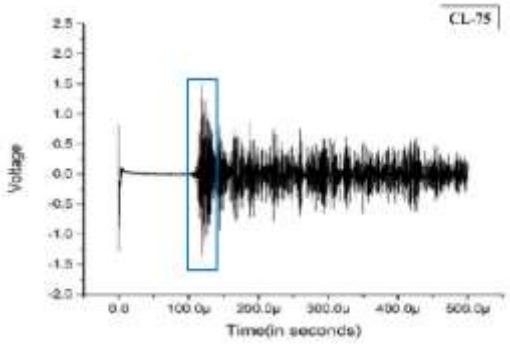

(c) CL-75

Total voltage 2.187V

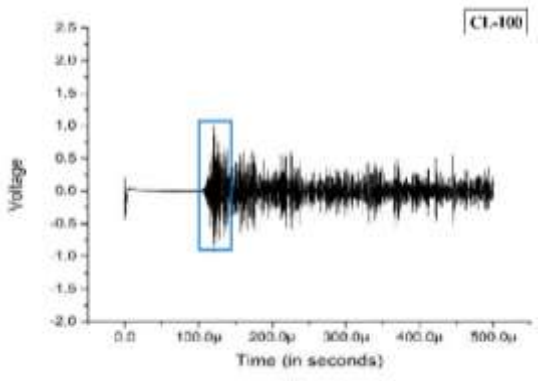

(d) CL-100

Total voltage 1.75V

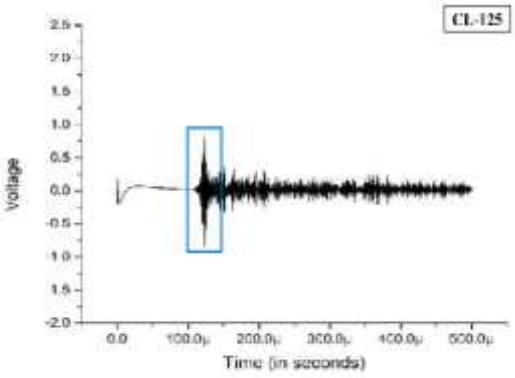

(e) CL-125

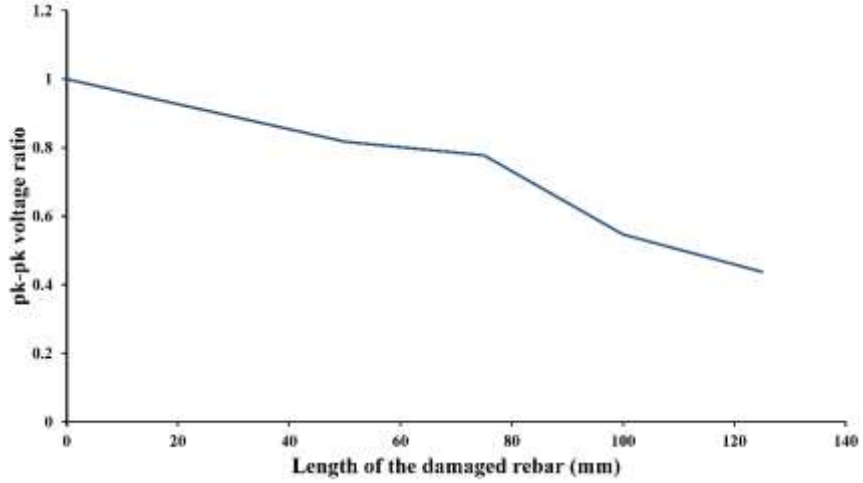

(f)

Figure 4.4. UGW signatures for the Simulated Damage 2 bars in concrete

Hence, it can be concluded that high frequency ultrasonic guided wave modes [L(0,7) for 12 mm bar in concrete at 1 MHz] propagated through rebars in concrete can easily pick up deterioration in bars in the form of area reduction indicating pitting and debonding or delamination from concrete by fall in transmitted signal strength. Hence, guided waves can be further used for monitoring actually corroding bars in concrete (Section 4.4.2).

4.2.2 Damage Monitoring Using IRT for Simulated Damage Specimen

Further, the bars with simulated corrosion damages (1 and 2) bars were also subjected to Infra-Red Thermography imaging and monitoring. **Figure 4.5** shows IRT image of a healthy rebar where maximum temperature recorded is 45.6 °C. No temperature difference on the rebar is observed and it is uniformly red from core and yellow on the surface indicating that the rebar has no undulation or cracks which leads to temperature differences indicating its healthy condition. IRT images for the bars in air as well as in concrete with Simulated Damage 1 and Damage 2 were also taken.

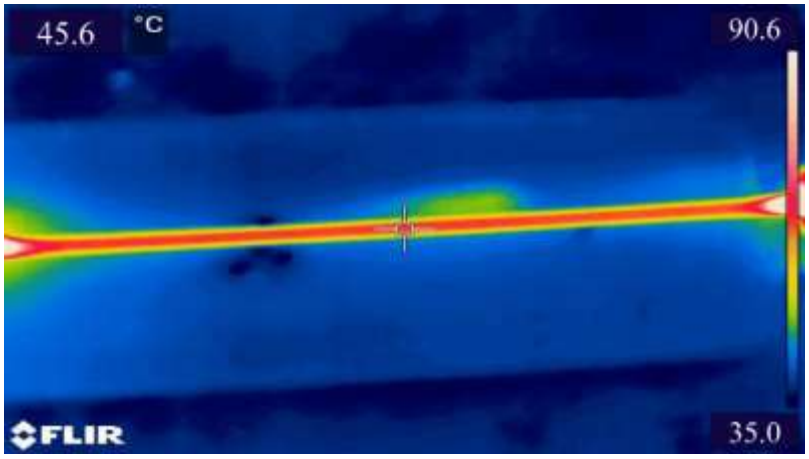

Figure 4.5. IRT image of healthy rebar in air

Figure 4.6 shows the IRT images for bars in air with Simulated damage 1 representative of reduced diameter indicating pitting effects of corrosion. It can be observed that there is a color difference at the locations where the reduction in diameter is done in the central 50 mm length. As the diameter reduces from D10 to D4, correspondingly temperature of the rebar in the centre increased from 41°C to 61°C respectively. During the electric heating of the metal the portion of the bar with reduced area of cross-section tends to be heated faster as compared to the rest of the bar leading to increased temperature in that portion of bar with simulated damage.

Similarly, in **Figure 4.7** it can be seen that the delaminated region shows different surface temperature from the rest of the rebar with an increase in length of de-bond as indicated by different colors in the IRT image. The temperature of L50 is lowest i.e. 32°C and L125 is the highest temperature at 71.3°C during heating. This is because with increase in debond length, the region heats faster than the surrounding healthy portion and shows increased temperature which leads to ease of picking up degradation in bars.

Hence, in IRT images, damaged portion of the rebar's in the form of reduced diameter or increasing debond is clearly depicted by variation in temperature which is well identified by color change in the IRT images. Hence, it can be concluded that IRT images are capable of giving pictorial representation of the exact location of damage. While UGW monitoring relates to the extent of damage, IRT picks up the exact location of damage. This was further investigated for bars with simulated damages when embedded in concrete (**Figure 4.8 and 4.9**).

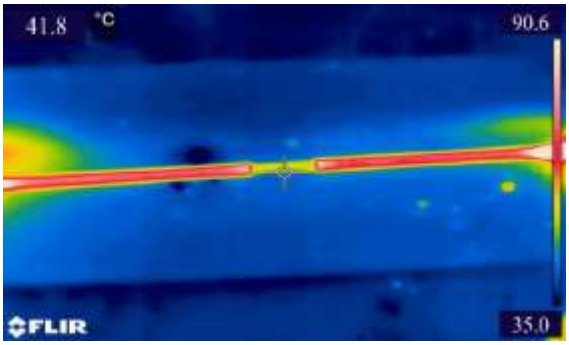

(a) D10

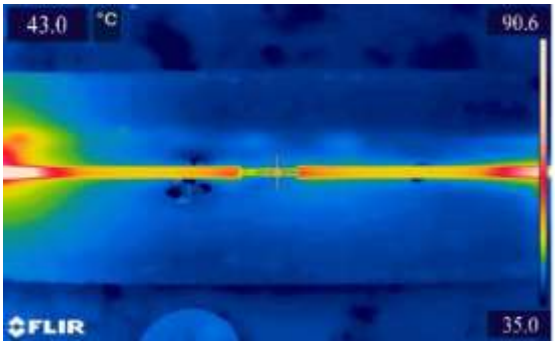

(b) D8

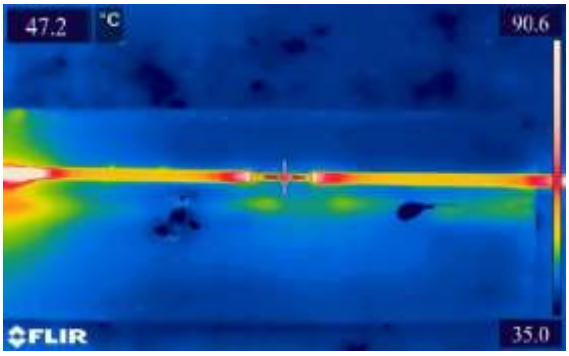

(c) D6

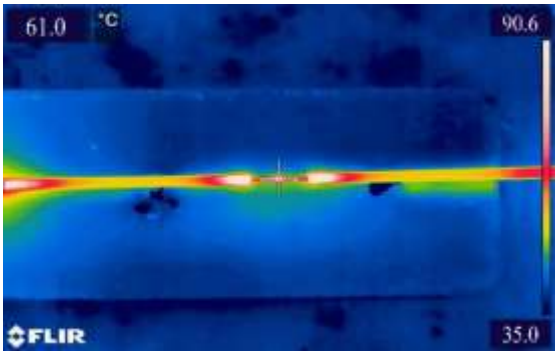

(d) D4

Figure 4.6. IRT images of rebar in air for Simulated Damage 1 (Pitting)

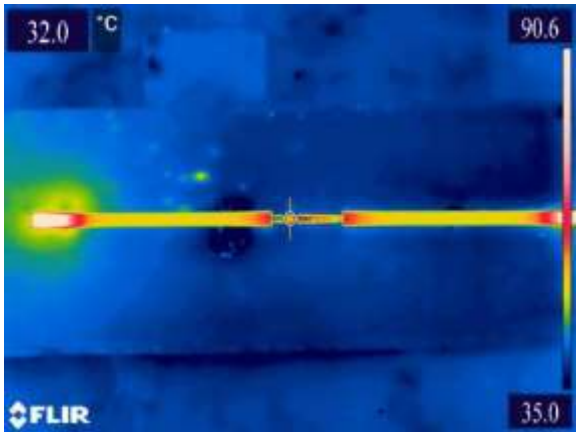

(a) L50

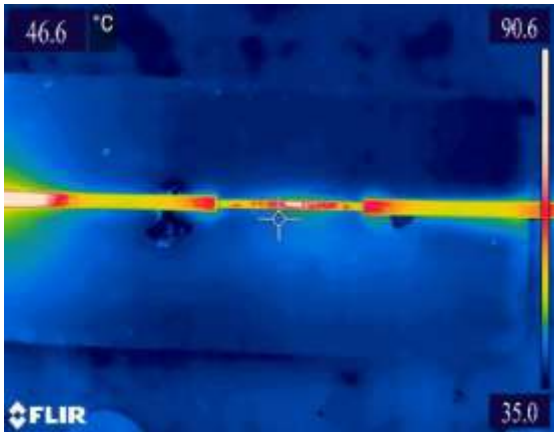

(b) L75

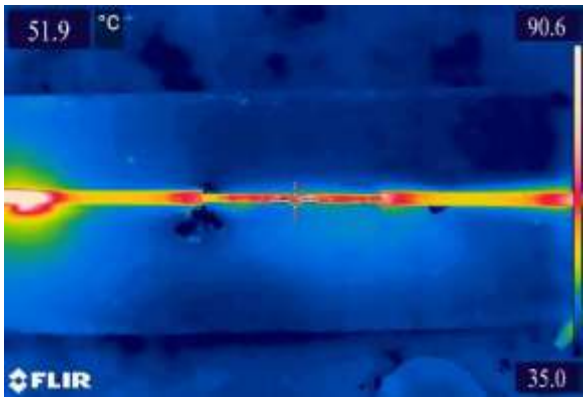

(c) L100

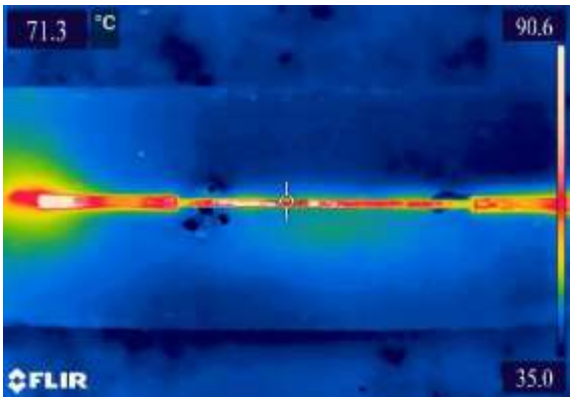

(d) L125

Figure 4.7. IRT images of rebar in air for Simulated Damage 2 (De-bond)

From the IRT images of bars in concrete with simulated damage 1 & 2, clear image of rebar inside concrete is visible. In IRT images of beams with Simulated Damage 1 increasing from CD10 to CD4, the temperature of the rebar increased in reduced diameter region at constant rate from 40°C to 52.6°C and gets heated up earlier than healthy bars (**Figure 4.8 a-d**). In the damaged region representing pitting corrosion variation in thermographic image color is different from the rest of the rebar indicating imperfection / damage in surface geometry leading to temperature variation. Similarly, the damage in the form of increasing debond is also very clearly visible in IRT images (**Figure 4.9 a-d**). As the de-bond length increases from L50 to L125 the temperature of the rebar in concrete increases from 38.2°C to 41.1°C. The change in temperature as compared to intensity of damage is less in bars embedded in concrete with simulated debond sample as with increase in damage length concrete dominates steel and thus ultimate change in surface temperature is less. Hence, it can be concluded that Infra-Red Thermographic imaging is capable of exactly locating simulated damage in the form of pitting and delamination in rebar in concrete. It is further explored for monitoring rebars in concrete undergoing actual corrosion in concrete.

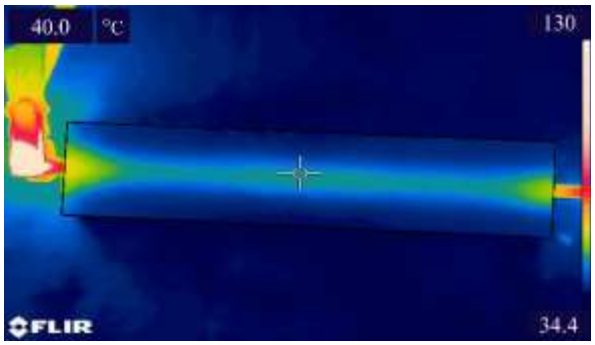

(a) D10

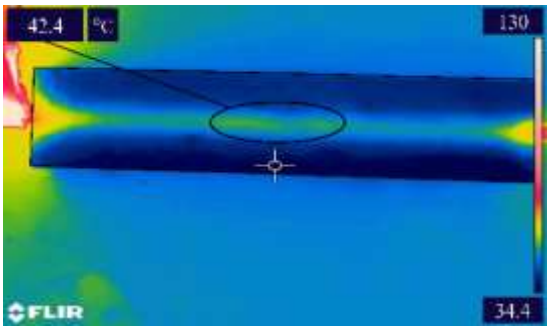

(b) D8

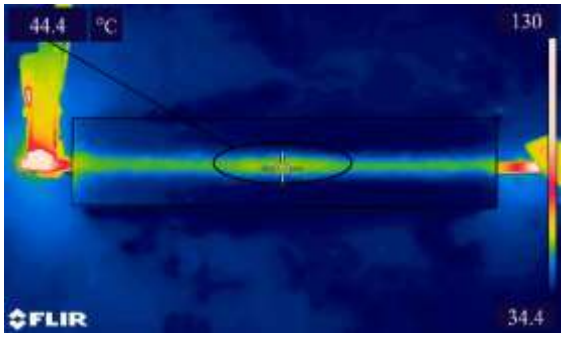

(c) D6

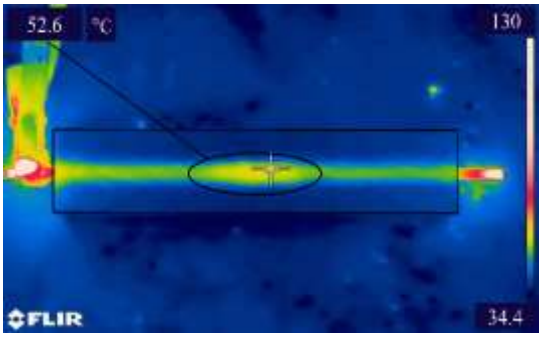

(d) D4

Figure 4.8. IRT images of rebar's in concrete for Simulated Damage 1 (Pitting)

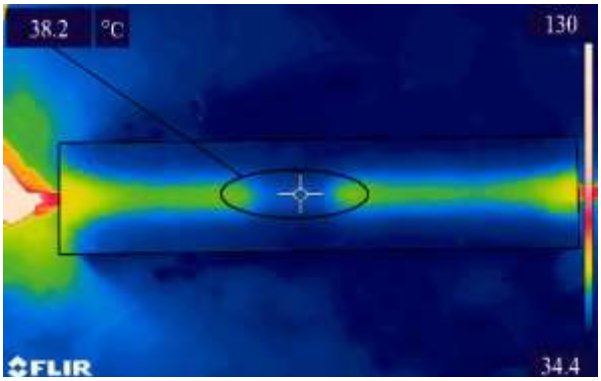

(a) L50

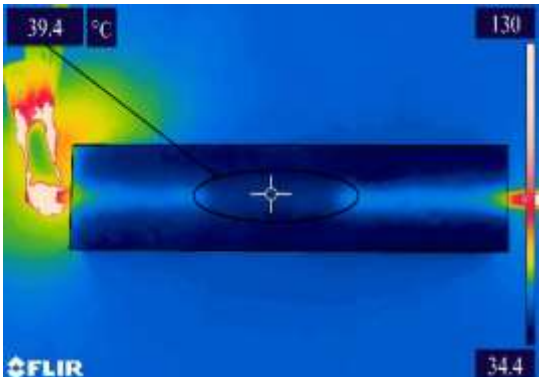

(b) L75

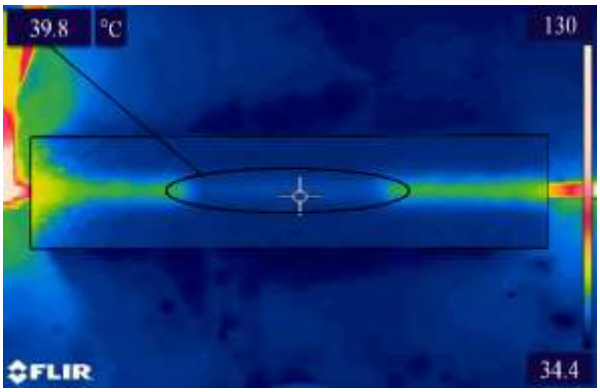

(c) L100

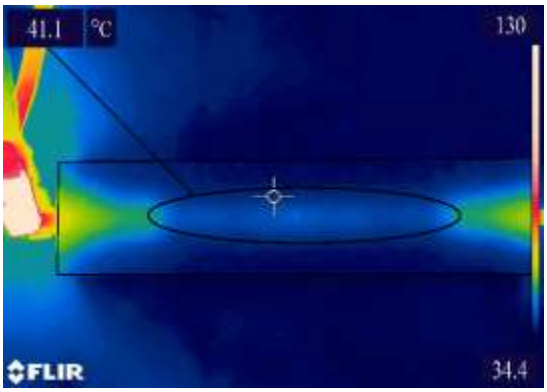

(d) L125

Figure 4.9 IRT images of rebar in concrete for Simulated Damage 2 (Debond)

4.3 DAMAGE MONITORING IN CORRODING RC BEAMS

The rebars embedded in concrete were subjected to accelerated impresses current corrosion for varying degrees and levels of corrosion and further monitored using IRT. During corrosion continuous non-destructive and in-situ monitoring of the beams was done by visual inspection of beams, Ultrasonic Guided Wave and AE techniques. Along with it, four beam specimens subjected to varying days of corrosion exposure (8, 19, 26 and 33) named as S8, S19, S26 and S33 were also subjected to IRT monitoring. Further, after corrosion to specific durations beams were visually observed for their deterioration inspection. The rebars extracted from corroded beams and the condition of the corroded beams is also assessed.

4.3.1 Visual Observations

Visual inspection of the RC beams for S8, S19, S26 and S33 are shown in **Figure 4.10**. It is observed in S8 beam, after 8 days of accelerated corrosion only minor visual corrosion effects were observed in the middle 100 mm length reflected by yellowish corrosion product which is also observed in the X-section. This indicates beginning of

corrosion in the S8 beam (**Figure 4.10 a**). With the progression of corrosion in S19 beam, reddish brown corrosion product is observed in the beam indicating increased rust formation. This exerts pressure on surrounding concrete which is weak in tension and hence appears as hair line cracks in the longitudinal direction and a transverse hair line crack after 19 days of accelerated corrosion (**Figure 4.10 b**). As corrosion level increases in S26 beam a large longitudinal crack appears in the entire beam surface along with numerous hairline transverse cracks. An important observation is the appearance of transverse crack in the middle of the beam pointing towards large expansive and tensile effect on surrounding concrete due to huge corrosion leading to busting stresses in concrete (**Figure 4.10 c**). Further in S33 beam both in longitudinal and transverse direction huge and widespread corrosion cracks are observed in the entire length of the beam.

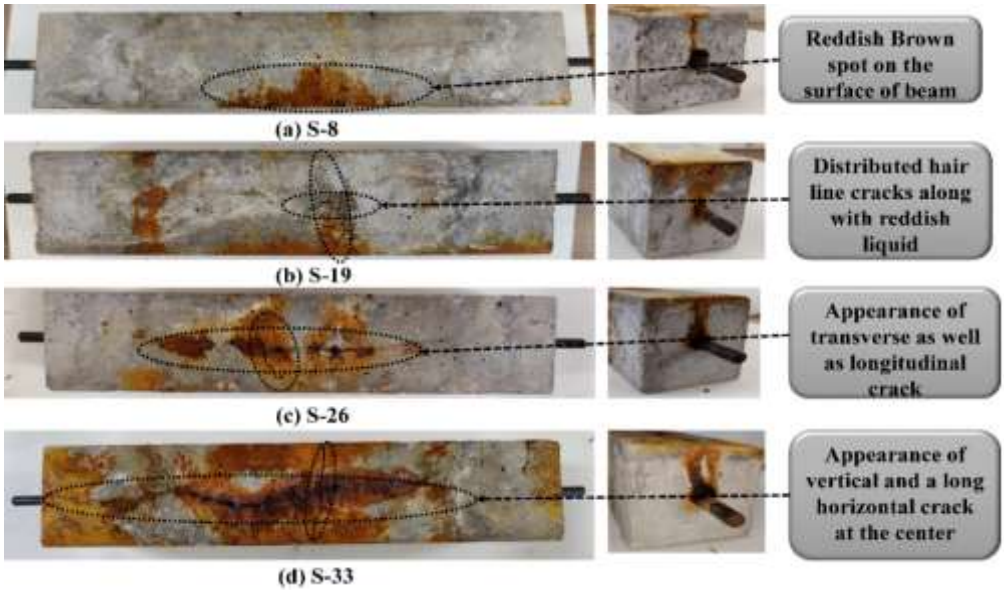

Figure 4.10. Visual images of corroding RC beam

For all RC beams corroded to different level of corrosion the rebars were extracted and also visually inspected. **Figure 4.11** represents the extracted rebar samples from RC beams corroded to varying level of corrosion. In S8 rebar very little corrosion product is seen and in S19 extracted rebar, initiation of surface corrosion is observed in the form of scaling off passive layer of oxides. In S26, corrosion pits were observed at various places in the bars where as in S33 rebar's pitting extends throughout the length of bars with deep grooves and pits at various places. Hence, it can be concluded that with increase in corrosion exposure, the embedded bar experiences increase in pitting

and rust product formation along the length of bar when subjected to accelerated chloride corrosion. Also the surrounding concrete experiences widespread longitudinal as well as transverse cracking with increases corrosion exposure along with widespread rust staining.

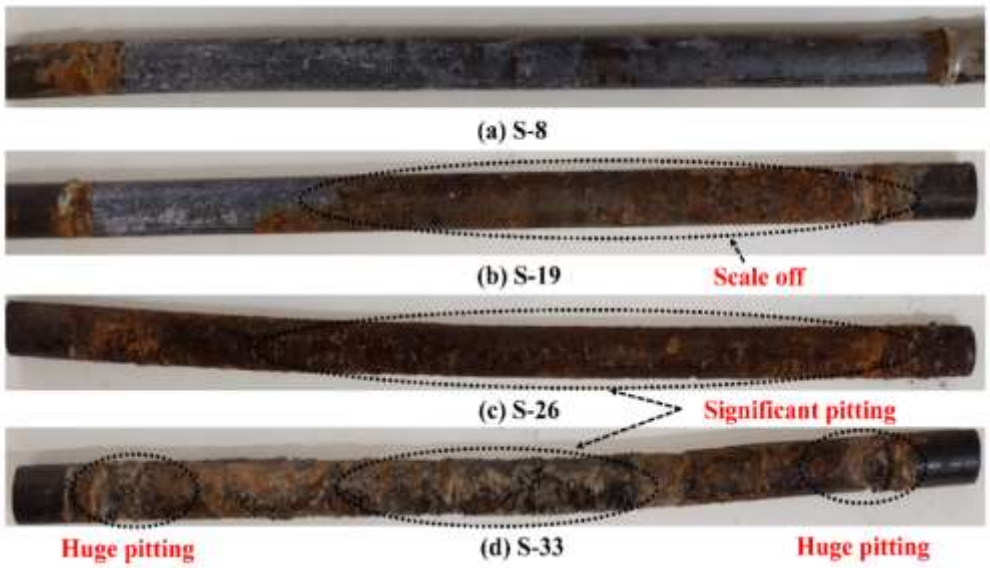

Figure 4.11. Rebar's extracted from the concrete samples

4.3.2 UGW Monitoring

The corroding concrete beams with rebars were also monitored using ultrasonic guided wave (UGW) signal of L (0,7) mode at 1 MHz in pulse transmission mode. It is important to note that UGW are propagated through rebars every 24 hours to record the transmitted signals as the rebars corroded. **Figure 4.12** shows the ultrasonic guided waves signals obtained in S33 sample which was corroded till 33 days until the UGW signal vanishes (**Figure 4.12 a**). The ultrasonic peak-peak voltage ratio with increasing corrosion exposure is shown in Figure 4.13. It is observed that with increasing accelerated impressed current corrosion consistent and continuous drop in signal strength is observed. Initially for 5-6 days no drop is observed pointing towards ingress of corrosion agents breaking down the passive layer but no significant effects on rebar in the form of area reduction / pitting. During this time, the breakdown of passive layer leads to debonding / delamination of bar from surrounding concrete which is not picked up by this high frequency L(0,7) mode at 1 MHz. This mode is sensitive to deterioration taking place in the core of the bar, rather than the surface owing to the energy being concentrated in the central core portion of the bar. Thus it is influenced by local

topography of bar rather than change in surface profile. It has been reported that lower frequency mode called surface seeking mode would be sensitive to bar profile changes like debonds and can easily pick up delamination of bar from surrounding concrete [42, 115]. The initial phase of breakdown of passive layer called delamination dominated zone and is picked up by low frequency mode which have not been studied in this work.

The UGW signal starts dropping after 6 days indicating the initiation and progression of corrosion in the form of pitting. Pitting leads to signal attenuation caused by waveguide scattering and multiple reflections causing reduction in the transmitted signal strength which falls at a rapid rate in later stages of corrosion. This is chloride induced corrosion leads to increased pit formation as observed visually with increased corrosion exposure. The ultrasonic signal completely vanishes in 33 days. Similar trends were observed in S8, S19, S26 and S33 beams where in a decline in UGW signal strength is observed with increase in corrosion level. The zone representing the corrosion mechanism in chloride environment is also depicted in **Figure 4.13**.

Total voltage 3.8 V

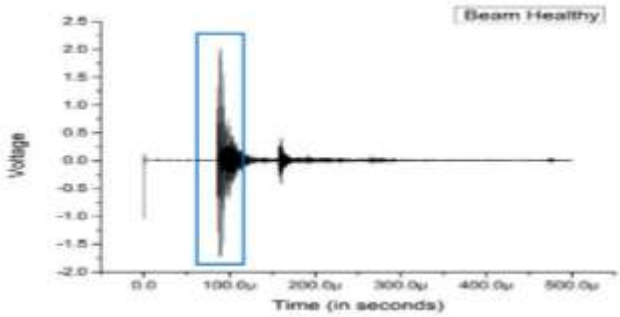

(a) Healthy

Total voltage 3.55V

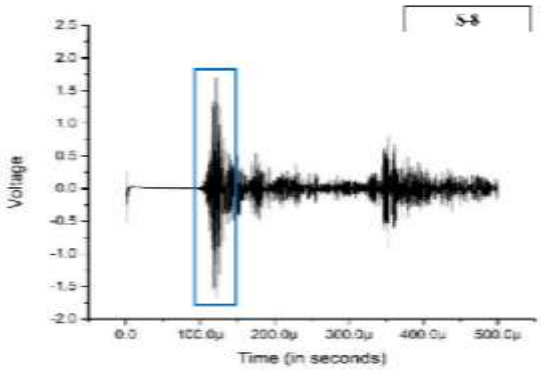

(b) S-8

Total voltage 1.993V

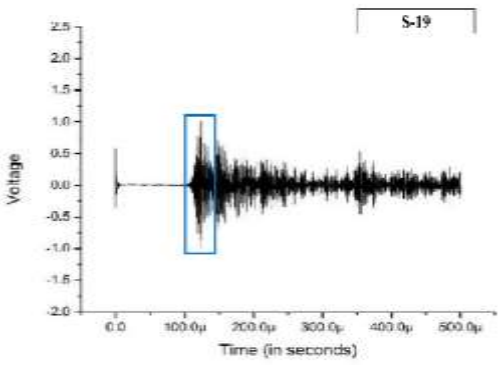

(c) S-19

Total voltage 1.071V

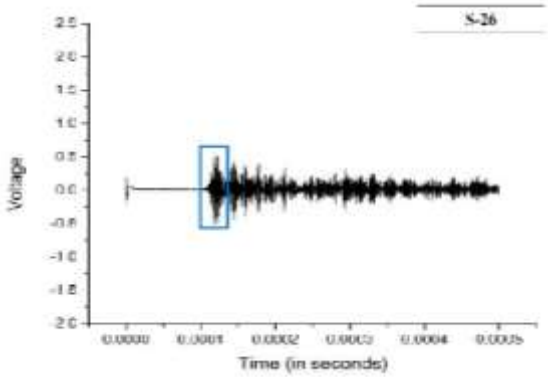

(d) S-26

Total voltage 0.231V

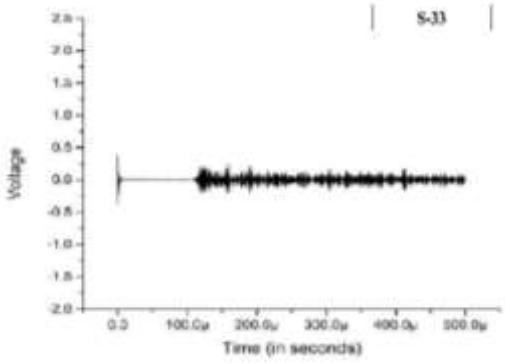

(e) S-33

Figure 4.12. UGW signature in corroded beam

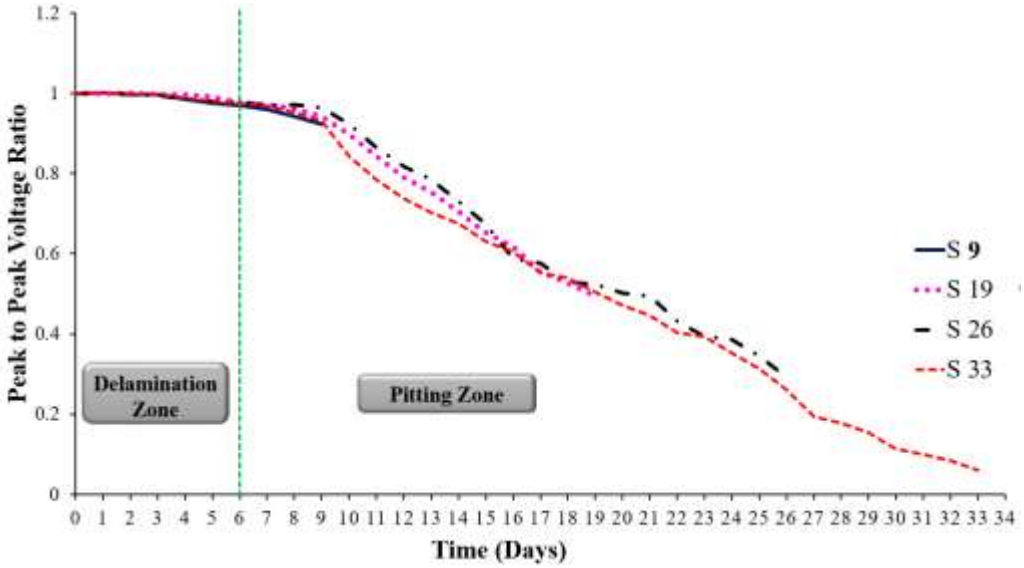

Figure 4.13. Peak to peak voltage ratio with corrosion

Another important observation is that the drop in signal strength with progressive corrosion closely follows drop in signal in Simulated Damage 1 (reduced diameter) bars in concrete (**Figure 4.2**). At 8 days, the UGW peak-peak signal voltage closely matches with D10 signal strength indicating that in 8 days of corrosion leads to an average reduction of 2 mm diameter of bars which closely matches with visual observation of extracted rebar's (**Figure 4.11 a** of S8). Similarly, a close match is observed between signal strength at S18 and D8, signal amplitude S26 and D6 and S33 and D4 indicating an average loss of 4mm, 6mm and 8mm at 19, 26 and 33 days of corrosion.

Since a close match is observed between the actual average diameter of the corroded bars at respective days of corrosion, a correlation has been attempted between ultrasonic pk-pk voltage ratio in actually corroding bars and average residual diameter at a particular stage (**Figure 4.14**). The empirical relationship between DR and R is given as below

$$D_R = 6.2492\ (\mathrm{R}) + 5.737 \quad (4.1)$$

Where, D_R- Average Residual Diameter

R- peak to peak voltage ratio at particular instant

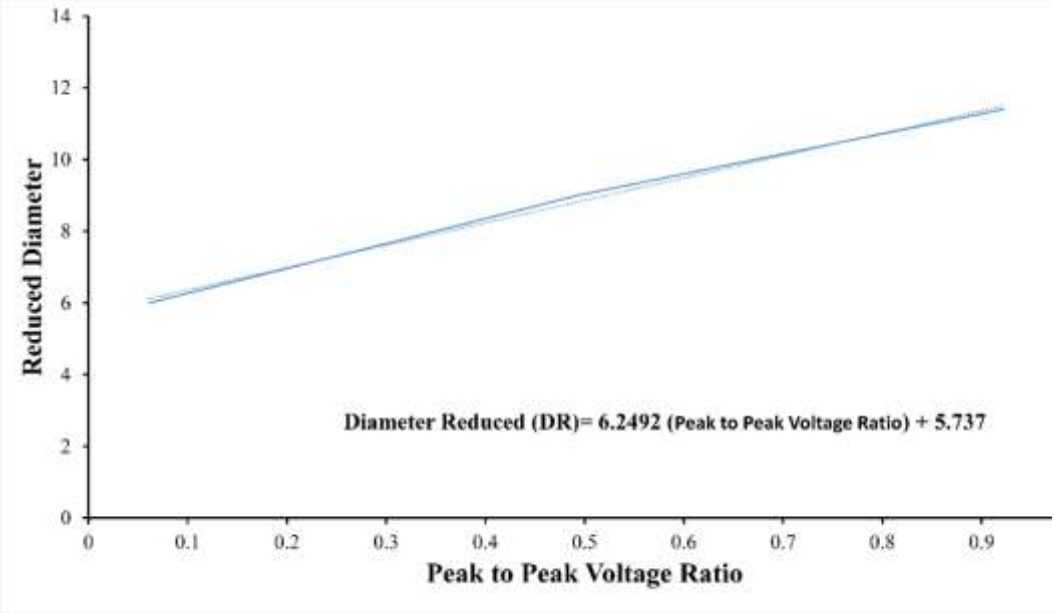

Figure 4.14. Actual reduced diameter Vs UGW Signal

Hence, UGW can be effectively used for picking up corrosion initiation and progression by using specific surface and core seeking guided wave modes. But it's important to note that GW are propagated through rebars in concrete and hence monitor the effect of corrosion in rebars only and not on surrounding concrete. It has been observed that UGW fails to identify corrosion in its initial stages and does not pin point the damage location. Hence, further AE technique is adopted to overcome these limitations of UGW along with IRT monitoring. AE has demonstrated potential in detecting initiation of corrosion along with its location. IRT gives a pictorial data which point out the exact location of damage beneath the surface. Thus combination of the

three NDT tools would lead to comprehensive damage monitoring strategy for rebars in concrete.

4.3.3 Acoustic Emission Monitoring

AE sensors were mounted on the surface of beam as briefed in Section 4.2.5 and **Figure 3.5**. It is important to note AE monitors the effects of corrosion in concrete as against UGW which measures deterioration in rebars only due to corrosion. AE parameters of cumulative AE hits, amplitude of AE hits and AE X-Y event plots are studied in detail to understand corrosion initiation and progression effects on surrounding concrete.

4.3.3.1. Cumulative AE Hits

Cumulative AE hits were recorded in concrete beams as it undergoes accelerated corrosion for 33 days (**Figure 4.15**). It is observed that AE hits start appearing right from the beginning of accelerated corrosion indicating initiation of micro-cracks due to corrosion in surrounding concrete. It is probably due to breakdown of passive layer leading to AE events of smaller amplitude in the surrounding concrete (delamination dominated zone) (**Figure 4.15**). AE hits increase up to 8 days slowly indicating the initiation stage of steel de-passivation resulting in micro-cracking in concrete in the beam. The average amplitude of AE hits in this initial stage ranges between 40-45 dB. This illustrates that AE monitoring effectively captures the corrosion activity right from the beginning while no significant change in UGW signal is observed (**Figure 4.13**) marked by slow increase in AE hits and relatively low amplitude indicating minor cracking in the surrounding concrete due to steel.

Further, AE hits increases at a faster rate with increase in corrosion beyond 8 days, indicating micro-cracking as a result of tensile pressure exerted by the rust product on the surrounding concrete. During this ***Phase-II Micro-Cracking Stage,*** a steep fall in peak to peak voltage ratio is also observed in UGW monitoring (**Figure 4.13**). Hence, Phase II of micro cracking indicates the transition phase where both delamination and pitting take place whereas in GW monitoring (from 8 to 19 day). In this stage, the average amplitude of AE hits lies the range of 55 dB to 70 dB which is higher than in phase I of AE monitoring (**Figure 4.16 b**). Further in 26 days a sudden sharp rise in AE hits is observed, pointing towards transformation of micro-cracks into macro-cracks in concrete leading to spread of corrosion in concrete and is termed as

Phase III Macro-Cracking phase of AE monitoring. It corroborates to pitting zone of GW monitoring where pitting dominates the corrosion mechanism and leads to macro-cracking in concrete. In this stage, amplitude of AE hits shows highest average value of 75 dB to 85 dB (**Figure 4.16 c**) pointing towards major AE activity in this zone. AE hits from 26 -33 days indicate a slow rise in AE events as major cracking has already occurred in Phase III. The AE hits recorded in this phase are due to the expansion of macro-cracks already present in the beam. Similar trends were observed in all other samples S8, S19 and S26. This indicates that the phenomenon of chloride induced corrosion is repeatable within experimental errors.

Hence, cumulative AE hits and their amplitudes provide a clear representation of initiation as well as progression of corrosion in the form of micro- and macro-cracking stages in concrete beams subjected to accelerated corrosion. AE hit plot correlates well with UGW for monitoring RC beam under corrosion but has over edge over UGW monitoring especially detecting initiation of corrosion in concrete along with its effect on surrounding concrete. UGW only measures the deterioration in rebars and doesn't reflect the effect on surrounding concrete which is more relevant for RC structures so that proper remedial measures can be taken before the corrosion reaches catastrophic level.

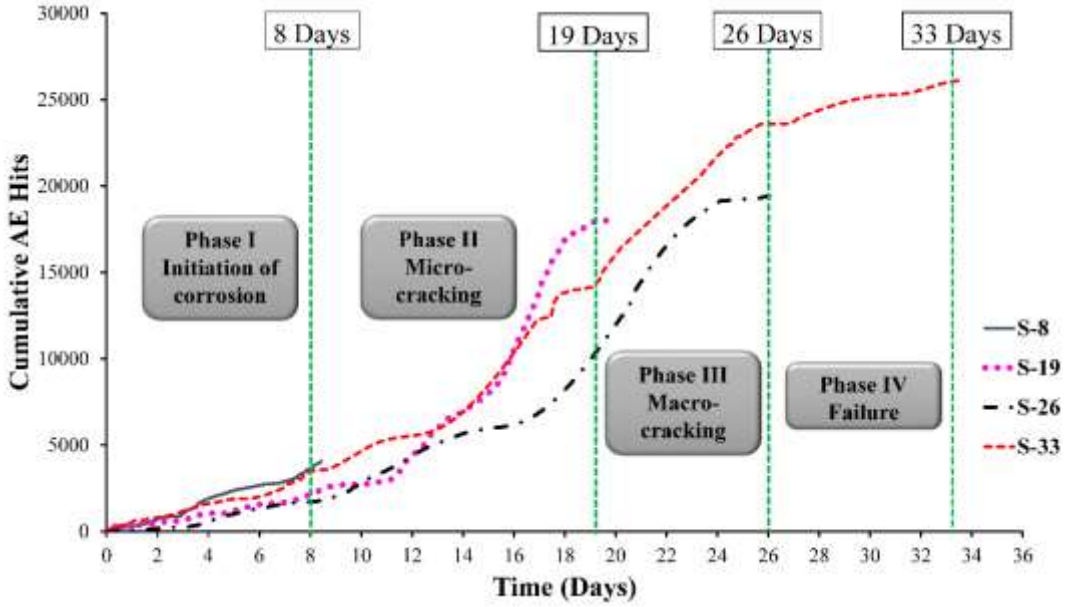

Figure 4.15. Cumulative AE hits Vs Time

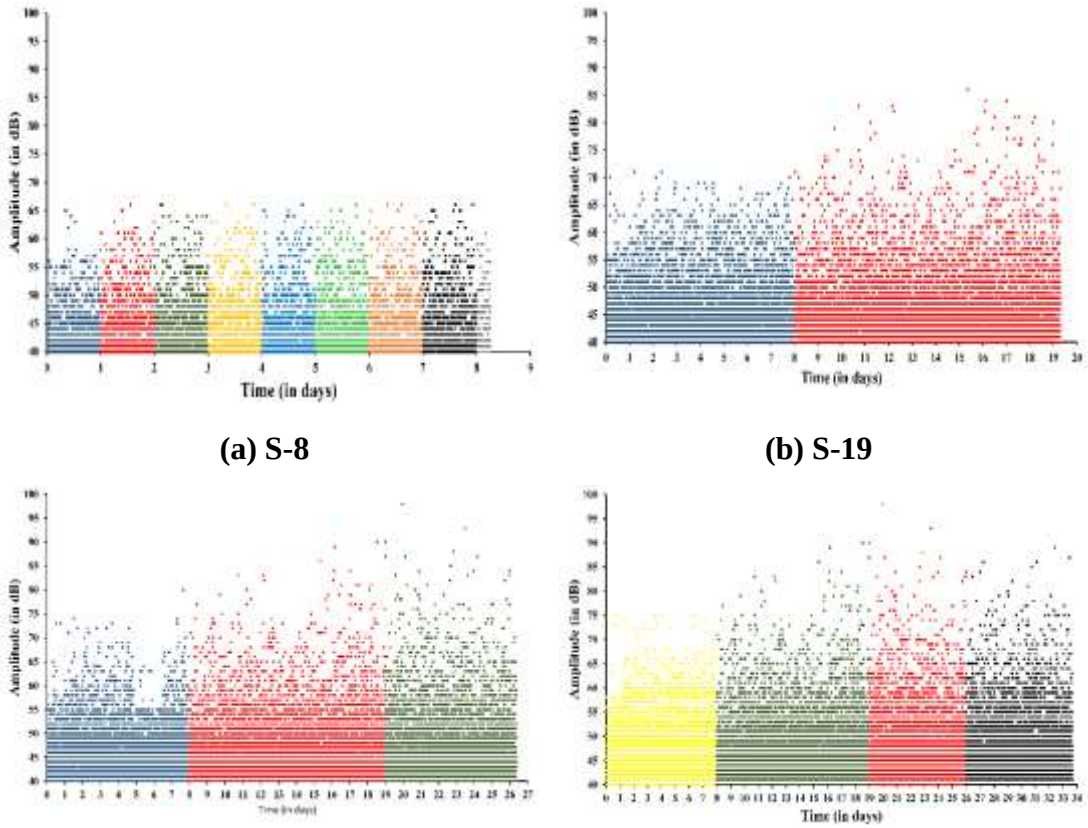

(a) S-8 **(b) S-19**

(C) S-26 **(d) S-33**

Figure 4.16. Amplitude of AE hits Vs Time

An attempt has also been made to relate AE activity in the form of percentage of AE hits with different phases of corrosion deterioration. About 20% of cumulative AE hits are observed to occur in Phase I representing initiation of corrosion. With increase in corrosion level, a major jump in percentage of AE hits is observed. In Phase II, about (~60-75%) AE hits are observed which represents major AE activity in the surrounding concrete as a result of micro-cracking. Further, constant increase in AE hits are observed until 95% of cumulative AE hits are recorded in Phase III of micro-cracking which indicates that most of the micro-cracks have coalesced into macro-cracks in their advanced stage of corrosion. These AE hits represents the expansion of micro-cracks into macro-cracks and ultimately leading to the failure of beam in Phase IV.

Further, the spread of AE activity in beams in X-Y direction is studied as AE X-Y event plots.

Table 4.1. Damage level in concrete due to corrosion

% AE hits	Damage Phase
14.5 to 16.3 %	I – Delamination Dominated Zone
60 to 75.24 %	II – Micro-cracking
75 to 95.02 %	III – Macro-cracking
Upto 100 %	IV - Failure

4.3.3.2 Damage localization using AE X-Y event plots

The pattern of cracking due to corrosion and its progression is represented and plotted in the form of 2-D AE X-Y event plots. The AE events recorded during the increasing corrosion exposure are pictorially represented at various stages (Figure 4.17). The red dots are the AE events recorded. AE events are primarily representative of cracking in concrete due to corrosion. The formation of voluminous rust product leads to tensile stresses in concrete. Concrete, being very poor in tension, cracks and energy is released as a result of cracking leading to AE events. In the initial stages of corrosion scattered AE events are being observed with no visual sign of cracks on the surface of beam, (Figure 4.17 a). This events are recorded due to minor cracking in surrounding concrete as a result of breaking down of passive layer on rebars in the initial stages of corrosion. After 8 days of accelerated corrosion (S-8) minor hairline cracks appear on the surface of concrete beam and the same is observed by increased red dots in AE event plot which continues till 19 days. In S-19 sample, a dense matrix of AE events is observed in the form of vertical and transverse loops as observed visually (Figure 4.17 b). From 19 to 26 days, a longitudinal crack at the centre is observed along with numerous transverse cracks throughout the length with reddish brown liquid oozing out of them (Figure 4.17 c). The same is represented by AE event plot which give a pictorial representation of cracks development in 2-D beneath the concrete surface. On further corrosion AE event map was crowded by events representing a major longitudinal crack along the length along with major transverse crack (Figure 4.17 d). Thus AE event plot provide a pictorial representation of initiation as well as progression of corrosion cracks inside concrete and well localizes the zone of major AE events where corrosion cracks are observed in actually corroding beams.

Hence, AE monitoring of RC structures for corrosion is successful in picking up initiation as well progression in the form of micro and macro-cracking in concrete along with pictorial representation of cracking evolution by AE event plots

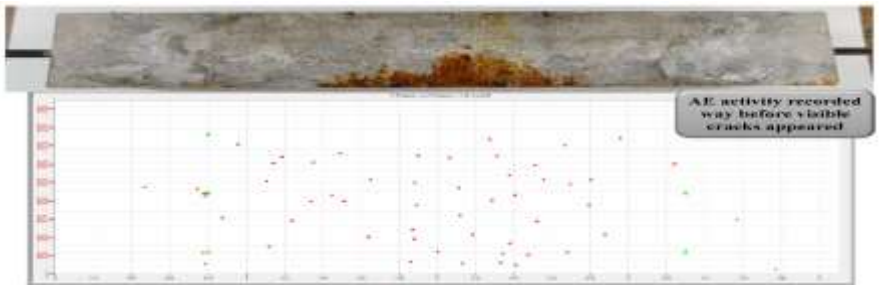

(a) S-8

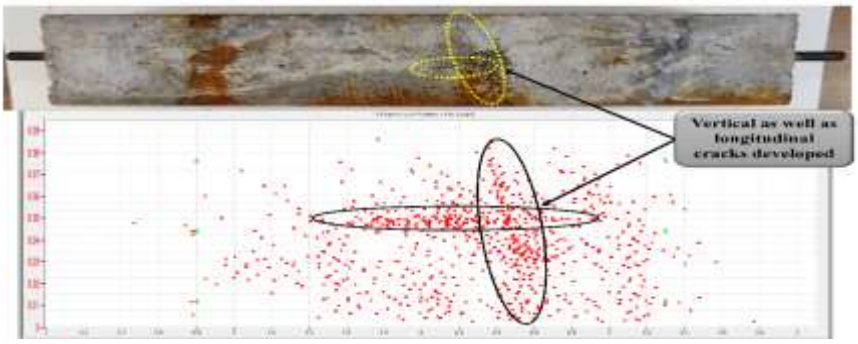

(b) S-19

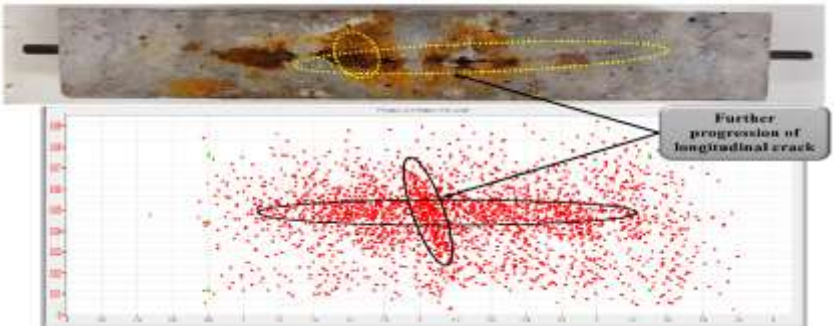

(c) S-26

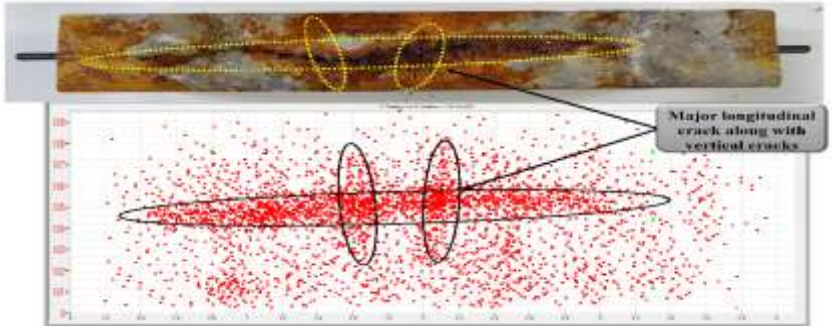

(d) S-33

Figure 4.17. AE X-Y event plot

4.3.4 IRT monitoring

IRT images were taken continuously for the corroding beams at regular intervals to illustrate sub-surface damage in the concrete beams or in embedded rebar's due to corrosion. **Figure 4.18 (a)** represents the IRT image in the healthy beam which uniform surface temperature noticed around the rebar which indicates healthy condition of rebar. **Figure 4.18 (b-e**) represent the IRT images of the beam sample at different degrees or levels of corrosion damage. IRT image of S-8 sample after 8 days of corrosion indicates no major surface temperature difference since there is only scaling off and minor initiation of corrosion as observed visually from the extracted bars from S-8 beam. But IRT images does indicate minor surface modification (**Figure 4.18 b**). Further as corrosion proceeds in S-19 beam, a considerable surface temperature variation is observed indicating signs of corrosion at various places of rebar and at the beam ends of rebar (**Figure 4.18 c**) in the form of temperature gradient. The damage portion is also represented by different color as rate of dispersing heat of corroded material is different as that of steel. In S-26 beam, major temperature difference is observed as corrosion activity is at its peak which are represented by red spots indicating pitting of rebar (**Figure 4.18 d**). For S-33 beam as a result of corrosion a large longitudinal crack appears on the surface which is also clearly distinguished by IRT image (**Figure 4.18 e**).

Hence, IRT imaging of bars undergoing corrosion in concrete is not only able to pick up initiation of corrosion but also its spread and actual location as corrosion progresses as indicated by color and temperature gradient in the thermography images. IRT clearly localizes the region of damage and also picks up consequential cracking in concrete (**Figure 4.18 e**) clearly observable as a major corrosion crack. This crack was observed in IRT image after 33 days of corrosion.

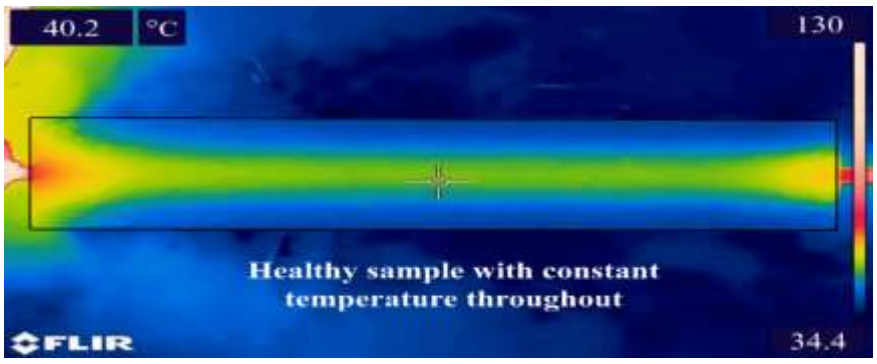

(a) Healthy RC beam

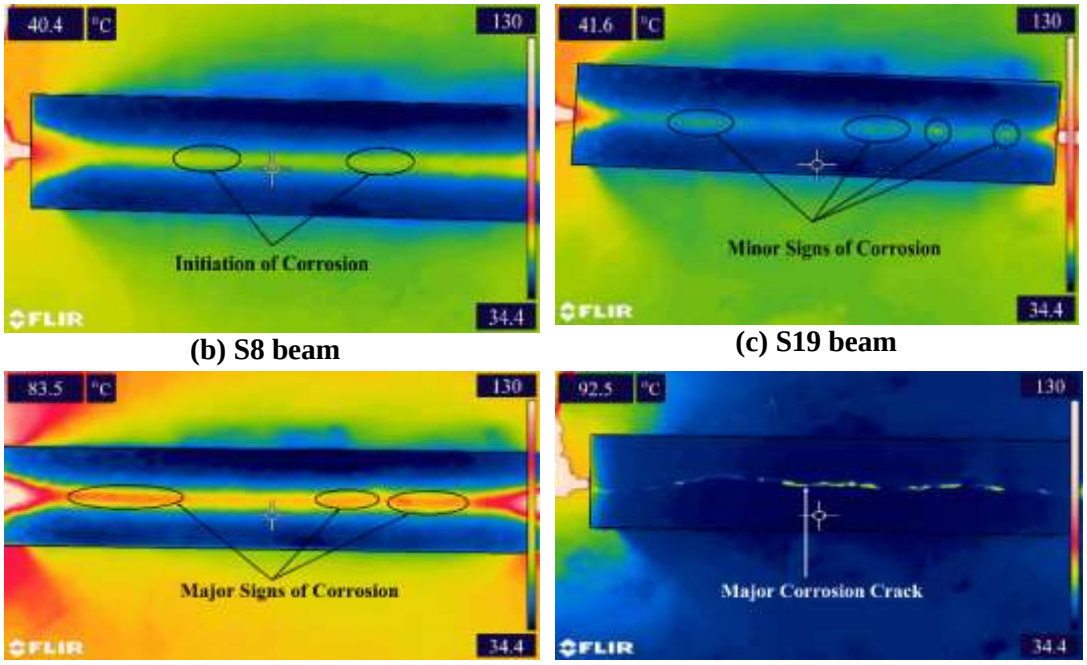

(b) S8 beam **(c) S19 beam**

(d) S26 beam **(e) S33 beam**

Figure 4.18. IRT images of RC beams on different time intervals

4.4 COMPARISON OF DAMAGE WITH TEMPERATURE PROFILE

The bars with Simulated Damage (1 and 2) and beams subjected to accelerated impressed current corrosion were monitored using Infra-red Thermography as discussed above. It has been observed that with increasing damage, there is a visible change in temperature profile of each specimen. Hence, this correlation is plotted with increasing damage in **Figure 4.19**. For the bars with simulated pitting damage, it is observed that there is steep rise in the surface temperature with increasing pitting level when bars are monitored in air as well as when embedded in concrete (Figure 4.19a). Similar variation in temperature profile is observed with simulated debond damage for bars in air but there is a very minor variation in temperature when bars with debond damage are embedded in concrete (Figure 4.19b). This may be due to the dispersion of heat in highly attenuative surrounding concrete. Thus, it can be concluded that to detect initiation of corrosion (debonding of bar from surrounding concrete) using other NDT techniques along with IRT.

Further in RC beams subjected to accelerated corrosion, it is observed that there is insignificant change in temperature profile of beam upto 10days (Small corrosion level) but with increase in corrosion, from surface scaling to pitting, there is a drastic change in surface temperature from 40ºC to 92ºC. Hence, it can be concluded that variation in

temperature profile in RC beams subjected to actual corrosion conditions can serve as an indicator of deterioration due to corrosion at later stages (Figure 4.19c).

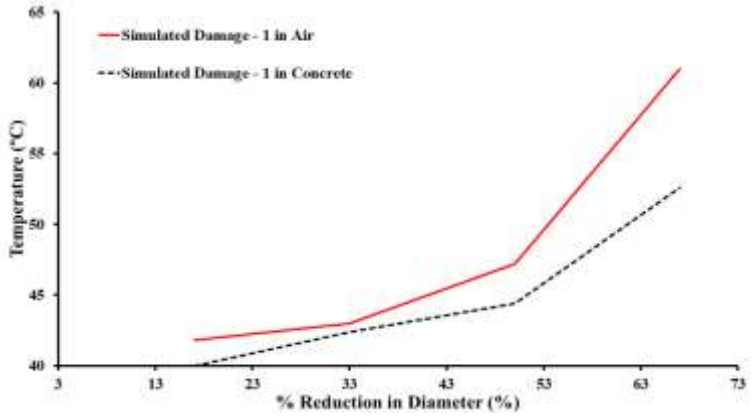

(a) Change in temperature for simulated Damage – 1 (Pitting)

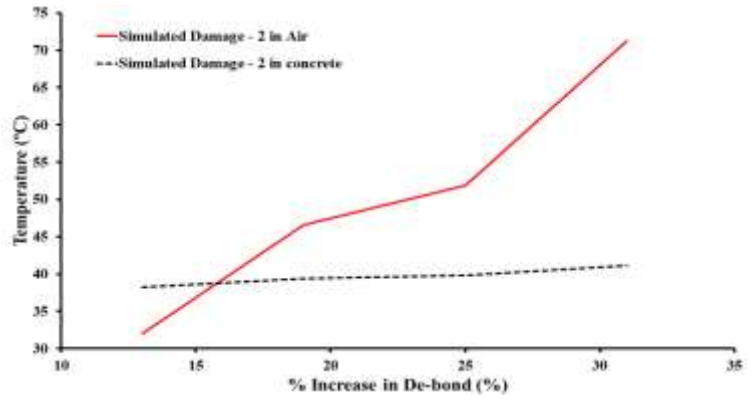

(b) Change in temperature for simulated Damage – 2 (De-bond)

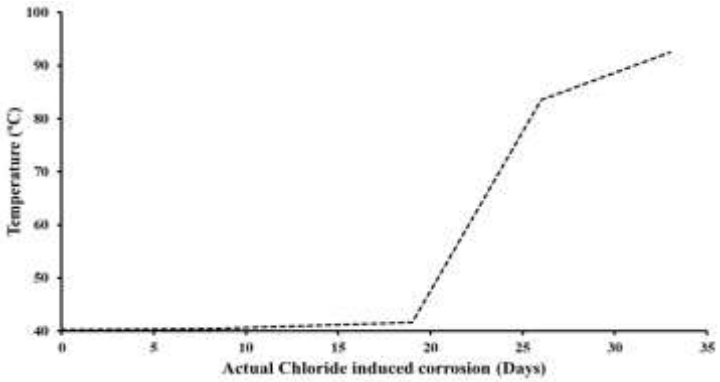

(c) Change in temperature wrt to Accelerated corrosion

Figure 4.19. Variation in temperature with increasing damage

4.5. COMPARISON OF NDT TOOLS

This work proposes a combined monitoring methodology for real time corrosion damage detection in RC structures. UGW for monitoring of rebar condition monitoring, AE for consequent cracking in surrounding concrete due to corrosion and

further IRT for imaging the deterioration in steel rebar's as well as concrete is suggested as NDT tool for monitoring corrosion in RC structure. UGW fails to pick up corrosion in the early stages and provide only likelihood of corrosion initially. It also requires the exposure of rebars at the end for monitoring condition of corroding beam. On the other hand, AE sensors are surface mounted on concrete structure for passive monitoring. It has the advantage of giving indication of initiation of corrosion along with damage progression. Also it has advantage of monitoring effect of corrosion on surrounding concrete. Additionally, AE monitoring of the structure does not disturb the working of structure. But AE sensors are to be mounted throughout the process of monitoring while UGW probes are mounted as and when observation are made. AE has also successfully gives a pictorial representation of AE events indicating corrosion cracking and damage state in the corroding RC beams. Amplitude of AE hits are also indicator of damage level in surrounding concrete.

IRT has the advantage of proving thermal images making use of temperature difference of material and air gaps developed due to corrosion to distinguish damage. It gives a clear pictorial representation / photograph of bars as well as surrounding concrete. Hence, judicious combination of active UGW and passive AE monitoring along with optical IRT serve as a potential health monitoring strategy to monitor corrosion right from its initiation to progression in RC structures.

4.6 CLOSING REMARKS

The chapter reports a combination of 3 non-destructive techniques based on wave propagation principles and thermographic imaging for corrosion in concrete before it is visible on surface. Bars with simulated damage (Damage 1 and 2) were monitored using Ultrasonic Guided Wave along with Infrared thermography in air as well as in concrete. Healthy bars of diameter 12 mm were cast in concrete beam and were subjected to accelerated corrosion and were simultaneously monitored using surface mounted AE sensors, ultrasonic guided waves and Infrared thermography. These results of simulated damage and actual corrosion using different NDT techniques were correlated and expression were derived. Also the effectiveness of 3 non-destructive tools of AE, UGW & IRT for real time corrosion monitoring is explored.

CHAPTER 5

MONITORING CORRODED AND CORROSION REPAIRED RC BEAMS USING VIBRATION MONITORING

5.1 GENERAL

Real size RC beams of 127 x 227 x 4100 mm were subjected to varying degrees of corrosion (10, 20, 30 and 40 days) and their vibration signatures are recorded using impact hammer set up. One set of corroded beams are subjected to different levels of corrosion repaired with GFRP sheets (R-10, R-20, R-30 and R-40) and also subjected to vibration monitoring to record the dynamic characteristics. Corroded and GFRP repaired corroded beams were further subjected to four-point flexural loading and their performance due to increasing corrosion and GFRP repair is assessed. Finally, an attempt has been made to correlate the Damage Index obtained from vibration diagnostic with ultimate load carrying capacity in corroded as well as GFRP repaired corroded beams obtained from flexural loading.

5.2 MONITORING DAMAGE IN CORRODED AND REPAIRED BEAMS

5.2.1 Visual Observations

Visual inspection of all corroded beams (C-10, C-20, C-30 and C-40) was done to determine the level of damage due to corrosion. Minor signs of corrosion were observed in C-10 beam with reddish brown patches at few places on the surface with very few minor hairline cracks (**Figure 5.1 a**). The number of these minor-cracks and reddish liquid oozing out these cracks increased in C-20 (**Figure 5.1 b**). Further C-30 beam, indicated severe corrosion damage as minor transverse cracks were also seen in addition to longitudinal cracks with widespread corrosion product oozing out of these cracks. Another significant change observed was the change in the colour of rust product from reddish brown to brownish -black pointing towards severe corrosion (**Figure 5.1 c**).

In C-40 beam, along with numerous transverse cracks a major longitudinal crack parallel to tensile reinforcement was observed (**Figure 5.1 d**). These cracks developed were as a result of tensile force exerted by the corrosion product on the concrete. Hence, as the level of corrosion increases, colour of rust product changes its colour from reddish brown to black which is an indicator progression of corrosion damage beneath the surface. Along with this development of micro-cracks and their transition to

transverse cracks along with longitudinal crack is a clear representation of severity of damage due to corrosion.

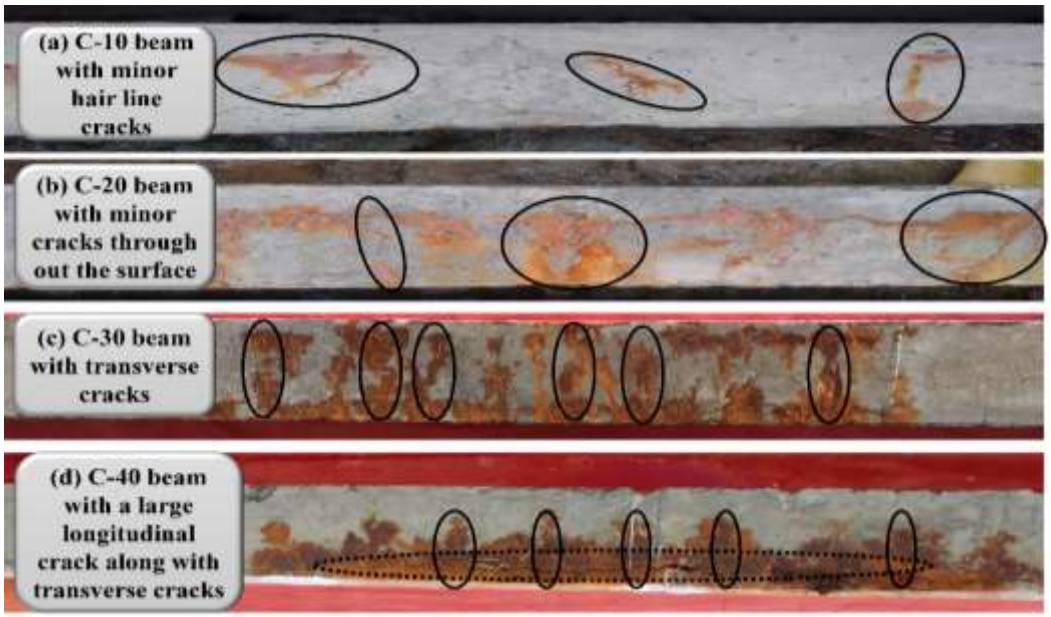

Figure 5.1. Beams corroded to different levels of accelerated corrosion

5.2.2 Corrosion Current

To ascertain the level of corrosion in various RC beams subjected to impressed current corrosion in chloride environment, corrosion current was recorded after every day. The increase in the corrosion current at constant voltage is an indicator of increasing corrosion of bars in concrete (**Figure 5.2**). Along with this RC beams were visually inspected to relate to various signs of corrosion. The corrosion current initially rises very slowly for 1-2 days and then becomes constant for 5-6 days owing to the resistance offered by the passive layer of oxides on rebar. Further the corrosion current increases steadily from 6 up to 32 days indicating the breakdown of passive layer by chloride ions and initiation and consistent progression of corrosion. A sudden jump in corrosion current values is observed at day 34 pointing towards severe damage to main steel in the form of pitting. It was observed that breach of passive layer and initiation of corrosion as depicted by rise in corrosion current was also confirmed by reddish brown liquid oozing out from various hair line cracks at different stages of corrosion. With increasing corrosion levels and progression of corrosion, the spread and width of cracks increased and change in colour of corrosion product from reddish brown to black was observed.

To quantify various level of corrosion, theoretical mass loss is calculated using Faradays' law which is compared with the actual mass loss experienced by the extracted bars after undergoing different extents of corrosion. In order to calculate actual mass loss, tensile and compression bars were extracted after flexural testing. Concrete and corrosion product stuck on the surface of bars was cleaned and then bars were thoroughly washed using acetone and the residual mass was noted. The extracted bars were also tested in fully compressed servo- controlled Universal Testing Machine (UTM, Hung Ta Instrument, Make, Taiwon of capacity- 1000 kN) for residual tensile strength measurements with increasing corrosion.

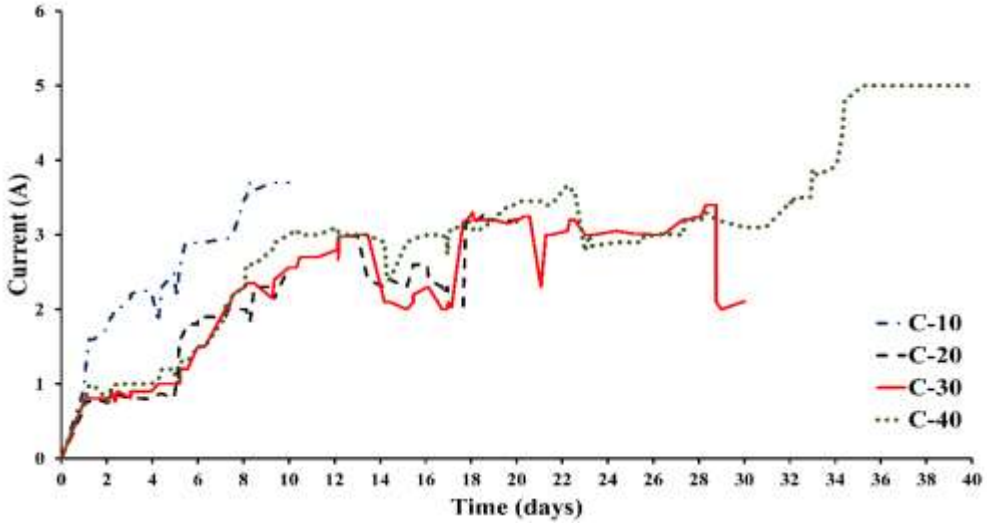

Figure. 5.2. Impressed corrosion current variation with time

Table 5.1. Destructive Test Parameters at varying corrosion levels

	Average mass loss (%)	Theoretical mass loss (%)	Ultimate Tensile Strength (N/mm^2)	Loss in Ultimate Tensile Strength (%)
C-0	0	0	680.7	0
C-10	8.3	7.8	512.4	24
C-20	11.4	10.5	481.1	29
C-30	24.3	21.9	371.9	45
C-40	33.2	34.9	326.2	52

Table 5.1 exhibits the actual as well as theoretical mass loss experienced by reinforcing bars at different stages of corrosion which closely match with each other. A distinguishing observation is significant fall in tensile strength as against relatively

small drop in mass loss. After 10 days and 20 days of accelerated corrosion, 8.3% and 11.4% mass loss is observed with significant 24% and 29% drop in tensile strength respectively. Similarly, in C30 and C-40 beam samples, 24.3% and 33.2% mass loss is observed with huge 45% and 52% loss in tensile strength respectively. This is very alarming and misleading as mass loss is insignificant in comparison to loss in tensile strength and can lead to catastrophic failures before giving an impending warning. Hence, it becomes very pertinent to monitor damage at different stages of loading to know the level of damage so that remedial measures can be taken at nascent stages.

5.2.3. Vibration Characteristics

For control, corroded and GFRP repaired corroded RC beams, changes in the dynamic characteristics with increasing damage and further repair is studied using global vibration diagnostics. The structures are made up of components possessing finite level of stiffness, rigidity, mass and non-perfect energy transfer characteristics. These properties are characterized by physical properties of structure such as Young's modulus, shear modulus, bulk modulus and mass distribution. As a result of damage and deterioration, there is change in mass and stiffness of the structure which directly influences the E and I of the structure leading to change in the modal parameters including FRF response. The FRF response is the function of these modal parameters and is studied for evaluation of damaged and repaired beams. The FRF signals obtained from corroded and corrosion repaired beams are compared with the baseline signal obtained from the control healthy beam to relate to the level of deterioration in corroded beams and further their improvement in characteristics in repaired beams. Experimental frequency of control beam (18 Hz) was observed very close to the theoretical fundamental frequency (19 Hz), indicating the accuracy of testing.

- ***Corroded Beams***

Figure 5.3 shows the FRF response of beams subjected to increased level of corrosion. **Table 5.2** represents the vibration characteristics of the corroded RC beams obtained from FRF plots. It is observed that with increasing corrosion damage, 7.4% drop in FRF signal amplitude is observed in C-10 beam as compared to C-0 beam with no significant shift in frequency. This may be due to improvement in bond between steel and the surrounding concrete as a result of formation of voluminous corrosion product having volume 4-6 times the original steel.

Table 5.2. Vibration characteristic of Corroded Beams

	Natural Frequency (Hz)	Amplitude ($m/s^2/N$) X 10^{-2}	Damage Index wrt FRF amplitude(%)
C-0	18	6.99	0
C-10	18	6.47	7.4
C-20	17	6.12	12.46
C-30	16	5.53	20.86
C-40	15	4.26	39.05

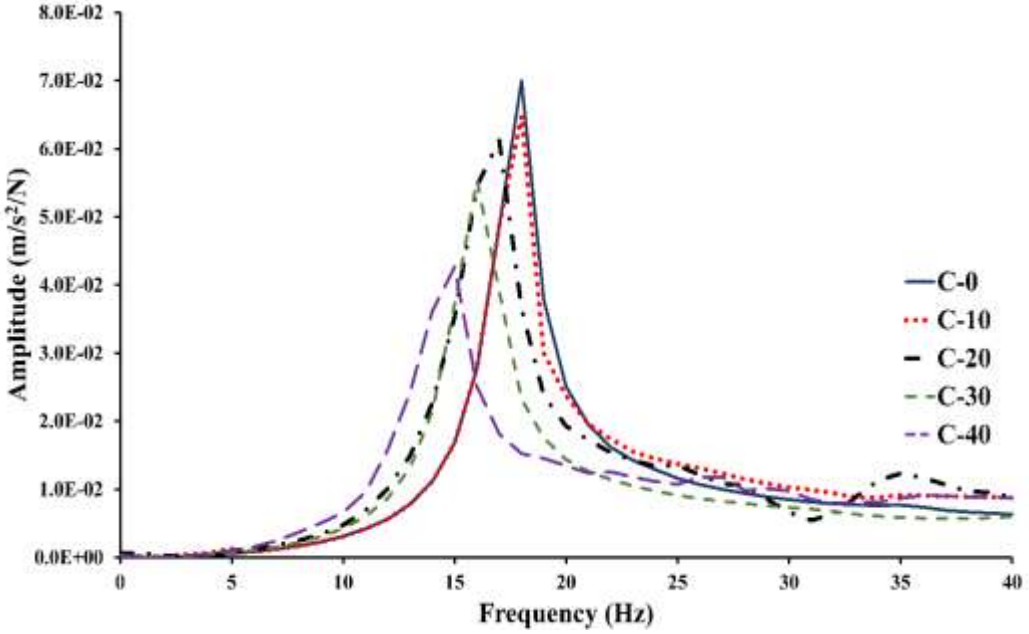

Figure. 5.3. FRF response of Corroded Beams

Further, in C-20 beam, a shift of 6.55% in fundamental frequency towards lower side is observed with a drop of 12.46% in FRF amplitude. It may be due to attenuation effect of voluminous corrosion product on vibration signals as well as due to development of micro-cracks at steel concrete interface due to expansive corrosion product since concrete is weak in tension which reduces the overall FRF amplitudes. With further increasing level of corrosion, in C-30 beam, an increased shift of 11.11% in fundamental frequency and drop of 20.86% in FRF amplitude is observed. Numerous cracks were observed due to tensile force exerted on the concrete by rust product. In heavily corroded C-40 beam, the integrity of beam is highly compromised, which leads to an alarming shift of 17% in fundamental frequency and drop of 39% in FRF amplitude.

To know the extent of damage in a structure, damage assessment is necessary which is done by calculating the Damage Index (DI). This index depends upon the specific damage parameters such as structural stiffness, strength degradation, stiffness degradation, deformation, energy dissipation and dynamic properties of structure. Various researchers developed different damage indexes depending upon specific dynamic properties, such as change in the natural frequency, mode shape and Frequency Response Function (FRF) [145] presented a damage index based on the change of frequency ratios. This method considers fundamental structural frequencies before and after damage. The authors concluded that if the new vibration signature obtained during a routine operation deviates from that of the baseline value, then the structure should be checked for possible local defects developed the Modal Flexibility Damage Index. [146] This index compares flexibility matrices from two sets of mode shapes [106] presented an FRF-based mode shape method that uses FRF data taken directly from structures without any intermediate steps. Typical vibration identification assumes that the dynamic property of a structure is a sensitive indicator of its physical integrity. When any of the properties like mass, stiffness, or damping of the structure changes due to a structural defect, the vibration response of the structure will also change concluded that the magnitude of FRF decreases with the increase in the level of damage in the RC building model [147]–[149]. There is large reduction (more than 50%) in FRF magnitude at state of first visible crack.

FRF based damage index is one of most effective way to relate to the health of the structure at different stages of damage. The change in fundamental frequency and magnitude of FRF of a system defines the damage extent and behaviour. So to assess and quantify the level of corrosion cracking in the RC beams, in this work FRF based Damage Index (DI) based on variation in FRF magnitude is used[57]. It is because change or shift in fundamental frequency vis-à-vis the extent of corrosion damage was not as significant as drop in FRF amplitude with increasing corrosion.

$$D.I\ (\%) = \frac{A_o - A_i}{A_o}\ X\ 100 \qquad (5.1)$$

Where: -

Ao = amplitude of healthy sample, Ai = amplitude of corroded beam

From Table 5.3, it is observed that DI increases for corroded beams with increasing corrosion levels from 7.4 % in C-10 to 39.05%in C-40 beam. With increasing corrosion level, corrosion cracks extend from steel-concrete interface to surrounding concrete and upto surface. This widespread cracking in concrete dissipates the vibration signal leading to fall in FRF amplitudes. Thus, as the damage due to corrosion increases, there is a drop in FRF amplitude of the vibration signal from 6.99 x 10^{-2} for C-0 beam to 6.47 x 10^{-2} for C-10, 6.12 x 10^{-2} for C-20, 5.53 x 10^{-2} for C-30 and 4.26 x 10^{-2} for C-40 beam leading to increase in DI from 7.4% for C-10 to 39.05% for C-40 beam. Hence, FRF magnitude based DI measures and quantifies the extent of deterioration caused by increasing corrosion in RC beams based on dynamic characteristics and can be used as a potential indicator of integrity of structures.

Hence, it can be concluded that with the increase in the level of corrosion, a shift in fundamental frequency is towards lower side along with a drop in FRF magnitude is observed pointing towards increasing degradation and damage due to cracking in concrete caused by increased corrosion exposure. Vibration monitoring can effectively pick up degradation due to increasing corrosion in RC beams marked by reduction in fundamental frequency and drop in FRF amplitudes well quantified by increasing DI values.

- ***GFRP repaired corroded Beams***

RC beams corroded to different levels were repaired using GFRP wraps and subjected to vibration monitoring. A significant improvement in fundamental frequency and FRF amplitudes was observed after repairing the corroded RC beams with GFRP wrapping (**Figure 5.4 and Table 5.3).** Damage index is also computed for repaired beams vis-à-vis with respect to original corrosion level.

Corrosion repaired R-10 beam shows an increase of 6.26% and 8.2% in fundamental frequency and FRF amplitude respectively in comparison to originally corroded C-10 beam. Also in comparison to the control beam (C-0), an increase of 6.26% and 0.85% in fundamental frequency and FRF amplitude respectively was observed in R-10 beam (**Figure 5.4 a**). This point out the fact that GFRP repaired corroded beam outperformed even the healthy beam which indicates the effectiveness of GFRP wrapping in corroded beams.

An improvement in the vibration parameters after repair of corroded beams occurs due to confinement of the cracked and damaged concrete by micro-concreting followed by GFRP wrapping. It leads to the improvement in the structural integrity of corroded specimens after repair. Similar observations are made with R-20 beam which shows an increase of 6.55% in fundamental frequency and 10.91% in FRF amplitude in comparison to originally corroded C-20 beam. (**Figure 5.4 b**). R-30 and R-40 beams also exhibited improved fundamental frequency and FRF amplitude in comparison to corroded C-30 and C-40 beams. While R-30 beam shows an increase of 6.88% and 14.56% in fundamental frequency and FRF amplitude in comparison to C-30 beam (**Figure 5.4 c**), R-40 exhibited an increase of 6.25% and 27.79% in fundamental frequency and FRF amplitude respectively in comparison to C-40 beam (**Figure 5.4 d**).

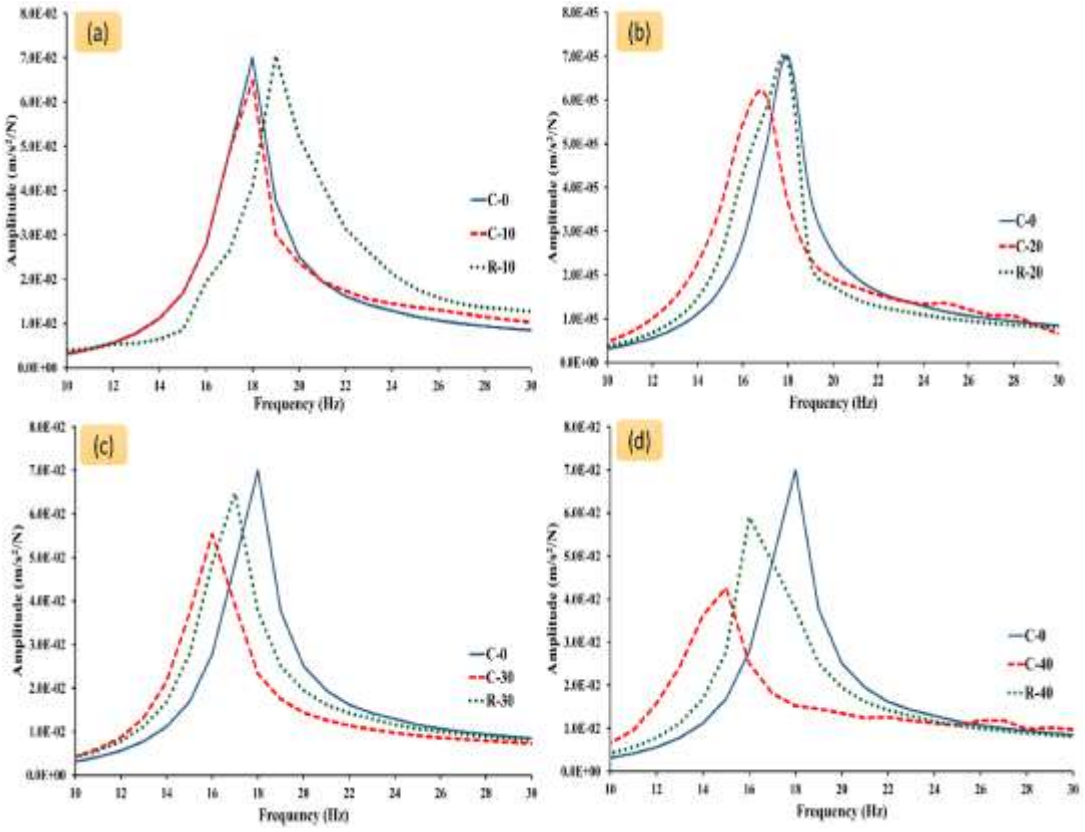

Figure. 5.4. Comparison of FRF signals of corroded and corrosion repaired beams

But the FRF magnitudes recorded in severely corroded C-30 and C-40 beams and further repaired beams was less in comparison to the original control beam. This indicates that even after repair with GFRP wraps, the original strength could not be recovered since these beams were in a highly dilapidated condition and steel rebars as

well as the concrete matrix was badly deteriorated. Beams couldn't recover their original strength and integrity even by replacing damaged concrete by high strength micro-concrete and GFRP wrapping.

Table 5.3. Vibration characteristics of GFRP repaired corroded beams

	Natural Frequency (Hz)	**Amplitude ($m/s^2/N$) X 10^{-2}**	**Damage Index wrt FRF amplitude (DI)**
C-0	18	6.99	0
R-10	19	7.05	-0.8
R-20	18	6.87	1.68
R-30	17	6.48	7.37
R-40	16	5.82	16.63

From **Table 5.3**, decreased DI values of repaired specimens as compared to corroded specimen depict the enhanced strength and integrity of RC beam. In R-10 and R-20 beam DI measured is -0.8 and 1.68 which represented their behaviour is almost equivalent to a healthy beam. Similar improvement in performance after repairing severely corroded beam R-30 is observed. In severely corroded and then repaired beam R-40 beam, a drop of 60 % in DI value is observed as compared to C-40 which is impressive but a Damage Index of 16.63 is on a relatively higher side. It indicates that the repair of corroded beams with GFRP wrapping will be most effective when the reinforced concrete structures are not heavily corroded and compromised. Hence, regular monitoring of RC structures for corrosion damage should be done so that proper remedial measures could be adopted well within time to prevent catastrophic damage. Vibration monitoring technique thus, has the potential to monitor integrity of RC structures for corrosion assessment even when they are repaired with GFRP wraps.

Hence, it can be concluded that vibration monitoring for system identification and damage detection can be applied to RC beams undergoing increasing levels of corrosion as well as can be effectively used for monitoring their performance when the RC beams are further strengthened and repaired against corrosion by GFRP wrapping. The variation in dynamic characteristics of FRF amplitudes and frequency is a good indicator for monitoring of condition of pre- and post-repair of RC structures subjected to corrosion. Thus, vibration monitoring technique scan serve as global health monitoring tool for investigating the performance of GFRP repaired RC structures also along with local techniques to localize damage regions.

5.3 FLEXURAL TESTING

5.3.1 Load- deflection Characteristics

All ten RC beams (one healthy, corroded and corrosion repaired beams) were tested under four-point bending. Load-deflection characteristics were observed to determine the change in ultimate load and deflection with the increase in corrosion level and effect of GFRP repairing in restoring the strength so as to relate the non-destructive global measurement parameters with actual condition of the beams.

Control beam (C-0) when tested in bending exhibited pure flexural failure at an ultimate load of 46.95 kN and deflection of 81.05 mm. The load-deflection plot shows two specific phases namely - Linear phase and Plastic phase. During initial stages of loading minor hairline cracks are observed on the tensile surface at a load of 7 kN. These hairline cracks became visible at a noticeable deflection of 14 mm and a load of 19kN. This linear trend continued until proportional limit of steel is reached at a load of 37 kN (**Figure 5.5**) and the corresponding zone is referred as Cracked Linear Zone. On further loading, the cracks spread and get distributed throughout the beam pointing towards steel yielding, which is also represented by minor increase in load corresponding to major increase in deflection. This zone is referred as Cracked Plastic Zone. Ultimately the control beam fails in pure flexure with concrete crushing in the compression zone and steel yielding in tension zone.

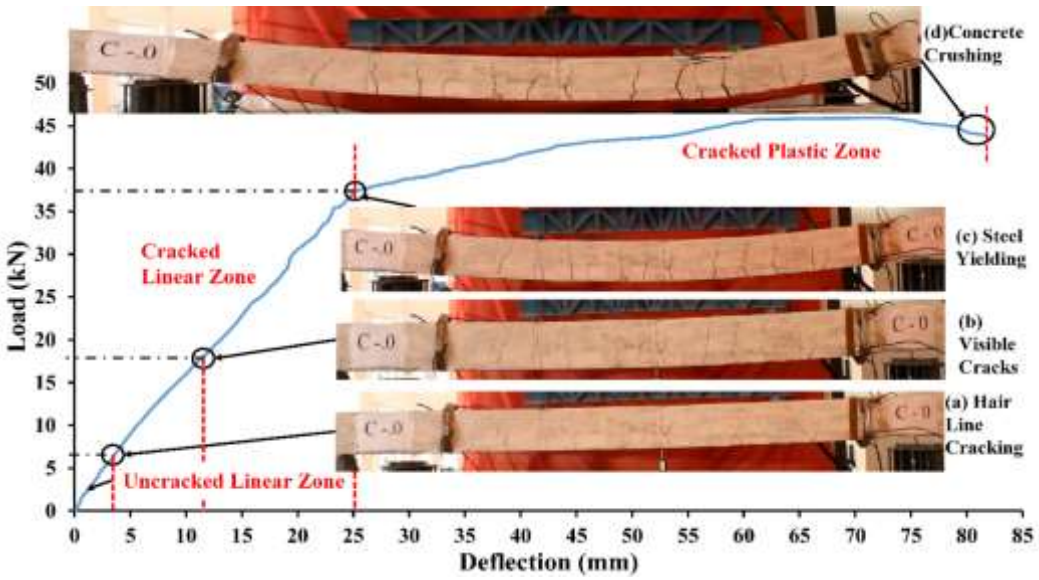

Figure. 5.5. Load deflection characteristics of control beam (C-0)

- ***Corroded Beams***

RC beams corroded to varying levels of corrosion, when subjected to flexural loading exhibit fall in ultimate loads and deflections with increase in corrosion level. In C-10 beam, a significant drop of 24.6% in ultimate load and 14.37% in deflection is observed in comparison to control beam (C-0) (**Figure 5.6 a**). This drop in ultimate load and mid-span deflection with minor hairline cracks on surface represents the deceptive behaviour of corrosion. Similarly, with few visible corrosion cracks in C-20 beam, a huge drop of 36.34% in ultimate load and 34.85% in mid-span deflection is observed in comparison to C-0 (**Figure 5.6 b**) (**Table 5.4**).

Table 5.4. Load-Deflection characteristics of beams

Samples	**Corroded beams**		**Samples**	**GFRP repaired beams**	
	Ultimate load (kN)	**Ultimate deflection (mm)**		**Ultimate load (kN)**	**Ultimate deflection (mm)**
C-0	46.95	81.05	**-**	-	-
C-10	34.63	69.4	**R-10**	46.3	96.28
C-20	29.25	52.8	**R-20**	42.5	91.83
C-30	20.24	46.39	**R-30**	32.02	77.31
C-40	14.94	30.95	**R-40**	26.73	50.44

Further, in case of heavily corroded beams (C-30 and C-40), a sudden brittle failure is observed which is alarming. In C-30 beam, corrosion cracks integrated to form a large vertical cracks and the beam ultimately failed suddenly at a load of 20.24 kN with an ultimate deflection of 46.39mm (**Figure 5.6 c**). In comparison to control beam, a drastic drop in load and deflection of 56.9% and 43.9% respectively is observed, which is very huge and alarming. Finally, in heavily damaged C-40 beam a sudden brittle failure is observed at an ultimate load of 14.95 kN and 30.95 mm mid-span deflection (**Figure 5.6 d**). Thus it clearly demonstrates the unpredictable behaviour of corrosion and its adverse effects which could ultimately lead to catastrophic failures if not intercepted at the right time and a proper remedial measure is not initiated.

Hence, corrosion, as expected, causes deterioration in the RC beams as depicted by a drastic fall in load carrying capacity with an increase in corrosion levels. Even at

initial stage of corrosion as identified visually, there is a considerable drop in the load carrying capacity of the beam, which is very misleading. Hence, it becomes mandatory to monitor and assess the damage in RC structures for corrosion, so that proper re-strengthening can be done before it leads to catastrophic failures ***GFRP repaired corroded Beams***

Corroded RC beams with varying level of corrosion were repaired with micro-concrete and GFRP wrapping when subjected to flexural loading showed enhanced load carrying capacity as compared to originally corroded beams. As a result of wrapping, change in the mode of failure is also observed from brittle failure (concrete crushing) to ductile failure (debonding of GFRP sheets). A tremendous increase in number of cracks in repaired beams was also observed as compared to corroded as well as control beams. This is attributed to the strain-hardening and multiple cracking characteristics of micro-concrete due to its micro structure in the repaired beams.

R-10 and R-20 beams reported impressive results as compared to original corroded beams (C-10 and C-20) marked by increase in load carrying capacity by 33.69% and 46.29% along with increase in mid-span deflections by 37.29% and 73.92% (**Figure 5.6 a&b**). The improved performance of GFRP repaired corroded beams is due to strengthening effect of high strength micro-concrete along with GFRP sheets which not only provides strength but also gives confinement to the beams, which enables them to behave as a single intact unit.

In heavily corroded RC beams (R-30 and R-40) an increase in ultimate load of 58.20% and 78.91% along with 70.32% and 62.97% increase in mid-span deflection in comparison to C-30 and C-40 beams is observed (**Figure 5.6 c&d**). When compared with the control beam (C-0), reduced ultimate load by 30.31% and 41.8%, and the deflection by 4.6% and 37.7% was observed. Thus drop in ultimate load and defection for R-30 and R-40 demonstrate the inadequacy of repair at this stage of corrosion. Hence, it is recommended to arrest corrosion in its early stages before it leads to a catastrophic failure. It is only possible if initiation and progression of corrosion at various stages of loading can be picked up by non-destructive testing tools like global vibration monitoring tools or local monitoring tools like Acoustic Emission as explained in chapter 6.

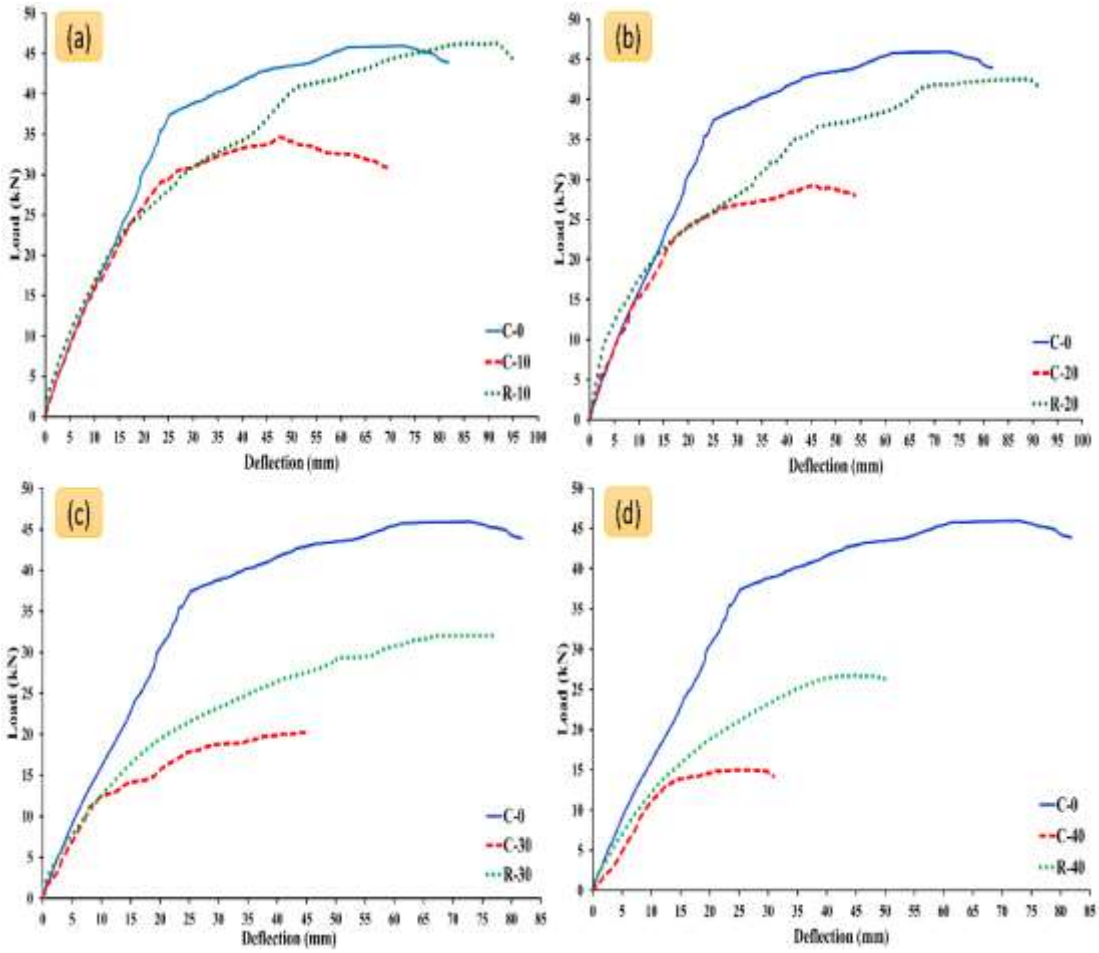

Figure 5.6. Load-Deflection characteristics of corroded and repaired beams

5.4 CORRELATION BETWEEN DI AND ULTIMATE LOAD

5.4.1 Corroded Beams

To assess the condition of RC beams at different levels of corrosion, an attempt is made to correlate vibration characteristics in the form of Damage Index (DI) with destructive parameters of ultimate load carrying capacity to facilitate non-destructive testing evaluation of corroding RC beams and further when they are repaired with GFRP wrapping.

As RC beams were corroded at different levels, a drop in ultimate load was observed. In C-10 beam, with few signs of corrosion, drop of 24.63% in ultimate load was observed. This fall in ultimate load with the increase in corrosion level was observed upto 67.48% for C-40 beam. This can be directly correlated with a consistent drop in FRF magnitude reported as DI (Equation 5.1) since the shift in frequency was

not as significant and prominent as fall in amplitudes with increasing corrosion level in RC beams (Refer **Table 5.2**).

A linear empirical correlation is established between ultimate load and DI (**Figure 5.7**) as given by the Equation (5.2) below. It will facilitate timely remedial measures to be adopted for prevention of further corrosion in RC beams. This correlation will give ultimate load carrying capacity in the RC beams at varying levels of corrosion based upon the Damage Index calculated from vibration diagnostics. Hence, it facilitates the use of vibration monitoring parameter of FRF magnitude for relating the ultimate load carrying of beam undergoing progressive accelerated corrosion.

$$(UL)_{tge} = -0.77\ (\mathrm{DI_i}) + 41.22 \tag{5.2}$$

Where

UL= Ultimate load carrying capacity at different instants in corroding beams

DIi = Damage Index at different instants in corroding beams

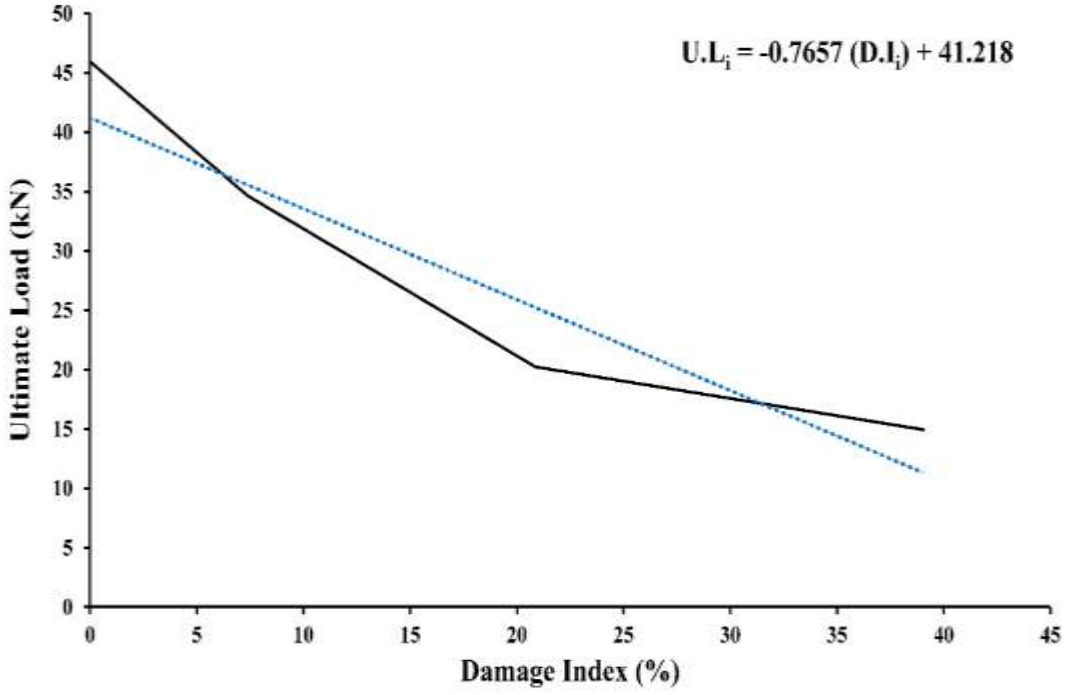

Figure 5.7. Correlation of DI with Ultimate Loads with increasing corrosion damage

5.4.2 GFRP Repaired Corroded Beams

An attempt is also made for correlating load carrying capacity of GFRP repaired corroded beams with Damage Index w.r.t FRF magnitude. Beams when repaired with micro-concrete and GFRP wraps, preformed well as compared to original corroded specimens, but a fall in ultimate load is observed with increasing DI even after repair as compared to healthy control beam (**Refer Table 5.3**). In R-30 and R-40 beams, a drop of 30.31% and 41.82% respectively in ultimate load as compared to C-0 is observed which is alarming. An empirical equation (5.3) is attempted to obtain a relationship between Ultimate Load and Damage Index for repaired beams (**Figure 5.8**).

$$(UL)_{tR} = -1.26\,(DI)_{tR} + 44.7 \tag{5.3}$$

Where:

$(UL)_{tR}$ = Ultimate load at different instants in GFRP repaired corroded samples

$(DI)_{tR}$ = Damage Index at different instants in GFRP repaired corroded sample

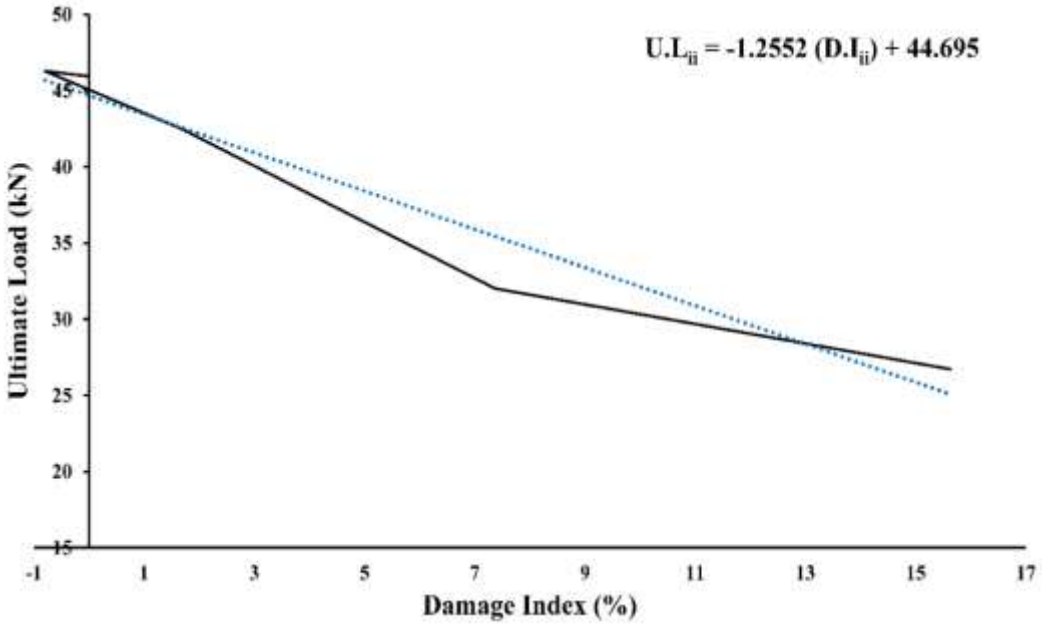

Figure 5.8. Correlation of DI with Ultimate Loads in GFRP repaired corroded samples

It is important to mention here that the empirical relationships given for corroded and FRP repaired corroded beams in Equations 5.2 and 5.3 respectively are limited to the experimental test parameters under which it is performed. Hence, it is recommended to monitor RC structures for corrosion related damage periodically using vibration monitoring technique, as an idea of drop in load carrying capacity can be measured using empirical relations, (Equation 5.2 and 5.3). It gives an indication that vibration diagnostics can serve to prevent massive damage and save rehabilitation cost in RC structures.

5.5 CLOSING REMARKS

This chapter focuses on the effective use of vibration monitoring technique for damage detection in both corroded and GFRP repaired corroded beams. With increasing corrosion level in RC beams, it is observed that vibration parameters of frequency and FRF magnitude of fundamental mode reduces, but these characteristics improve after GFRP repair pointing towards strength regain and enhancement post-repair. It is also well supported by improvement in the flexural characteristics of the repaired beams and a change in failure mode from brittle to ductile. The proposed non-destructive and in-situ monitoring technique provides an extra edge over the existing NDT tools in terms of detecting damage beneath the surface even after FRP repair.

CHAPTER 6

MONITORING CORRODED AND GFRP REPAIRED CORRODED BEAMS USING ACOUSTIC EMISSION TECHNIQUE

6.1. GENERAL

In this chapter, Acoustic Emission technique is employed as a non-destructive testing tool to study the behaviour of corroded and GFRP repaired corroded beams when subjected to flexural loading. AE sensors are mounted on beams and AE monitoring is done during flexural testing. Acoustic Emission parameters of cumulative AE hits and their amplitudes along with AE X-Y event plots are used to relate to the effect of corrosion on the performance of bars and further to the role played by GFRP wrapping in strengthening and regaining of strength after corrosion**.** AE event plots give a pictorial representation of actual development and progression of micro- and macro-cracking inside concrete as the corroded and corrosion reinforced beams are subjected to flexural loading. This chapter reports an effort to develop a novel methodology for assessing the performance of GFRP wrapped corroded RC structures using AE techniques. This approach facilitates non-destructive evaluation of FRP repaired RC structures with a prior indication of their damage post repair.

6.2 ACOUSTIC EMISSION MONITORING

Six AE sensors were mounted on the surface of the beams in a triangular pattern to record the AE activity during flexure testing of corroded and GFRP repaired corroded beams. AE hits and their respective amplitudes, AE X-Y event plots were plotted along with flexure testing to understand the mechanism of propagation of cracking in beams in corroded as well as GFRP repaired beams.

6.2.1 Cumulative AE hits

- ***Control Beam***

Initiation and progression of cracks in C-0 are demonstrated by cumulative AE hits plot depicted by well-defined AE phases (I-IV) (**Figure 6.1**).

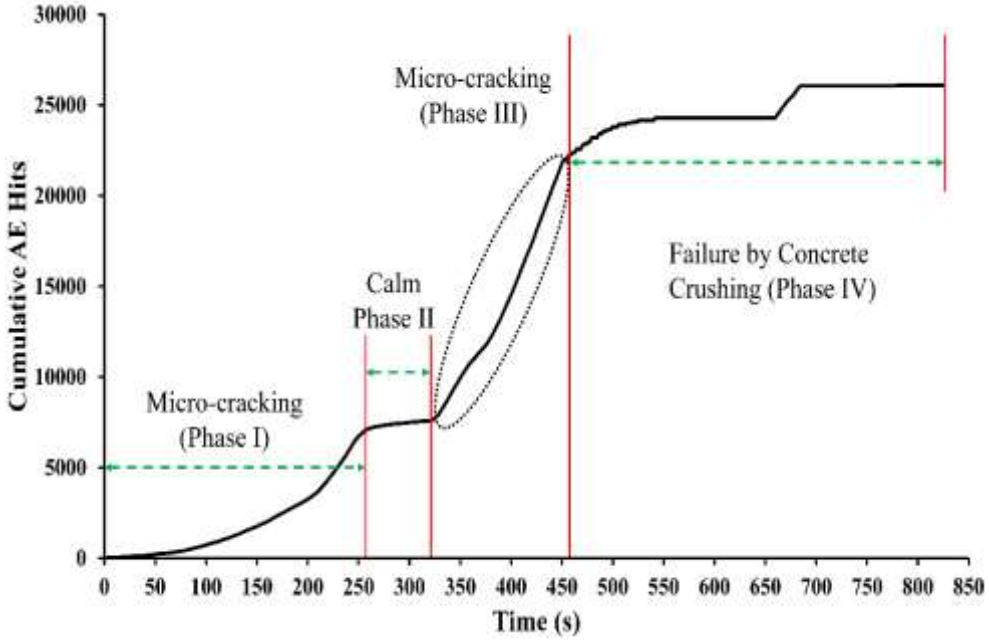

Figure. 6.1. Cumulative AE hits (Healthy beam C-0)

During the initial stages of loading, small AE activity is recorded even though there is no visible sign of cracking. This initial AE phase can be related to the uncracked linear zone of P-Δ curve (**Figure 5.5**). With further increase in loading, an increase in the AE activity up to 250 seconds pointing towards small acoustic events with average amplitude in the range of 50-60 dB (**Figure 5.3**). It probably relates to initiation of micro-cracking in concrete around reinforcement (Cracked Linear Zone) and is termed as '***Micro-Cracking AE Phase I'***. During this phase, no major cracks are observed visually on the beam. Hence, AE hit map indicates initiation of micro-cracking inside concrete well before it is visible on the surface. Further for a small duration, no significant AE activity is observed in the ***'Calm Phase II'*** indicating probable coalescing together of micro-cracks with no active AE activity. The amplitude, as well as the number of AE hits, drop in this phase.

But as the beam is further loaded, a sudden and significant jump is observed in AE hits pointing towards the integration of micro-cracks to macro-cracking in "***Macro-Cracking Phase III***". The amplitude, as well as number of AE hits significantly increase in this stage, and the average amplitude of AE hits rise to 65-70 dB. It is also well illustrated by the appearance of numerous flexural cracks on the surface of the beam during testing. As the beam is further loaded, the number of cumulative AE hits reduces and almost becomes constant pointing towards the failure of the beam in Phase IV. This is due to attenuation of AE signals caused by significantly cracked beam.

Hence, the plot of cumulative AE hits and their amplitudes give a clear indication of different phases of cracking in a concrete beam right from the initiation of cracking to its progression and give a prior warning of failure in RC beams under flexural loading.

- ***Corroded Beams***

Further, as corroded beams are subjected to flexural loading, it is observed that mildly corroded C-10 beam, having minute visible cracks, exhibits similar AE hits and phases trends as C-0 but with an overall reduction in AE hits due to attenuation of the signals caused by initial cracks due to corrosion (**Figure 6.2 a**).

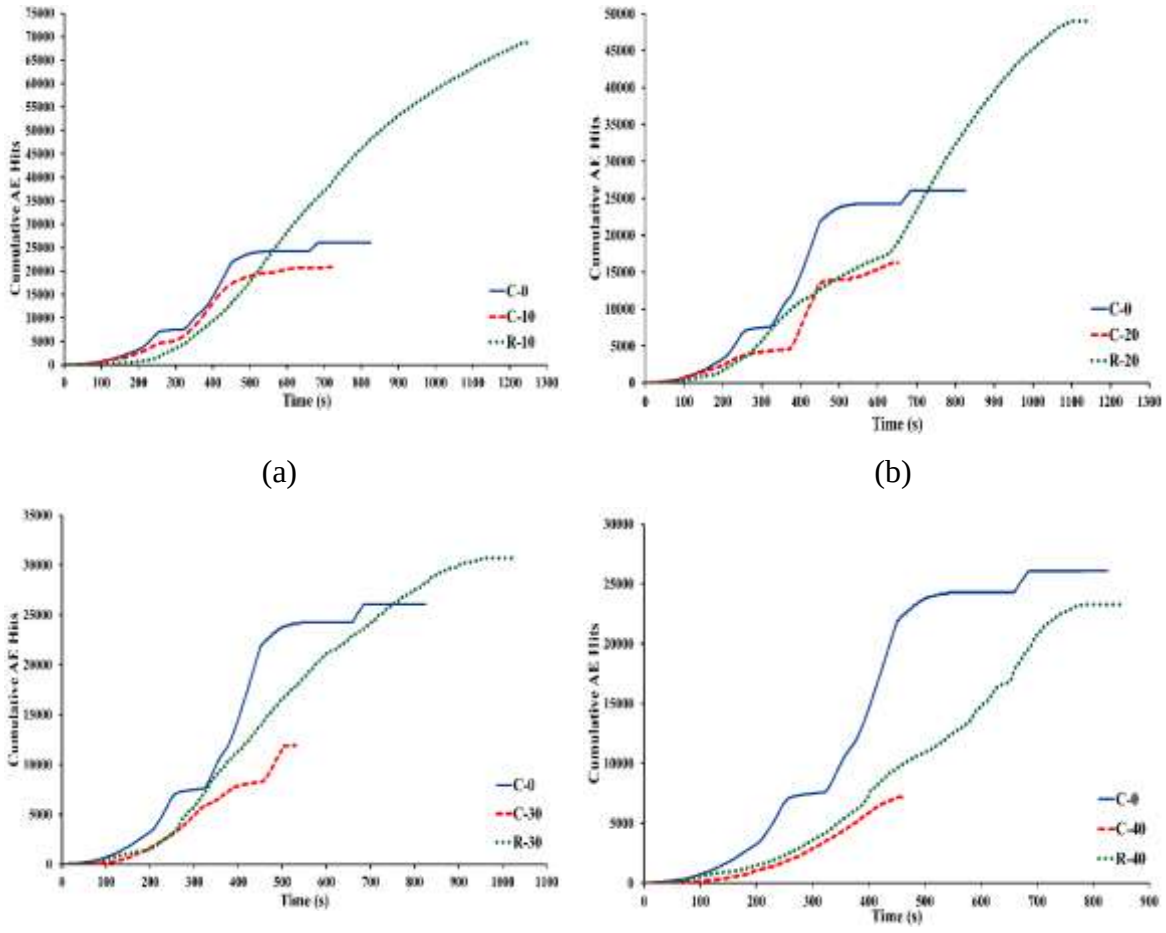

Figure 6.2. Cumulative AE Hits for corroded and repaired beams

But in C-20 beam, the number of AE hits reduces significantly with a huge delay in the appearance of different phases of AE activity. It is due to micro-cracks already present in the corroded beam in the initial stages of loading and with further loading micro-cracks integrate into macro-cracks in Phase-III (**Figure 6.2 b**). This phase lasts

for a short duration and leads to sudden failure in Phase IV. The average amplitude of AE hits is almost similar to that in C-0. (**Figure 6.3 a&c**).

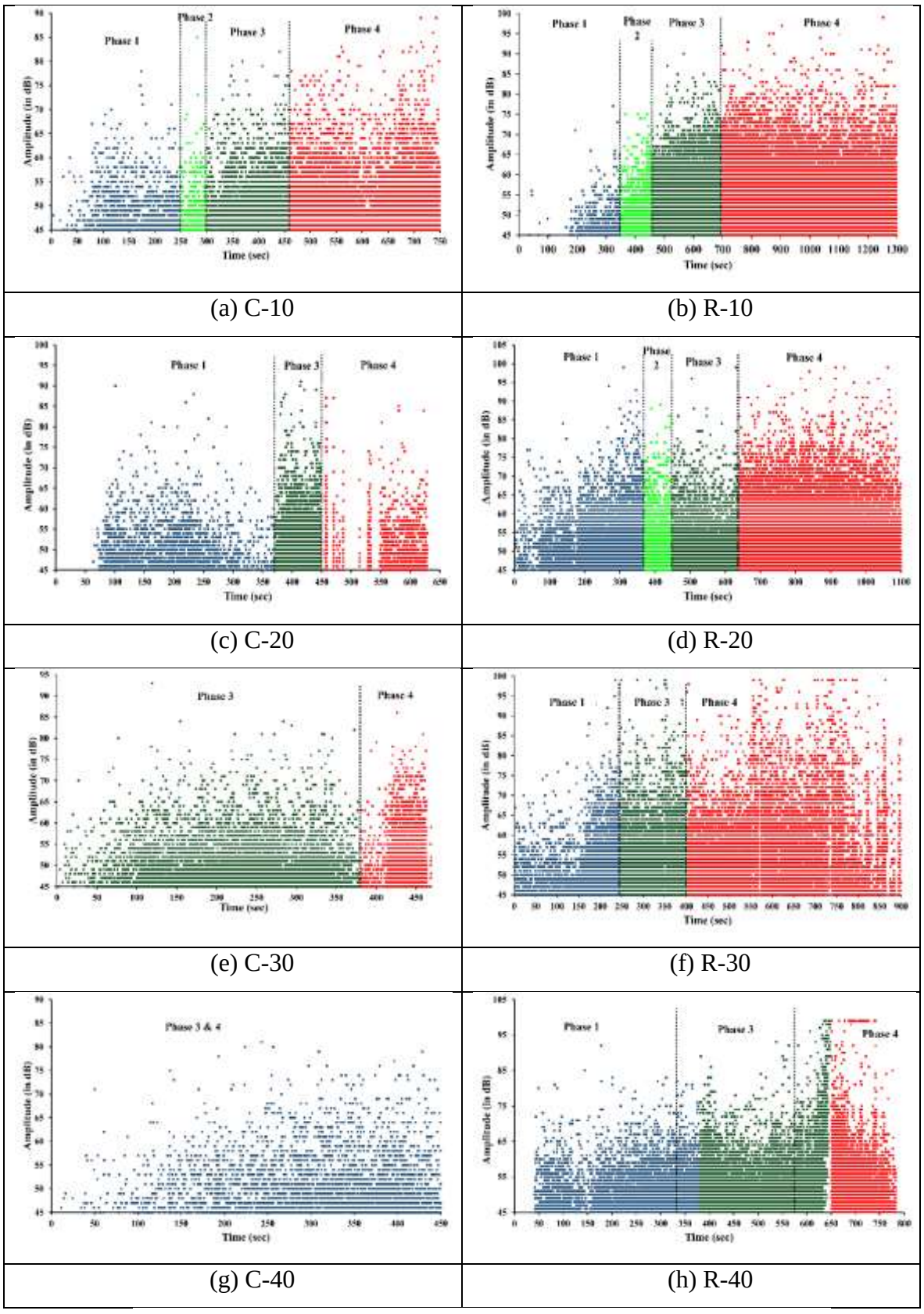

(a) C-10 (b) R-10

(c) C-20 (d) R-20

(e) C-30 (f) R-30

(g) C-40 (h) R-40

Figure 6.3. Amplitude of AE hits in corroded and repaired beams

On the other hand, in badly corroded beams (C-30 and C-40), no initial micro-cracking and calm phases are observed due to already pre-cracked condition of these beams. Only macro-cracking Phase III and failure Phase IV are observed due to coalescing of cracks lead to macro-cracking and ultimate failure (**Figure 6.2 c&d**). The pre-cracked condition of the corroded beams is well indicated by a significant drop in AE hits plots with depletion of various AE phases with an increase in corrosion.

- ***GFRP repaired beams***

When beams corroded to different levels are repaired and further subjected to flexural loading, there is a significant improvement in strength and deformation capabilities of corroded beams. It is also well tracked by a sudden increase in AE hits after repair of corroded beams. GFRP repaired beams showed outstanding performance as compared to corroded samples. Phase-I representing the initiation of micro-cracking is observed in all specimens (R-10, R-20, R-30 and R-40) as damaged and spalled concrete in corroded beams are replaced with micro-concrete. For R-10, a significant 3 times increase in cumulative AE hits is observed as compared to control beam C-0 (**Figure 6.2 a&b**). This increase in the number of AE hits is directly representative of micro-cracking in newly filled micro-concrete. The repaired beam behaves like a sound beam and is indicative of its integrity after repair (**Figure 6.2 a**).

Similarly, R-20 also records a significant increase in AE hits (almost double) when compared with C-0 (**Figure 6.2 b**). Phase I and III representatives of micro-cracking and macro-cracking appears distinctly in the repaired beams with a large increase in AE hits. Also, a significant increase in the average amplitude of AE hits in Phase I and III of 65 dB, and 70 dB is observed in R-10 and R-20 beams as compared to C-10 and C-20 of 55 dB and 65 db. Repairing by removing cracked and spalled concrete, micro-concreting and further GFRP wrapping improves the flexural behaviour of mildly corroded beams significantly. It is well corroborated by load deflection behaviour and significant enhancement of strength as well as ductility (**Figure 6.2 b**).

Heavily corroded R-30 and R-40, which were repaired after heavy corrosion with micro-concrete and GFRP wrapping also significantly recovered post repair which is indicated by the increase in the total number of AE hits for R-30 as well as R-40 beams which were greater than originally corroded C-30 and C-40 beams. Phase I and II of AE activity which was absent in corroded C-30 and C-40 beams reappear as a result of

repair with micro-concrete and GFRP repair. Well defined phases of AE activity indicate improvement in the integrity of badly corroded C-30 and C-40 beam. GFRP plays a key role in strengthening corroded samples (**Figure 6.2 c&d**). This is also well supported by load deflection behaviour of these beams (**Figure 5.6 c&d**). But a significant improvement in ductility is observed in comparison to originally corroded C-30 and C-40 beams. The failure mode changes in both beams from brittle to ductile.

The results clearly demonstrate the importance and effectiveness of AE technique in real time degradation monitoring of RC beams subjected to simultaneous loading and corrosion and further monitoring of GFRP repaired corroded beams.

6.2.2 AE X-Y Event Plots

For real time monitoring, AE X-Yevent plots provide a pictorial representation of the origin of cracks even when they are not visible on the surface. Initiation and progression of cracks can be tracked within the region covered by the sensors. A close relation is observed between actual micro- and macro cracks appearing in the corroded beam and the AE X-Y event plots (**Figure. 6.5**)

For corroded beams, a significant drop in AE events is observed. For C-10, as a result of corrosion, micro-cracks were already present below the surface. As, the beam is loaded, these micro-cracks tend to extend and were successfully captured by AE events before they were visible on the surface (**Figure. 6.5 a**). In C-20, micro-cracks were already present on the surface, and on further loading, the micro-cracks integrated into macro-cracks and led to ultimate failure. The same was represented by a reduced number of AE events in C-20 as compared to C-0 and C-10. (**Figure. 6.4 & 6.5 c**). A significant drop in the number of AE event is observed in heavily corroded beams (C-30 and C-40) as numerous transverse and longitudinal cracks were present previously due to pre-corrosion (**Figure. 6.5 e&g**).

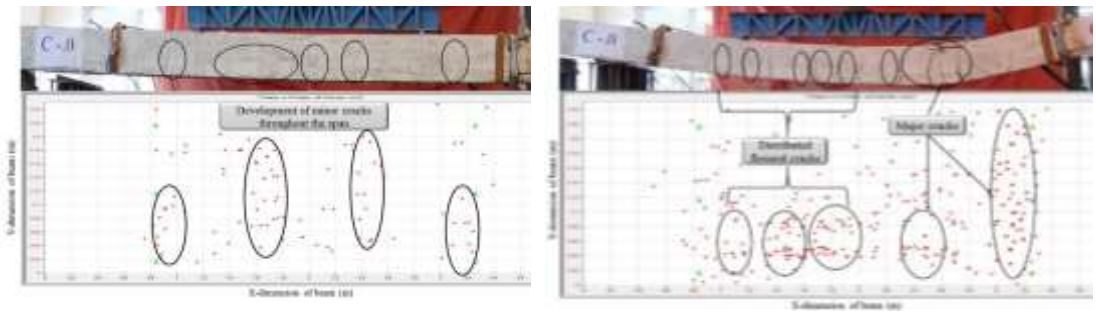

Initial stage Final stage

Figure 6.4. AE XY event plot for C-0

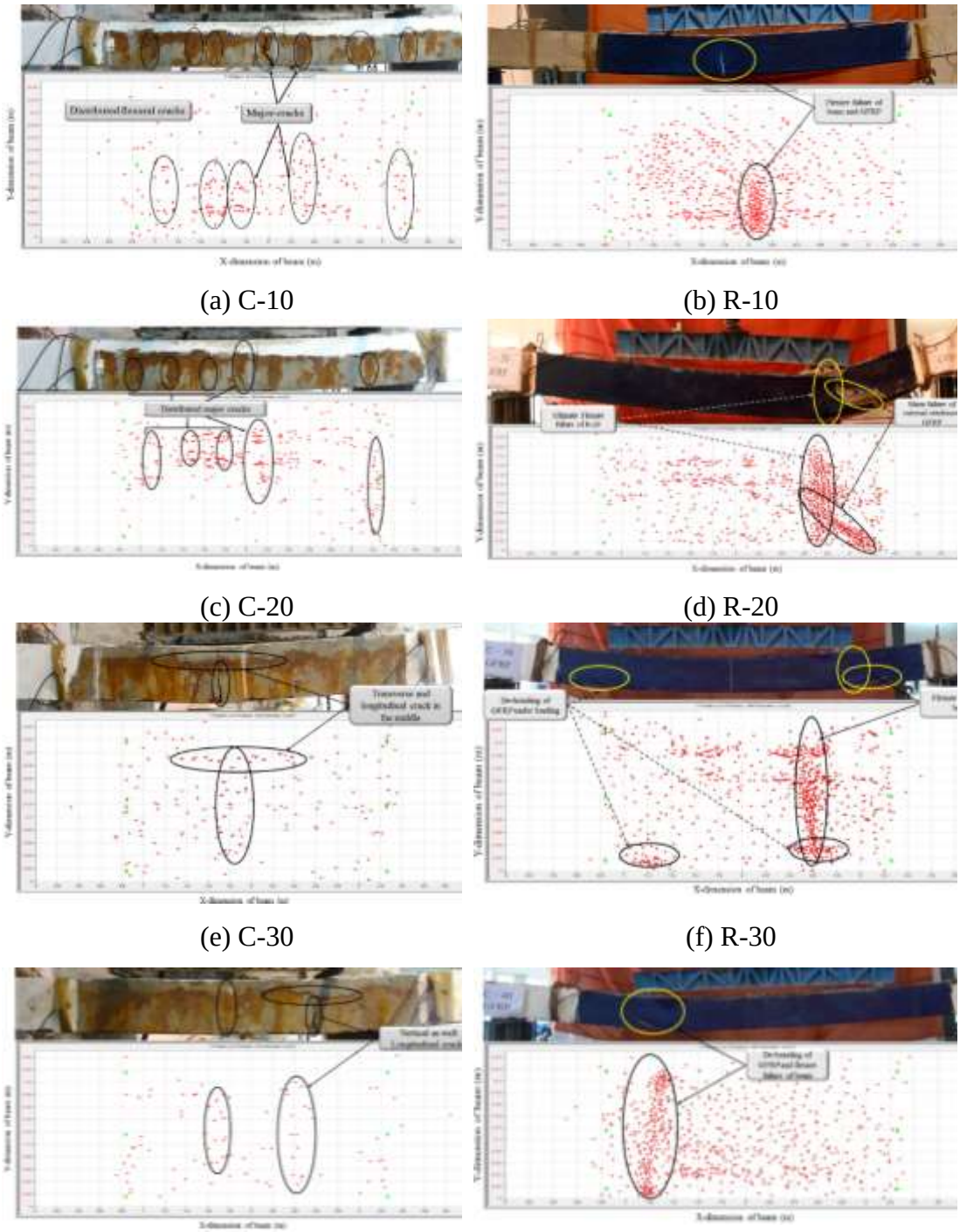

(a) C-10 (b) R-10

(c) C-20 (d) R-20

(e) C-30 (f) R-30

(g) C-40 (h) R-40

Figure 6.5. AE XY event plot

AE X-Y event plot for repaired corroded RC beams presented a tremendous increase in AE events as compared to control and corroded beams. As R-10 was subjected to increased loading, the surge in a number of AE events is observed. On

further loading, failure of GFRP sheets was clearly demonstrated by an increased number of AE events as compared to the control beam (C-0) (**Figure 6.5 b**). This entire behaviour of beam from the initiation of cracks to final failure under loading was represented and correlated closely to the actual condition of beam. R-20 beams showed a similar trend of increase as that of R-10 beams, with a slight increase in the number of total AE events. This attributes to the fact that GFRP plays a major role in intercepting load as steel is compromised, which is well illustrated by the AE event plot (**Figure 6.5 d**). Similarly, for heavily corroded repaired beams R-30 and R-40, a jump in the total number of AE events is observed as compared to originally corroded beams. This increase in AE events plot illustrates the effect of micro-concrete and GFRP sheets in rehabilitating the structural strength. Cracks were observed at the same location where a sudden cluster of AE events was observed (**Figure 6.5 f&h**). Continuous increase in AE hits with loading in repaired beams pointing that it can take the larger load before failure by de-bonding of GFRP and concrete.

Hence, it is concluded that AE plays a crucial role in detecting the initiation and progression of cracks in both corroded and repaired specimens as given by AE hits and their amplitude along with pictorial representation by X-Y AE event plots.

6.3 CORRELATION BETWEEN DESTRUCTIVE AND AE PARAMETERS

To assess the condition of RC beams at different levels of corrosion, an attempt is made to correlate cumulative AE hits with destructive parameters of ultimate load carrying capacity to facilitate non-destructive testing evaluation of corroding RC beams and further when they are repaired with GFRP wrapping.

6.3.1 Corroded Beams

As RC beams were corroded at different levels, a drop in ultimate load was observed. In C-10 beam, with few signs of corrosion, drop of 24.63% in ultimate load was observed. This fall in ultimate load with the increase in corrosion level was observed upto 67.48% for C-40 beam. This can be directly correlated with a consistent drop in cumulative AE hits (**Table 6.1**) with increasing corrosion level in RC beams.

Hence, the drop in cumulative AE hits is a good indicator of increasing corrosion levels in RC beams and can facilitate non-destructive evaluation of RC structures.

Table 6.1 Comparison of AE parameters and Ultimate Load for corroded RC beams

	Cumulative AE hits	Ultimate load (kN)
C-0	26000	46.95
C-10	20822	34.63
C-20	16271	29.24
C-30	11919	20.24
C-40	9094	14.94

6.3.2 GFRP Repaired Corroded Beams

An attempt is made to correlate load carrying capacity of GFRP repaired corroded beams with AE parameter of Cumulative AE hits. Beams when repaired with micro-concrete and GFRP wraps, preformed well as compared to their original corroded specimens as well as controlled beams. It is observed that cumulative AE hits in (R-10, R-20 and R-30) are much higher than C-0 as well as when compared with their reference corroded samples (C-10, C-20 and C-30). The trend of increasing SE hits is similar to increase in ultimate load as a result of repair when compared with control as well as their reference corroded samples **(Table 6.2)**. This increase in number of hits directly represents the effectiveness of micro concrete and GFPR repair in corrosion damage structures. Bu in -40 samples, though same micro concrete abed FGR wrapping is done but the detrition in damage to the corrosion leading to large reduction inn cross sectional area of steel is too high. Hence the number of AE hits drops and ultimate load carrying capacity is closer to control beams as compared to other repaired beams. Hence, AE hits are a potential non-destructive extent of deterioration as well as a good indicator of effectiveness of repair against corrosion.

Table 6.2 Comparison of AE parameters and Ultimate load for GFRP repaired corroded RC beams

	Cumulative AE hits	Ultimate load (kN)
C-0	26000	46.95
R-10	68687	96.28
R-20	49027	91.83
R-30	30711	77.31
R-40	23271	50.446

Hence, it is recommended to monitor RC structures for corrosion related damage periodically using Acoustic Emission Technique. An idea of drop in load carrying capacity and hence strength of beam can be judged/related to the cumulative AE hits recorded at an instant. It gives an indication that Acoustic Emission Technique can serve to prevent massive damage and save rehabilitation cost in RC structures due to corrosion.

6.4 CLOSING REMARKS

This chapter evaluate the flexural behaviour and performance of Glass Fiber Reinforced Polymer (GFRP) repaired. Reinforced Concrete (RC) beams corroded to different levels using Acoustic Emission (AE) techniques. A significant improvement in the flexural characteristics of the GFRP repaired corroded beams is observed with a change in failure mode from brittle to ductile. The benefits of GFRP repair in corroded RC beams are further clearly demonstrated by AE monitoring parameters of cumulative AE hits and their amplitudes. A significant improvement in the number of AE hits and the reappearance of AE cracking phases after repair of corroded beams indicate the efficiency of AE technique to monitor repaired structures also. A pictorial representation of the development of micro-cracks beneath the surface of concrete and GFRP to the formation of macro-cracks is well demonstrated in an AE event plot. The assessment of local damage in RC beams using AE techniques subjected to simultaneous loading and corrosion and their further repair would facilitate in-situ non-destructive evaluation of actual RC structures in future for detecting damage beneath the surface even after FRP repair.

CHAPTER 7

CONCLUSIONS

7.1 GENERAL

This work reports the effect of corrosion and GFRP repair on the dynamic properties of RC structure. The work is divided into three sub division, first section deals with the monitoring real time corrosion using NDT tools of AE, UGW and IRT. The second section deals with the monitoring of corroded and corrosion repaired RC beams using vibration monitoring. Finally, the same were tested under flexural loading and simultaneously monitored using surface mounted AE sensors.

7.2 MONITORING REAL TIME CORROSION USING NDT TOOLS

In this study, the real time monitoring of initiation and progression of corrosion damage is attempted using a combination of Active guided waves, passive Acoustic Emission and IRT.

1. In bar, simulating pitting corrosion in the form of area reduction in bars in a constant length, a drop in ultrasonic signal strength is observed with reducing diameter. It is due to a lesser transmitted signal strength through the rebar caused by area reduction leading to attenuation in signal, when bars are tested in air as well as when they are embedded in concrete. When the rebars are embedded in concrete a significant drop in ultrasonic signal strength observed due to leakage into the surrounding concrete. The ultrasonic guided waves mode chosen for study is core sensitive mode sensitive to bar profile deterioration and here is slightly affected by reducing diameter simulating pitting.

2. In bars simulating de-bond effect of corrosion, with increasing length of debond in bars in air and in concrete, drop in signal strength is not very high as observed with reduced diameter simulating pitting. But at larger length of de-bond, signal dissipation increases leading to drop in peak to peak voltage in the transmitted signals.

3. Real time monitoring of corrosion in rebars in concrete using ultrasonic guided wave approach indicates that it is not very effective in picking up the initiation of corrosion but very effectively picks progression of corrosion at later stages. It is

well indicated by significant drop in ultrasonic transmitted signal strength voltages.

4. Chloride induced corrosion in rebar in concrete is well picked up by core seeking guided wave mode well depicted by delamination phase, transition phase and pitting phases.

5. AE successfully picks up initiation of corrosion along with its progression. It is well depicted by various micro-cracking and macro-cracking phases at different stages of corrosion, distinguished on the basis of slope of cumulative AE hit plot and the amplitude of AE hits. Cumulative AE hit plot clearly distinguishes between various stages of chloride induced corrosion in RC beam which is well complimented by drop in UGW voltages and the phase of corrosion as depicted by guided wave approach. This is due to the core-seeking nature of guided wave mode used for damage monitoring.

6. The initiation and progression of corrosion damage is also well picked up by change in amplitude of AE hits. Initiation of corrosion in phase I is marked by low amplitude events of 55 dB indicating beginning of hairline or minor cracking. As the effect of corrosion damage increases into the surrounding concrete, the amplitude of AE hits increases from 55 dB to 70 dB in phase III micro-cracking phase. The increasing amplitude of AE hits point towards progression in AE activity of larger magnitude in the form of macro-cracking in concrete

7. AE X-Y plot clearly demonstrate the initiation and progression of cracks in pictorial representation. As the level of corrosion increase AE X-Y plot represented in the form dots become dense at area exposed to corrosion and the same is verified by the corrosion cracks appeared at the surface in later stages.

8. IR technique effectively picked up location of damage in bar with rise in temperature in the middle portion of bar with simulated damages as well as in concrete due to the reduced diameter of bar. Reduced cross-section of bar tends to heat at a faster rate thus it gives a clear representation of damage. For bars in concrete undergoing actual corrosion, there is minor difference in temperature in the initial stage of corrosion but with the progression of corrosion marked change

in temperature is observed in the corrosion rebar in concrete. It is because the further rust produced get heated at a fast rate than the parent steel.

9. IRT successfully gives a pictorial representation as well as exact localization of damage due to corrosion in surrounding concrete which is clearly visible in thermograms and finally a large crack in concrete is observed in IRT images at advanced stages of corrosion.

10. A comprehensive combined non-destructive tests methodology for picking up actual corrosion in concrete is proposed in this work using local Acoustic Emission, Ultrasonic Guided Waves and Infra-Red Thermography techniques. Guided wave effectively picks up rebar deterioration using specific guided wave modes propagated through it. AE picks up effect of corrosion on surrounding concrete well picked up amplitude and number of AE hits and marked by different cracking stages whereas IRT gives a pictorial representation of progressive damage as well as localizes damages due to corrosion in concrete.

7.3 MONITORING CORRODED AND CORROSION REPAIRED RC BEAMS USING VIBRATION MONITORING

1. RC beams subjected to increasing levels of corrosion indicate severe deterioration beginning with minor hairline cracks with reddish brown corrosion product oozing out and further spreads in the form of numerous and widely distributed transverse cracks and large longitudinal cracks parallel to reinforcement. Severe deterioration in badly corroded RC beams demands for timely monitoring and maintenance to avoid catastrophic failures in structures.
2. Changes in corrosion current with increasing corrosion points towards the corrosion mechanism in RC structures. Initial drop in corrosion current indicates the resistance offered to corrosion by passive layer of oxides on embedded steel in concrete. But as corrosion progresses, breakdown of passive layer leads to corrosion initiation and progression indicated by increase in corrosion current. Corrosion current can be used as an initial indicator of corrosion initiation in RC structures but fails to quantify the extent of corrosion deterioration in RC structures.
3. Beams corroded to different levels when subjected to vibration monitoring and reported a shift and drop in fundamental frequency and significant drop in FRF

amplitudes with increasing corrosion levels. This is due to attenuation of vibration signal produced by impact of hammer and picked up by accelerometer due to increasing corrosion cracks.

4. With increase in corrosion levels a significant decrease in ultimate load carrying capacity and mid-span deflections is observed when the corroded beams are subjected to flexural loading as area of steel reduces which ultimately compromises its ductility. A significant improvement in these flexural characteristics is observed when replicates of these corroded beams were repaired using micro-concrete and GFRP wrapping.
5. Micro-concrete and GFRP repair of corroded RC beams leads to a significant improvement in dynamic characteristics of beams both in frequency as well as FRF amplitudes. It points towards effective strength regain after repair due to the replacement of spalled concrete with sound micro-concrete and confinement offered by U-shaped GFRP wraps which enabled beam to behave as good as control beam.
6. Increasing corrosion leads to significant drop in dynamic vibration parameter of FRF amplitudes as well as drop in load carrying characteristics of the RC beams. Hence, to facilitate non-destructive evaluation of corroded beams, an empirical correlation is attempted between FRF amplitude based Damage Index and load carrying capacities both in corroded as well as corrosion repaired beams.

7.4 MONITORING CORRODED AND GFRP REPAIRED CORRODED BEAMS USING ACOUSTIC EMISSION TECHNIQUE

1. AE monitoring of corroded and GFRP repaired corroded RC beams when subjected to flexural loading successfully detects the cracking behaviour. It is well picked up by variation in various AE waveform parameters such as number of AE hit and their amplitudes and AE X-Y event plots.
2. Variation in a number of AE hits and their corresponding amplitudes with an increase in corrosion level portrays the condition of RC beam at different levels of corrosion. With the increase in corrosion levels, a significant drop in cumulative AE hits along with depletion of different AE cracking phases is observed due to the attenuation of the captured AE signals caused by pre-existing cracks. AE monitoring provides an extra edge of detecting initiation and

progression of damage and cracks much before they are observed on the surface, thus making it more desirable and an efficient non-destructive tool.

3. The repair of corroded beams using GFRP wrapping causes reappearance of the AE phases with an increase in the number of cumulative AE hits pointing towards improved integrity of the beams after GFRP repair. Successful AE monitoring of corroded and further GFRP repaired corroded beams establish it as a good potential real time NDT candidate for RC beams subjected to simultaneous corrosion and loading.
4. AE X-Y event plots give a pictorial representation of actual cracking inside the concrete much before it is observed on the surface. A close mapping is observed between the actual cracking pattern observed visually in the beams and the AE X-Y events plots. AE event plot can play a key role in monitoring GFRP repaired RC specimen because as wraps otherwise restrict the visual observation of cracks. All the cracking events right from initiation to the progression of micro-cracks into macro-cracks is well presented by AE X-Y event plots.

7.5 FUTURE SCOPE OF WORK

The research effort in this work can be further explained as follows:

1. Investigate the combined effect of vis-a-vis sustained loading with real-time corrosion in RC structures to develop a real time damage monitoring tool. The effect of combined corrosion and sustained loading using vibration monitoring to relate to practical situations to which the RC structures are subjected would be an interesting future scope of work.
2. Repairing of corroded beams using other repair strategies and monitoring their vis a vis effectiveness under loads.
3. Monitoring the effectiveness of various repair strategies against corrosion using NDT tools.
4. Develop corrosion models in RC structures using numerical modelling tools vis-a-via various repair strategies.

LIST OF PUBLICATIONS

1. Garhwal, Sunil, Shruti Sharma, and Sandeep Kumar Sharma. "Acoustic Emission Monitoring of RC Beams Corroded to Different Levels Under Flexural Loading." Arabian Journal for Science and Engineering (2020): 1-17.

2. Garhwal, Sunil, Shruti Sharma, and Sandeep Kumar Sharma. "Monitoring the flexural performance of GFRP repaired corroded reinforced concrete beams using passive acoustic emission technique." Structural Concrete (2020).
3. Garhwal, Sunil, Shruti Sharma, and Sandeep Kumar Sharma. “Monitoring Performance of Corroded and GFRP Repaired Corroded Reinforced Concrete Beams using Vibration Diagnostics” Nondestructive Testing and Evaluation. (Under review)
4. Garhwal, Sunil, Shruti Sharma, and Sandeep Kumar Sharma. “Monitoring Real Time Corrosion in RC beams Using a Combination of AE, UGW and IRT Technique” Journal of Nondestructive Evaluation. (Under review)

REFERENCES

[1] T. El Maaddawy, K. Soudki, and T. Topper, “Long-term performance of corrosion-damaged reinforced concrete beams,” *ACI Struct. J.*, 2005, doi: 10.14359/14660.

[2] S. A. Alghamdi and S. Ahmad, “On Durability of Reinforced Concrete Structures: A Design Methodology for RC Beams and Columns in Corrosive Environments,” *Arab. J. Sci. Eng.*, 2018, doi: 10.1007/s13369-018-3101-x.

[3] L. Wu, X. Kou, and M. Jiang, “Probabilistic Corrosion Initiation Time Assessment of Existing Concrete Structures Under Marine Environment,” *Arab. J. Sci. Eng.*, 2015, doi: 10.1007/s13369-015-1774-y.

[4] R. Zhang, A. Castel, and R. François, “The corrosion pattern of reinforcement and its influence on serviceability of reinforced concrete members in chloride environment,” *Cem. Concr. Res.*, 2009, doi: 10.1016/j.cemconres.2009.07.025.

[5] A. A. Almusallam, A. S. Al-Gahtani, A. R. Aziz, and Rasheeduzzafar, “Effect of reinforcement corrosion on bond strength,” *Constr. Build. Mater.*, 1996, doi: 10.1016/0950-0618(95)00077-1.

[6] S. Ahmad, “Reinforcement corrosion in concrete structures, its monitoring and service life prediction - A review,” *Cement and Concrete Composites*. 2003, doi: 10.1016/S0958-9465(02)00086-0.

[7] M. W. T. Mak, P. Desnerck, and J. M. Lees, “Corrosion-induced cracking and bond strength in reinforced concrete,” *Constr. Build. Mater.*, 2019, doi: 10.1016/j.conbuildmat.2019.02.151.

[8] Y. Ma, Z. Guo, L. Wang, and J. Zhang, “Experimental investigation of corrosion effect on bond behavior between reinforcing bar and concrete,” *Constr. Build. Mater.*, 2017, doi: 10.1016/j.conbuildmat.2017.06.169.

[9] A. Tarighat and B. Zehtab, “Structural reliability of reinforced concrete beams/columns under simultaneous static loads and steel reinforcement corrosion,” *Arab. J. Sci. Eng.*, vol. 41, no. 10, pp. 3945–3958, 2016.

[10] R. Zhang, A. Castel, and R. François, “Concrete cover cracking with

reinforcement corrosion of RC beam during chloride-induced corrosion process," *Cem. Concr. Res.*, vol. 40, no. 3, pp. 415–425, 2010.

[11] A. Sharma, S. Sharma, S. Sharma, and A. Mukherjee, "Monitoring invisible corrosion in concrete using a combination of wave propagation techniques," *Cem. Concr. Compos.*, 2018, doi: 10.1016/j.cemconcomp.2018.03.014.

[12] C. M. Hansson, "Concrete: the advanced industrial material of the 21st century," *Metall. Mater. Trans. A Phys. Metall. Mater. Sci.*, 1995, doi: 10.1007/BF02647584.

[13] H. W. Song and V. Saraswathy, "Corrosion monitoring of reinforced concrete structures - A review," *Int. J. Electrochem. Sci.*, 2007.

[14] S. Sharma and A. Mukherjee, "Monitoring Corrosion in Oxide and Chloride Environments Using Ultrasonic Guided Waves," *J. Mater. Civ. Eng.*, 2011, doi: 10.1061/(asce)mt.1943-5533.0000144.

[15] M. Ormellese, M. Berra, F. Bolzoni, and T. Pastore, "Corrosion inhibitors for chlorides induced corrosion in reinforced concrete structures," *Cem. Concr. Res.*, vol. 36, no. 3, pp. 536–547, 2006.

[16] G. Batis and E. Rakanta, "Corrosion of steel reinforcement due to atmospheric pollution," *Cem. Concr. Compos.*, vol. 27, no. 2, pp. 269–275, 2005.

[17] K. Y. Ann and H.-W. Song, "Chloride threshold level for corrosion of steel in concrete," *Corros. Sci.*, vol. 49, no. 11, pp. 4113–4133, 2007.

[18] R. Arndt and F. Jalinoos, "NDE for corrosion detection in reinforced concrete structures—A benchmark approach," *Proc. Non-destructive Test. Civ. Eng.*, 2009.

[19] A. Zaki, H. K. Chai, D. G. Aggelis, and N. Alver, "Non-destructive evaluation for corrosion monitoring in concrete: A review and capability of acoustic emission technique," *Sensors (Switzerland)*, 2015, doi: 10.3390/s150819069.

[20] S. Gadve, A. Mukherjee, and S. N. Malhotra, "Corrosion of steel reinforcements embedded in FRP wrapped concrete," *Constr. Build. Mater.*, 2009, doi: 10.1016/j.conbuildmat.2008.01.008.

[21] F. Wu and F. K. Chang, “Debond detection using embedded piezoelectric elements in reinforced concrete structures - Part I: Experiment,” *Struct. Heal. Monit.*, 2006, doi: 10.1177/1475921706057978.

[22] S. Sharma and A. Mukherjee, “Monitoring corrosion in oxide and chloride environments using ultrasonic guided waves,” *J. Mater. Civ. Eng.*, 2011, doi: 10.1061/(ASCE)MT.1943-5533.0000144.

[23] P. R. Vassie, “The half-cell potential method of locating corroding reinforcement in concrete structures,” *TRRL Appl. Guid.*, no. AG 9, 1991.

[24] P. V. Bahekar and S. S. Gadve, “Impressed current cathodic protection of rebar in concrete using Carbon FRP laminate,” *Constr. Build. Mater.*, 2017, doi: 10.1016/j.conbuildmat.2017.08.145.

[25] S. Patil, B. Karkare, and S. Goyal, “Acoustic emission vis-à-vis electrochemical techniques for corrosion monitoring of reinforced concrete element,” *Constr. Build. Mater.*, vol. 68, pp. 326–332, 2014.

[26] M. K. ElBatanouny, J. Mangual, P. H. Ziehl, and F. Matta, “Early corrosion detection in prestressed concrete girders using acoustic emission,” *J. Mater. Civ. Eng.*, 2014, doi: 10.1061/(ASCE)MT.1943-5533.0000845.

[27] Y. yan Lu, J. yue Hu, S. Li, and W. shui Tang, “Active and passive protection of steel reinforcement in concrete column using carbon fibre reinforced polymer against corrosion,” *Electrochim. Acta*, 2018, doi: 10.1016/j.electacta.2018.05.037.

[28] J. A. González, J. M. Miranda, N. Birbilis, and S. Feliu, “Electrochemical techniques for studying corrosion of reinforcing steel: Limitations and advantages,” *Corrosion*, 2005, doi: 10.5006/1.3278158.

[29] L. Bourreau *et al.*, “Uncertainty assessment of concrete electrical resistivity measurements on a coastal bridge,” *Struct. Infrastruct. Eng.*, 2019, doi: 10.1080/15732479.2018.1557703.

[30] J. Swarup and P. C. Sharma, “Electrochemical techniques for the monitoring of corrosion of reinforcement in concrete structures,” *Bull. Electrochem.*, 1996.

[31] B. Elsener, “Corrosion rate of steel in concrete—Measurements beyond the Tafel law,” *Corros. Sci.*, vol. 47, no. 12, pp. 3019–3033, 2005.

[32] M. Maalej, S. F. U. Ahmed, and P. Paramasivam, “Corrosion durability and structural response of functionally-graded concrete beams,” *J. Adv. Concr. Technol.*, 2003, doi: 10.3151/jact.1.307.

[33] J. M. López-Higuera, L. R. Cobo, A. Q. Incera, and A. Cobo, “Fiber optic sensors in structural health monitoring,” *J. Light. Technol.*, 2011, doi: 10.1109/JLT.2011.2106479.

[34] D. S. Kim and H. W. Kim, “Non-destructive testing and evaluation of civil infrastructures using stress wave propagation,” 2004, doi: 10.4028/www.scientific.net/kem.270-273.1616.

[35] A. Mukherjee and S. J. Arwikar, “Performance of externally bonded GFRP sheets on concrete in tropical environments. Part II: Microstructural tests,” *Compos. Struct.*, 2007, doi: 10.1016/j.compstruct.2006.05.002.

[36] H. Shan, J. Xu, Z. Wang, L. Jiang, and N. Xu, “Electrochemical chloride removal in reinforced concrete structures: Improvement of effectiveness by simultaneous migration of silicate ion,” *Constr. Build. Mater.*, 2016, doi: 10.1016/j.conbuildmat.2016.09.137.

[37] D. G. Aggelis, E. Z. Kordatos, D. V. Soulioti, and T. E. Matikas, “Combined use of thermography and ultrasound for the characterization of subsurface cracks in concrete,” *Constr. Build. Mater.*, 2010, doi: 10.1016/j.conbuildmat.2010.04.014.

[38] A. Sharma, S. Sharma, S. Sharma, and A. Mukherjee, “Investigation of deterioration in corroding reinforced concrete beams using active and passive techniques,” *Constr. Build. Mater.*, 2018, doi: 10.1016/j.conbuildmat.2017.11.165.

[39] S. Sharma and A. Mukherjee, “Nondestructive evaluation of corrosion in varying environments using guided waves,” *Res. Nondestruct. Eval.*, 2013, doi: 10.1080/09349847.2012.699609.

[40] W. Zhu, J. L. Rose, J. N. Barshinger, and V. S. Agarwala, “Ultrasonic guided

wave NDT for hidden corrosion detection," *Res. Nondestruct. Eval.*, 1998, doi: 10.1080/09349849809409629.

[41] P. Fromme, F. Bernhard, and B. Masserey, "High-frequency guided ultrasonic waves to monitor corrosion thickness loss," 2017, doi: 10.1063/1.4974574.

[42] A. Sharma, S. Sharma, S. Sharma, and A. Mukherjee, "Ultrasonic guided waves for monitoring corrosion of FRP wrapped concrete structures," *Constr. Build. Mater.*, 2015, doi: 10.1016/j.conbuildmat.2015.08.084.

[43] A. Bossio *et al.*, "Nondestructive assessment of corrosion of reinforcing bars through surface concrete cracks," *Struct. Concr.*, 2017, doi: 10.1002/suco.201600034.

[44] S. G. Shah and J. M. C. Kishen, "Use of acoustic emissions in flexural fatigue crack growth studies on concrete," *Eng. Fract. Mech.*, vol. 87, pp. 36–47, 2012.

[45] S. G. Shah and J. M. C. Kishen, "Fracture behavior of concrete–concrete interface using acoustic emission technique," *Eng. Fract. Mech.*, vol. 77, no. 6, pp. 908–924, 2010.

[46] D. L. Carnì, C. Scuro, F. Lamonaca, R. S. Olivito, and D. Grimaldi, "Damage analysis of concrete structures by means of acoustic emissions technique," *Compos. Part B Eng.*, 2017, doi: 10.1016/j.compositesb.2016.10.031.

[47] A. Carpinteri, G. Lacidogna, and G. Niccolini, "Critical behaviour in concrete structures and damage localization by acoustic emission," *Key Eng. Mater.*, 2006, doi: 10.4028/0-87849-994-6.305.

[48] M. Daniyal and S. Akhtar, "Corrosion assessment and control techniques for reinforced concrete structures: a review," *J. Build. Pathol. Rehabil.*, 2020, doi: 10.1007/s41024-019-0067-3.

[49] M. Di Benedetti and A. Nanni, "Acoustic emission intensity analysis for in situ evaluation of reinforced concrete slabs," *J. Mater. Civ. Eng.*, 2014, doi: 10.1061/(ASCE)MT.1943-5533.0000794.

[50] B. Elsener, C. Andrade, J. Gulikers, R. Polder, and M. Raupach, "Half-cell potential measurements—Potential mapping on reinforced concrete structures,"

Mater. Struct., 2003, doi: 10.1007/bf02481526.

[51] Y. Kawasaki, T. Wakuda, T. Kobarai, and M. Ohtsu, "Corrosion mechanisms in reinforced concrete by acoustic emission," *Constr. Build. Mater.*, 2013, doi: 10.1016/j.conbuildmat.2013.02.020.

[52] H. A. Elfergani, R. Pullin, and K. M. Holford, "Damage assessment of corrosion in prestressed concrete by acoustic emission," *Constr. Build. Mater.*, 2013, doi: 10.1016/j.conbuildmat.2012.11.071.

[53] M. Ohtsu and Y. Tomoda, "Corrosion process in reinforced concrete identified by acoustic emission," *Mater. Trans.*, 2007, doi: 10.2320/matertrans.I-MRA2007844.

[54] L. Chung, I. K. Paik, S. H. Cho, and Y. S. Roh, "Infrared thermographic technique to measure corrosion in reinforcing bar," 2006, doi: 10.4028/www.scientific.net/kem.321-323.821.

[55] W. L. Lai, S. C. Kou, C. S. Poon, W. F. Tsang, and C. C. Lai, "Characterization of the deterioration of externally bonded CFRP-concrete composites using quantitative infrared thermography," *Cem. Concr. Compos.*, 2010, doi: 10.1016/j.cemconcomp.2010.03.008.

[56] D. G. Aggelis, E. Z. Kordatos, M. Strantza, D. V. Soulioti, and T. E. Matikas, "NDT approach for characterization of subsurface cracks in concrete," *Constr. Build. Mater.*, 2011, doi: 10.1016/j.conbuildmat.2010.12.045.

[57] K. Kobayashi and N. Banthia, "Corrosion detection in reinforced concrete using induction heating and infrared thermography," *J. Civ. Struct. Heal. Monit.*, 2011, doi: 10.1007/s13349-010-0002-4.

[58] S. Baek, W. Xue, M. Q. Feng, and S. Kwon, "Nondestructive corrosion detection in RC through integrated heat induction and IR thermography," *J. Nondestruct. Eval.*, 2012, doi: 10.1007/s10921-012-0133-0.

[59] J. R. Brown and H. R. Hamilton, "Quantitative infrared thermography inspection for FRP applied to concrete using single pixel analysis," *Constr. Build. Mater.*, 2013, doi: 10.1016/j.conbuildmat.2009.12.016.

[60] V. Munoz *et al.*, “Damage detection in CFRP by coupling acoustic emission and infrared thermography,” *Compos. Part B Eng.*, 2016, doi: 10.1016/j.compositesb.2015.09.011.

[61] F. Khan, M. Bolhassani, A. Kontsos, A. Hamid, and I. Bartoli, “Modeling and experimental implementation of infrared thermography on concrete masonry structures,” *Infrared Phys. Technol.*, 2015, doi: 10.1016/j.infrared.2015.02.001.

[62] P. D. Pastuszak, “Characterization of Defects in Curved Composite Structures Using Active Infrared Thermography,” 2016, doi: 10.1016/j.proeng.2016.08.373.

[63] Y. Ma, F. Xu, L. Wang, J. Zhang, and X. Zhang, “Influence of corrosion-induced cracking on structural behavior of reinforced concrete arch ribs,” *Eng. Struct.*, 2016, doi: 10.1016/j.engstruct.2016.03.008.

[64] B. Sangoju, K. Ramanjaneyulu, A. Kanchanadevi, and S. Saibabu, “Fire Damage to Concrete Furnace-Supporting Structure and Formulation of Repair Methodology,” *J. Perform. Constr. Facil.*, 2018, doi: 10.1061/(ASCE)CF.1943-5509.0001142.

[65] T. Türker and A. Bayraktar, “Vibration based modal testing of a scaled reinforced concrete building for construction stages,” *Bull. Earthq. Eng.*, 2017, doi: 10.1007/s10518-015-9852-9.

[66] M. U. Hanif, Z. Ibrahim, H. X. Lim, and Y. X. Hang, “Effect of incremental static damage on modal frequencies of reinforced concrete beams,” *Int. J. Integr. Eng.*, 2018, doi: 10.30880/ijie.2018.10.02.020.

[67] Q. S. Li, J. Q. Fang, and A. P. Jeary, “Calculation of vertical dynamic characteristics of tall buildings with viscous damping,” *Int. J. Solids Struct.*, 1998, doi: 10.1016/S0020-7683(98)00021-3.

[68] D. Lu, J. Meng, S. Zhang, Y. Shi, K. Dai, and Z. Huang, “Damping ratios of reinforced concrete structures under actual ground motion excitations,” 2020, doi: 10.1007/978-3-030-12115-0_36.

[69] L. Zhang, Y. Xia, J. A. Lozano-Galant, and L. Sun, “Mass-Stiffness Combined Perturbation Method for Mode Shape Monitoring of Bridge Structures,” *Shock*

Vib., 2019, doi: 10.1155/2019/7320196.

[70] B. Xu, G. Song, and S. F. Masri, “Damage detection for a frame structure model using vibration displacement measurement,” *Struct. Heal. Monit.*, 2012, doi: 10.1177/1475921711430437.

[71] S. Ahmad and Z. Shabir, “Effect of Water Cement ratio on Corrosion of Reinforced concrete,” 2005.

[72] M. C. García-Alonso *et al.*, “Corrosion behaviour of new stainless steels reinforcing bars embedded in concrete,” *Cem. Concr. Res.*, 2007, doi: 10.1016/j.cemconres.2007.06.003.

[73] K. Saravanan, S. Sathiyanarayanan, S. Muralidharan, S. S. Azim, and G. Venkatachari, “Performance evaluation of polyaniline pigmented epoxy coating for corrosion protection of steel in concrete environment,” *Prog. Org. Coatings*, 2007, doi: 10.1016/j.porgcoat.2007.03.002.

[74] J. T. Pérez-Quiroz, J. Terán, M. J. Herrera, M. Martínez, and J. Genescá, “Assessment of stainless steel reinforcement for concrete structures rehabilitation,” *J. Constr. Steel Res.*, 2008, doi: 10.1016/j.jcsr.2008.07.024.

[75] G. Luckeneder, R. Autengruber, K.-H. Stellnberger, and J. F. T. Kurz, “Corrosion Protection of Galvanized Press-Hardening Steel : Main Influencing Factors and Mechanisms,” *Galvatech 2015 Conf. Proc.*, 2015.

[76] V. de K. Ortolan, T. Hilgert, J. J. Howland, L. F. O. Silva, and B. F. Tutikian, “Comparative assessment of corrosion of concrete reinforced with unprotected steel and hot-dip galvanized steel,” *Rev. la Constr.*, 2017, doi: 10.7764/RDLC.16.2.238.

[77] Y. Zhou *et al.*, “Experimental investigations on corrosion resistance of innovative steel-FRP composite bars using X-ray microcomputed tomography,” *Compos. Part B Eng.*, 2019, doi: 10.1016/j.compositesb.2018.10.069.

[78] M. G. Sohail, M. Salih, N. Al Nuaimi, and R. Kahraman, “Corrosion performance of mild steel and epoxy coated rebar in concrete under simulated harsh environment,” *Int. J. Build. Pathol. Adapt.*, 2019, doi: 10.1108/IJBPA-

12-2018-0099.

[79] D. Zhao, J. Pan, Y. Zhou, L. Sui, and Z. Ye, “New types of steel-FRP composite bar with round steel bar inner core: Mechanical properties and bonding performances in concrete,” *Constr. Build. Mater.*, 2020, doi: 10.1016/j.conbuildmat.2020.118062.

[80] M. D. Macdonald and A. J. J. Calder, “Bonded steel plating for strengthening concrete structures,” *Int. J. Adhes. Adhes.*, 1982, doi: 10.1016/0143-7496(82)90125-7.

[81] W. C. Tang, R. V. Balendran, A. Nadeem, and H. Y. Leung, “Flexural strengthening of reinforced lightweight polystyrene aggregate concrete beams with near-surface mounted GFRP bars,” *Build. Environ.*, 2006, doi: 10.1016/j.buildenv.2005.05.029.

[82] B. Kondraivendhan and B. Pradhan, “Effect of ferrocement confinement on behavior of concrete,” *Constr. Build. Mater.*, 2009, doi: 10.1016/j.conbuildmat.2008.08.004.

[83] S. Jayasree, N. Ganesan, and R. Abraham, “Effect of ferrocement jacketing on the flexural behaviour of beams with corroded reinforcements,” *Constr. Build. Mater.*, 2016, doi: 10.1016/j.conbuildmat.2016.05.131.

[84] A. Mukherjee, T. E. Boothby, C. E. Bakis, M. V. Joshi, and S. R. Maitra, “Mechanical behavior of fiber-reinforced polymer-wrapped concrete columns - Complicating effects,” *J. Compos. Constr.*, 2004, doi: 10.1061/(ASCE)1090-0268(2004)8:2(97).

[85] A. Mukherjee and S. J. Arwikar, “Performance of externally bonded GFRP sheets on concrete in tropical environments. Part I: Structural scale tests,” *Compos. Struct.*, 2007, doi: 10.1016/j.compstruct.2006.05.013.

[86] M. Balachandran and S. Christian Johnson, “Retrofitting of reinforced concrete beam with externally bonded CFRP,” *Int. J. Appl. Eng. Res.*, 2014.

[87] T. P. Meikandaan and A. Ramachandra Murthy, “Flexural behaviour of RC beam wrapped with GFRP sheets,” *International Journal of Civil Engineering and Technology*. 2017.

[88] C. E. Bakis *et al.*, “Guide for the design and construction of externally bonded FRP systems for strengthening concrete structures,” *Rep. by ACI Comm.*, vol. 440, no. 2002, 2002.

[89] P. N. Balaguru, A. Nanni, and J. Giancaspro, *FRP composites for reinforced and prestressed concrete structures : a guide to fundamentals and design for repair and retrofit*. 2009.

[90] S. Masoud, K. Soudki, and T. Topper, “CFRP-strengthened and corroded RC beams under monotonic and fatigue loads,” *J. Compos. Constr.*, 2001, doi: 10.1061/(ASCE)1090-0268(2001)5:4(228).

[91] J. F. Bonacci and M. Maalej, “Externally bonded fiber-reinforced polymer for rehabilitation of corrosion damaged concrete beams,” *ACI Struct. J.*, 2000, doi: 10.14359/8805.

[92] K. A. Soudki and T. G. Sherwood, “Behaviour of reinforced concrete beams strengthened with carbon fibre reinforced polymer laminates subjected to corrosion damage,” *Can. J. Civ. Eng.*, 2000, doi: 10.1139/l00-052.

[93] I. A. Wootton, L. K. Spainhour, and N. Yazdani, “Corrosion of steel reinforcement in carbon fiber-reinforced polymer wrapped concrete cylinders,” *J. Compos. Constr.*, vol. 7, no. 4, pp. 339–347, 2003.

[94] M. Badawi and K. Soudki, “Control of corrosion-induced damage in reinforced concrete beams using carbon fiber-reinforced polymer laminates,” *J. Compos. Constr.*, vol. 9, no. 2, pp. 195–201, 2005.

[95] T. El Maaddawy and K. Soudki, “Carbon-fiber-reinforced polymer repair to extend service life of corroded reinforced concrete beams,” *J. Compos. Constr.*, vol. 9, no. 2, pp. 187–194, 2005.

[96] S. Masoud and K. Soudki, “Evaluation of corrosion activity in FRP repaired RC beams,” *Cem. Concr. Compos.*, vol. 28, no. 10, pp. 969–977, 2006.

[97] A. Mukherjee, S. Gadve, and S. Malhotra, “Active protection of FRP wrapped reinforced concrete structures against corrosion,” in *Concrete Solutions*, 2009.

[98] T. El Maaddawy, A. Chahrour, and K. Soudki, “Effect of fiber-reinforced

polymer wraps on corrosion activity and concrete cracking in chloride-contaminated concrete cylinders," *J. Compos. Constr.*, vol. 10, no. 2, pp. 139–147, 2006.

[99] R. Sen, "Advances in the application of FRP for repairing corrosion damage," *Prog. Struct. Eng. Mater.*, 2003, doi: 10.1002/pse.147.

[100] S. Gadve, A. Mukherjee, and S. N. Malhotra, "Corrosion protection of fiber-reinforced polymer-wrapped reinforced concrete," *ACI Mater. J.*, 2010, doi: 10.14359/51663860.

[101] K. W. Neale, M. Demers, and P. Labossiere, "FRP protection and rehabilitation of corrosion-damaged reinforced concrete columns," *Int. J. Mater. Prod. Technol.*, vol. 23, no. 3–4, pp. 348–371, 2005.

[102] S. Gadve, A. Mukherjee, and S. N. Malhotra, "Active protection of fiber-reinforced polymerwrapped reinforced concrete structures against corrosion," *Corrosion*, 2011, doi: 10.5006/1.3549564.

[103] A. Sharma, S. Aneja, S. Sharma, and R. Gupta, "Elastic wave based evaluation of CFRP protected RC structures subjected to corrosion," *Constr. Build. Mater.*, vol. 287, p. 123081, 2021.

[104] V. N. Bindal, *Transducers for ultrasonic flaw detection*. Alpha Science Int'l Ltd., 1999.

[105] B. N. Pavlakovic, M. J. S. Lowe, and P. Cawley, "High-frequency low-loss ultrasonic modes in imbedded bars," *J. Appl. Mech.*, vol. 68, no. 1, pp. 67–75, 2001.

[106] N. M. M. Maia, J. M. M. Silva, E. A. M. Almas, and R. P. C. Sampaio, "Damage detection in structures: From mode shape to frequency response function methods," *Mech. Syst. Signal Process.*, 2003, doi: 10.1006/mssp.2002.1506.

[107] A. A. Torres-Acosta, M. J. Fabela-Gallegos, D. V. Vega, and M. M. Madrid, "Vibration Monitoring to Detect Corrosion Degradation in Reinforced Concrete Beams," 2003.

[108] S. Sharma and A. Mukherjee, “Longitudinal guided waves for monitoring chloride corrosion in reinforcing bars in concrete,” *Struct. Heal. Monit.*, 2010, doi: 10.1177/1475921710365415.

[109] S. Sharma and A. Mukherjee, “Ultrasonic guided waves for monitoring corrosion in submerged plates,” *Struct. Control Heal. Monit.*, 2015, doi: 10.1002/stc.1657.

[110] A. Farhidzadeh and S. Salamone, “Reference-free corrosion damage diagnosis in steel strands using guided ultrasonic waves,” *Ultrasonics*, vol. 57, pp. 198–208, 2015.

[111] K. Beena, S. Shruti, S. Sandeep, and K. Naveen, “Monitoring degradation in concrete filled steel tubular sections using guided waves,” *Smart Struct. Syst.*, vol. 19, no. 4, pp. 371–382, 2017.

[112] W. M. Kairu, M. M. Gatari, M. L. Muia, S. W. Mumenya, and P. Rajagopal, “Structural health monitoring of reinforced concrete structures using guided waves,” *Rev. Prog. Quant. Nondestruct. Eval.*, 2019.

[113] R. C. Sriramadasu, S. Banerjee, and Y. Lu, “Detection and assessment of pitting corrosion in rebars using scattering of ultrasonic guided waves,” *NDT E Int.*, vol. 101, pp. 53–61, 2019.

[114] C. U. Grosse and M. Ohtsu, *Acoustic emission testing*. Springer Science & Business Media, 2008.

[115] D.-J. Yoon, W. J. Weiss, and S. P. Shah, “Assessing Damage in Corroded Reinforced Concrete Using Acoustic Emission,” *J. Eng. Mech.*, 2000, doi: 10.1061/(asce)0733-9399(2000)126:3(273).

[116] Y. Kawasaki, Y. Tomoda, and M. Ohtsu, “AE monitoring of corrosion process in cyclic wet–dry test,” *Constr. Build. Mater.*, vol. 24, no. 12, pp. 2353–2357, 2010.

[117] A. A. Abouhussien and A. A. A. Hassan, “Acoustic Emission Monitoring of Corrosion Damage Propagation in Large-Scale Reinforced Concrete Beams,” *J. Perform. Constr. Facil.*, 2018, doi: 10.1061/(ASCE)CF.1943-5509.0001127.

[118] A. Nair, C. S. Cai, and X. Kong, “Acoustic emission pattern recognition in CFRP retrofitted RC beams for failure mode identification,” *Compos. Part B Eng.*, vol. 161, pp. 691–701, 2019.

[119] P. R. Prem, M. Verma, and P. S. Ambily, “Damage characterization of reinforced concrete beams under different failure modes using acoustic emission,” in *Structures*, 2021, vol. 30, pp. 174–187.

[120] S. Bagavathiappan, B. B. Lahiri, T. Saravanan, J. Philip, and T. Jayakumar, “Infrared thermography for condition monitoring - A review,” *Infrared Physics and Technology*. 2013, doi: 10.1016/j.infrared.2013.03.006.

[121] P. Meinlschmidt, “Thermographic detection of defects in wood and wood-based materials,” 2005.

[122] S. Hiasa, R. Birgul, and F. N. Catbas, “Effect of Defect Size on Subsurface Defect Detectability and Defect Depth Estimation for Concrete Structures by Infrared Thermography,” *J. Nondestruct. Eval.*, 2017, doi: 10.1007/s10921-017-0435-3.

[123] X. Maldague, “Theory and practice of infrared technology for nondestructive testing,” 2001.

[124] L. Chung, I. K. Paik, S. H. Cho, and Y. S. Roh, “Infrared Thermographic Technique to Measure Corrosion in Reinforcing Bar,” *Key Eng. Mater.*, 2006, doi: 10.4028/www.scientific.net/kem.321-323.821.

[125] B. Milovanović and I. Banjad Pečur, “Review of active IR thermography for detection and characterization of defects in reinforced concrete,” *J. Imaging*, vol. 2, no. 2, p. 11, 2016.

[126] M. Janků, P. Cikrle, J. Grošek, O. Anton, and J. Stryk, “Comparison of infrared thermography, ground-penetrating radar and ultrasonic pulse echo for detecting delaminations in concrete bridges,” *Constr. Build. Mater.*, vol. 225, pp. 1098–1111, 2019.

[127] H. A. Razak and F. C. Choi, “The effect of corrosion on the natural frequency and modal damping of reinforced concrete beams,” *Eng. Struct.*, 2001, doi: 10.1016/S0141-0296(01)00005-0.

[128] R. Burgueño, V. M. Karbhari, F. Seible, and R. T. Kolozs, “Experimental dynamic characterization of an FRP composite bridge superstructure assembly,” *Compos. Struct.*, vol. 54, no. 4, pp. 427–444, 2001.

[129] C. Y. Kao and S.-L. Hung, “Detection of structural damage via free vibration responses generated by approximating artificial neural networks,” *Comput. Struct.*, vol. 81, no. 28–29, pp. 2631–2644, 2003.

[130] N. Baghiee, M. Reza Esfahani, and K. Moslem, “Studies on damage and FRP strengthening of reinforced concrete beams by vibration monitoring,” *Eng. Struct.*, 2009, doi: 10.1016/j.engstruct.2008.12.009.

[131] D. R. Prasad and D. R. Seshu, “Study on change in modal parameters of RC beams due to fatigue type damage,” 2010.

[132] A. N. Ede, B. U. Ngene, and G. Bamigboye, “Vibration-Based Structural Health Monitoring: Theoretical Foundations and Experimental Validation on Reinforced Concrete Beams,” *ANALELE Univ. “EFTIMIE MURGU” REŞIŢA*, vol. 22, no. 2, 2015.

[133] R. Capozucca, “Vibration analysis of damaged RC beams strengthened with GFRP,” *Compos. Struct.*, vol. 200, pp. 624–634, 2018.

[134] A. S. Kırlangıç, “Nonlinear vibration-based estimation of corrosion-induced deterioration in reinforced concrete,” *J. Civ. Struct. Heal. Monit.*, vol. 10, pp. 639–651, 2020.

[135] A. Pourrastegar and H. Marzouk, “Vibration-Based Nondestructive Damage Detection for Concrete Plates,” *ACI Struct. J.*, vol. 118, no. 6, pp. 117–129, 2021.

[136] IS 456:2000, “Plain and Reinforced Concrete Code of Practice,” *Indian Stand.*, 2000.

[137] S. Sharma and A. Mukherjee, “Ultrasonic guided waves for monitoring the setting process of concretes with varying workabilities,” *Constr. Build. Mater.*, 2014, doi: 10.1016/j.conbuildmat.2014.09.018.

[138] C. U. Grosse and M. Ohtsu, *Acoustic emission testing: Basics for Research-*

Applications in Civil Engineering. 2008.

[139] hans A. Büchholdt, *Structural Dynamics for Engineers*. 1997.

[140] R. G. Rohrmann, M. Baessler, S. Said, W. Schmid, and W. F. Ruecker, "Structural causes of temperature affected modal data of civil structures obtained by long time monitoring," *Proc. Int. Modal Anal. Conf. - IMAC*, 2000.

[141] A. G. Chassiakos, S. F. Masri, R. D. Nayeri, J. P. Caffrey, G. Tzong, and H. P. Chen, "Use of vibration monitoring data to track structural changes in a retrofitted building," *Struct. Control Heal. Monit.*, 2007, doi: 10.1002/stc.155.

[142] A. ASTM, "C881 Standard Specification for Epoxy-Resin-Base Bonding Systems for Concrete," *Am. Soc. Test. Mater. West Conshohocken, PA, USA*, 2015.

[143] ASTM, *A370: Standard Test Methods and Definitions for Mechanical Testing of Steel Products*. 2014.

[144] A. Standard, "ASTM C109-standard test method for compressive strength of hydraulic cement mortars," *ASTM Int. West Conshohocken, PA*, 2008.

[145] E. DiPasquale and A. S. Cakmak, "Seismic damage assessment using linear models," *Soil Dyn. Earthq. Eng.*, 1990, doi: 10.1016/S0267-7261(05)80010-7.

[146] G. C. Yao, K. C. Chang, and G. C. Lee, "Damage diagnosis of steel frames using vibrational signature analysis," *J. Eng. Mech.*, 1992, doi: 10.1061/(ASCE)0733-9399(1992)118:9(1949).

[147] V. Kanwar, N. Kwatra, and P. Aggarwal, "Damage detection for framed RCC buildings using ANN modeling," *Int. J. Damage Mech.*, 2007, doi: 10.1177/1056789506065939.

[148] A. Vimuttasoongviriya, N. Kwatra, and M. Kumar, "The effect of lateral quasi-static loading on damage indexes based on modal parameters of retrofitted RC frame model," 2010.

[149] V. S. Kanwar, R. P. Singh, N. Kwatra, and P. Aggarwal, "Monitoring of RCC structures affected by earthquakes," *Geomatics, Nat. Hazards Risk*, 2016, doi: 10.1080/19475705.2013.866984.

[150] A. Vimuttasoongviriya, N. Kwatra, and M. Kumar, “Vibration Monitoring and Damage Assessment of a Retrofitted RC Frame Model,” *Curr. Appl. Sci. Technol.*, vol. 11, no. 2, pp. 43–53, 2011.